Electrical creation of spin polarization in silicon devices with magnetic tunnel contacts

Sharma, Sandeep

Electrical Creation of Spin Polarization in Silicon Devices with Magnetic Tunnel Contacts

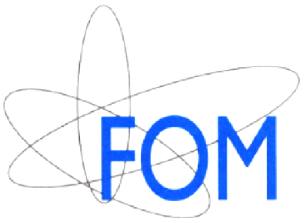

The work described in this thesis was performed in the group Physics of Nanodevices of the Zernike Institute for Advanced Materials at the University of Groningen, The Netherlands. Part of the research work was done at the National Institute of Advanced Industrial Science and Technology (AIST) in Tsukuba, Japan, and at the MESA+ Institute for Nanotechnology of the University of Twente, The Netherlands. The project was financially supported by the Dutch Foundation for Fundamental Research on Matter (FOM), the Netherlands.

Printed by: Grafimedia, 9747 AC Groningen

RIJKSUNIVERSITEIT GRONINGEN

Electrical Creation of Spin Polarization in Silicon Devices with Magnetic Tunnel Contacts

Proefschrift

ter verkrijging van het doctoraat in de
Wiskunde en Natuurwetenschappen
aan de Rijksuniversiteit Groningen
op gezag van de
Rector Magnificus, dr. E. Sterken,
in het openbaar te verdedigen op
maandag 25 maart 2013
om 11.00 uur

door

Sandeep Sharma

geboren op 25 mei 1979

te Hamirpur, India

Promotor:	Prof. dr. ir. B.J. van Wees
Copromotor:	Dr. R. Jansen
Beoordelingscommissie:	Prof. dr. ir. G.E.W. Bauer Prof. dr. ir. H.J.M. Swagten Prof. dr. D. Weiss

Zernike Institute PhD thesis series 2013-09
ISSN: 1570-1530
ISBN: 978-90-367-6070-6
ISBN: 978-90-367-6115-4 (Electronic version)

UNIVERSITY OF GRONINGEN

Electrical Creation of Spin Polarization in Silicon Devices with Magnetic Tunnel Contacts

Dissertation

to obtain the doctorate in the
Faculty of Mathematics and Natural Science
at the University of Groningen
under the authority of the
rector magnificus, dr. E. Sterken,
to be publicly defended
on Monday 25 March 2013
at 11.00 a.m.

by

Sandeep Sharma

born on 25 May 1979

at Hamirpur, India

Promotor:	Prof. dr. ir. B.J. van Wees
Copromotor:	Dr. R. Jansen
Reading Committee:	Prof. dr. ir. G.E.W. Bauer Prof. dr. ir. H.J.M. Swagten Prof. dr. D. Weiss

Zernike Institute PhD thesis series 2013-09
ISSN: 1570-1530
ISBN: 978-90-367-6070-6
ISBN: 978-90-367-6115-4 (Electronic version)

Contents

Chapter 1

Introduction

In this chapter, we introduce the topic of the thesis. A brief history of the development of metal-based spintronics devices is presented. Followed by these developments the prospects of a spin-based semiconductor technology are discussed. We identify the fundamental requirements for a spin-based semiconductor technology and explain why silicon is selected as a semiconductor material. To achieve the ultimate goal of implementing spin functionality in the semiconductor we emphasize the use of a magnetic tunnel contacts to Si. The advantages of the use of a tunnel insulator are discussed. We discuss the core objective of the thesis, which is to explore and/or find solutions for the fundamental issues of spin creation and detection in a semiconductor using spin-tunnel contacts. At the end of the chapter we give an outline of the thesis.

1.1 Why semiconductor spintronics ?

The invention of the metal oxide field effect transistor (MOSFET) during the sixties[1] has revolutionized the human life with a wide range of applications including smart phones, ipods, digital-tv, digital cameras, personal computers, video games and various other devices. The MOSFET, together with the diode, capacitor and a bipolar transistor form the basic building blocks of all kinds of digital or analog integrated-circuits. These electronic devices exploit the most salient property of the electrons: the electric charge. Such devices are based on the transport, manipulation and short-term storage of electrical charge, which represents the data as a volatile memory. The performance of such devices depends on how fast and efficiently charge manipulation and storage operation can be performed. The remarkable performance of these devices is attributed to the scaling of the dimensions of the MOSFET. Although the reduction in the dimensions of the MOSFET enabled most of the performance

enhancement, it cannot continue definitely[2]. It is limited by the fact that device dimensions will reach the physical limits very soon and it will no longer be possible to further enhance the device performance by simple scaling. Confronted with this challenge, alternative solutions are sought, where new device architectures with enhanced performance and new functionality are developed [3]. Semiconductor spintronics is an example of such a new technology, which aims at harnessing the spin angular momentum of the electron in solid state devices.

Similar to an electric charge, the spin angular momentum is the intrinsic fundamental property of the electron, responsible for the static magnetic properties of the magnetic materials. Although the concept of the spin was proposed long before in 1925 [4], it gained practical importance after the discovery of the giant magnetoresistive (GMR) effect in ferromagnetic thin film multilayers [5, 6]. Read sensors based on the GMR effect have been successfully integrated in computer hard drives since the mid-1990's. Later, the room temperature demonstration of the large tunnel magnetoresistance (TMR) in magnetic tunnel junctions (MTJs) showed great promise for their use in read head sensors and they were soon implemented. It also lead to the commercialization of the MTJs based magnetic random access memory (MRAM) [7]. Initial version of this type of magnetic memory used the magnetic field for writing operation. This magnetic field is induced by the current passing through the world line and bit line in MRAM. Such type of MRAM requires a larger current for writing operation when the MTJ size is reduced[8, 9]. Thus, this approach limits the scaling of the MRAM. Recently, another technique known as spin transfer torque (STT) magnetization switching has received greater attention. The write current for this type of MRAM scales down with the cell size. It does not require additional write word line, which leads to the reduction in cell size, enabling higher storage density[10, 11]. Thus, metal-based spintronics devices have seen a tremendous growth in a very short span of time.

Followed by these developments there have been significant efforts to have a control on the spin degree of freedom in a semiconductor and combine the unique features of the semiconductors and ferromagnets. These efforts are propelled by the fact that including the spin functionality in semiconductors may offer new avenues that are inaccessible in metal-based spintronics devices. The primary motivation behind this is the fact that the properties of semiconductors can be controlled by doping (density and type), light and by electrostatic gates, providing amplification and transistor action. The semiconducting materials also possess larger spin lifetime, enabling the spin information to survive for longer duration. On the other hand, ferromagnets have non-volatile memory functionality at ambient temperature. Yet, the magnetization can be switched rapidly and with unlimited endurance. The combination of these features yields an alternative information technology in which memory and logic

functions are integrated, and data is encoded in the direction of the electron's spin. Success in this field could lead to more efficient, fast operating devices with reduced power consumption compared with conventional semiconductor devices[12–15].

A technological assessment of the potential and the merits of this newly emerging technology is essential. For that purpose the devices and prototype circuits need to be realized, their characteristics and limitations determined, and their performance parameters quantified. Despite the efforts by various research groups across the globe, realizing a spin-functional semiconductor device at room temperature has been a long standing goal but an elusive one. Although some progress has been made in this direction, a complete prototype demonstration is still not available. To reap the expected benefits of a spin-based semiconductor technology, it is essential that spin-functional devices can operate at room temperature.

The motivation of the present work is to identify and establish the fundamental requirements for realization of spin-functional devices in semiconductors, particularly in silicon. In this thesis we will examine the basic requirements and address some of the issues. These developments may form the foundation of the spin-based semiconductor technology. In the following section, we explain why we have chosen Si as the host semiconductor.

1.2 Why silicon ?

Most of the initial developments in semiconductor spintronics were limited to GaAs, a direct band gap material where optical techniques could be employed for creating and detecting the spin polarization[16]. These optical investigations have given us considerable insight into spin dynamics and the lifetime and spin relaxation mechanisms in GaAs. Here, we will focus on silicon.

The interest in silicon stems from the fact that it has a lattice with inversion symmetry, and lower spin-orbit interaction due to its smaller atomic mass. Further, due to the absence of nuclear spin in the most abundant isotope of Si, the spin relaxation via hyperfine interaction is almost negligible. All these properties make the spin lifetime in Si large. Thus, spin information can be transmitted over large distances without loosing the spin coherence. But above all, Si is the mainstream semiconductor. The existing technology base for Si makes it more favorable to investigate the spin-related phenomena.

The efforts to induce spins into Si date back to early seventies. In 1968 it was shown by Lampel that a non-equilibrium spin polarization of the electrons in Si can be induced by illuminating the material with circularly polarized light[17]. Unfortunately, the steady state spin polarization was only a few percent in Si because spin-relaxation is much faster than carrier recombination, owing to the indirect band gap.

Therefore, optical orientation or luminescence are less efficient for the creation and detection of spin polarization in Si. One needs to look for an alternative efficient approach that is purely electrical. An example of such an approach is an all-electrical injection and detection of the spin-polarized carriers in a semiconductor. For e.g., in a magnetic tunnel contact to a semiconductor, the current across the junction is spin polarized due to the different tunneling conductance for majority ($\uparrow$) and minority ($\downarrow$) spins and this can be used to inject spins into the semiconductor. The injected spins undergo spin relaxation and the spin polarization reduces to zero if a continuous supply of spins is not maintained. Thus, under steady state condition a non-equilibrium spin accumulation can be created electrically in a semiconductor. This is preferred over the optical methods, as it offers a technologically viable method to integrate spin and charge-based devices on a common platform. In the following section we will discuss the basic requirements of semiconductor spintronics and the use of magnetic tunnel contacts to a semiconductor for realizing semiconductor based spin-functional devices.

1.3 Requirements of semiconductor spintronics

In order to have spin functionality in semiconductor devices, the following essential requirements need to be fulfilled simultaneously:

(1) Injection of spin-polarized carriers from a ferromagnet into semiconductor,

(2) Transport of spin-polarized carriers through the semiconductor channel, without loosing the spin information,

(3) Detection of spin-polarized carriers by a ferromagnetic drain contact,

(4) Electrical manipulation of the spins in the channel,

(5) Achieving all above mentioned conditions at room temperature and preferably in n-type and p-type semiconductor.

Earlier developments in semiconductor spintronics revealed that even achieving the first goal is not a trivial task. It was initially thought that the simplest way for injecting spins into Si (or any semiconductor) would be to make a direct contact between a ferromagnet (FM) and Si. However, the electrical spin injection from a FM into a highly resistive material (for e.g., a SC), which is in direct contact with the ferromagnet, was found to be highly inefficient due to the conductivity mismatch problem[18]. The spin accumulation created by the injection current at such an interface prefers to flow back into the less resistive ferromagnetic injector rather than diffusing into the

high resistive SC material. The spins, flowing back into the ferromagnet, readily loose their spin orientation and no significant spin polarization is created in the semiconductor.

Another problem in making direct contact of transition metal ferromagnets with silicon is the formation of silicide. It is known that silicide formation on Si occurs even at room temperature [19]. The magnetic atoms diffuse into Si but the associated magnetic moments do not align with each other as they do inside a ferromagnet. As a result, the spin orientation of the electrons injected into silicon is randomized by the strong spin-scattering events due to randomly-oriented magnetic moments of the metal atoms. The spin polarization of the current across the interface region reduces significantly and the spin polarization inside the Si becomes negligible[19, 20]. Instead of a direct contact between ferromagnet and silicon, we use a different approach, originally proposed by Rashba to alleviate the conductivity mismatch, i.e., to use a tunnel barrier between the ferromagnet and the semiconductor [21–23]. Introducing a tunnel barrier between FM and semiconductor has following three advantages.

(1) It avoids the formation of silicide at the interface between the ferromagnet and silicon. The silicide layer causes significant spin flips, reducing the spin polarization of the tunnel current into silicon.

(2) A tunnel barrier provides a large spin-dependent resistance, i.e., the conductance for one spin orientation (majority) is higher compared to the spins (minority) with opposite orientation. As a result, the spin polarization of the current across the interface is enhanced. Note that technology for creating magnetic tunnel contacts with high tunnel spin polarization is well developed, thanks to metal-based spintronics.

(3) Finally, the high tunnel resistance prevents the back flow of the spins that have been injected into silicon. Due to this weak coupling between the FM and the spins in the silicon, the probability to loose the spin information by tunneling back into FM is lowered. Spin detection via a tunnel barrier can be considered as an ideal spin voltage probe. Thus, efficient spin injection and detection would be possible by using spin-tunnel contacts to silicon or other semiconductors.

Therefore, world-wide efforts have focused on this convenient and technologically viable approach to create and detect spin polarization in semiconductors. Another approach, based on hot electrons was used by Appelbaum and coworkers. Using this, they demonstrated electrical spin transport in silicon in 2007[24]. Remarkable

results were subsequently obtained, including spin transport and coherent spin precession over a large distance of 350 micron of (undoped) Si at low temperature[25]. Unfortunately, the hot-electron approach has a major drawback in that the current levels are too small. Most of the current is lost due to the fast energy relaxation of the hot electrons in the ferromagnetic metals, and the current in the detection circuit of the device is only a minute fraction ($\approx 10^{-4}$) of the injected current[24].

Jonker et al. in 2007 reported electrical spin injection from an Fe/Al_2O_3 tunnel contact into silicon at low temperature[26]. The detection of the spin polarization was done optically, using a light emitting diode (LED) structure in which circularly-polarized luminescence is produced when the injected spin-polarized carriers recombine, as first demonstrated for other semiconductors [27]. Later that year, van 't Erve et al. reported electrical injection and detection of spin in silicon at 10 K with ferromagnetic tunnel contacts [28]. The breakthrough to room temperature was made in 2009 when we reported the first all-electrical creation and detection of spin polarization at 300 K in a semiconductor, for both n-type and p-type silicon [29] as described in chapter 3 of this thesis. Since then, the magnetic tunnel contacts have been successfully used for creating and detecting spin polarization in other semiconductors [29–33]. This has established magnetic tunnel contacts as a robust, reliable and efficient method to induce and probe spins in semiconductor at the relevant temperature scale. Because of this, they are now widely employed and, in fact, have become the standard in semiconductor spintronics. In this thesis, we therefore concentrate on silicon spintronic devices with ferromagnetic tunnel contacts.

1.4 Motivation and thesis outline

As discussed in the previous sections, the success in spin-based semiconductor technology may lead to the development of new information storage devices and architectures which are efficient and have low power dissipation. For achieving these goals certain fundamental issues related to spin injection into a semiconductor need to be satisfied.

The central objective of the thesis is to investigate the solutions for the basic requirements of a spin-based semiconductor technology. It includes the creation, detection and control of the spin polarization in silicon (n and p-type) at room temperature. We will address these issues by using silicon/oxide/ferromagnet tunnel devices. Understanding of the parameters which control the spin-polarized transport across a magnetic tunnel contact to silicon is essential. We will study how the use of different barrier materials, thickness of the barrier, type of ferromagnet and roughness of the tunnel interface influence the spin accumulation and spin lifetime and dynamics of spins in silicon. The variation of the spin signals with voltage, current

density and temperature will be investigated. In addition, we also include a study of the magnetization direction dependent spin-polarized transport in these devices. This thesis is divided into three main parts. In the first part, we describe the principle of electrical spin injection into a semiconductor. The second part describes the fundamental results of spin injection and detection in Si at room temperature. This part also includes the detailed study of how spin signal varies with parameters like the voltage, the current density, temperature, interface roughness, barrier thickness and tunnel barrier materials (Al_2O_3 and MgO). The third part of the thesis is devoted to the investigation of the tunneling anisotropy in Si/oxide/ferromagnet devices. For all measurements, we have used the three-terminal geometry for spin injection and detection. Below we present an outline of the work covered in this thesis.

Chapter 2 describes the basic principle of spin injection and detection with a magnetic tunnel contact to a semiconductor. Spin injection through a spin-tunnel contact is described in a linear approximation. We present a detailed description of the spin-detection method which utilizes the Hanle effect. We examine the role of spin diffusion on data analysis and describe the three-terminal and two-terminal measurement geometries. Spin signals in semiconductor based magnetic tunnel devices are suspected to have spurious signals like magnetoresistance and local hall effect. To rule out these artefacts, the use of a control experiment, employing a non-magnetic layer at interface between a ferromagnet and oxide is emphasized.

Chapter 3 presents the experimental results on ferromagnetic tunnel devices with an amorphous Al_2O_3 tunnel barrier, showing that spin polarization in silicon (n-type as well as p-type) was created successfully at room temperature. The variation of the spin signals with voltage, current density and temperature is presented. We present three-terminal Hanle measurements on a control device and investigate the effect of roughness on the Hanle measurements and on the extraction of the spin lifetime. We also compare the signal magnitude to existing theory.

Chapter 4 presents an alternative approach for realizing spin-tunnel devices to Si using crystalline MgO/Fe tunnel contacts instead of devices with an amorphous tunnel barrier. We describe the preparation method and structural characterization of these devices. The conditions of obtaining crystalline MgO/Fe tunnel contacts on Si are presented. We present the basic results on spin injection into p-type as well as n-type silicon at room temperature. Finally, we discuss the influence of the Si surface preparation on the measured Hanle, inverted Hanle signals, the linewidth of Hanle signal and correlate it with the roughness of the tunnel interface.

Chapter 5 provides a more detailed study of the magnitude of the spin accumulation created in a semiconductor. The focus is to investigate how the spin-signal obtained in a Hanle measurement varies with the thickness of the tunnel barrier. We present the spin transport data obtained on silicon based tunnel devices with amor-

phous Al_2O_3 and crystalline MgO tunnel barriers. We compare the experimental data with the available theoretical models which consider the direct tunneling, two-step tunneling and direct as well as two-step tunneling in parallel. To rule out spin signal enhancement by two-step tunneling via localized interface states, we present measurements on control devices in which the semiconductor is replaced by a non-magnetic metal (Ru) electrode. Further, to establish that the measured signals are genuine and originate from spin polarized transport, we present measurements on a control sample in which spin injection is known to be absent.

Chapter 6 is devoted to the investigations of the tunneling anisotropy in Si/Al_2O_3/ ferromagnet devices. We explore the tunneling anisotropy in three-terminal geometry, when the magnetization is rotated from *in-plane* to *out-of-plane*. We discuss the different contributions to the tunneling anisotropy and show that these can be distinguished using magnetic tunnel contacts on n as well as p-type silicon with different ferromagnets (Fe and Ni). This is followed by the description of the fitting equation which contains a term associated with tunneling anisotropic magnetoresistance and another term arising from an anisotropic spin accumulation inside silicon. A strategy to interpret the experimental results is included at the end of the chapter.

In chapter 7, we investigate the influence of the crystalline quality of the tunnel contact on tunneling anisotropy. We describe *in-plane* as well as *out-of-plane* tunneling anisotropy in crystalline Fe/MgO/Si tunnel devices. In addition, *in-plane* tunneling anisotropy is studied on silicon based tunnel devices with a poly-crystalline MgO/Fe tunnel contact and for devices with an amorphous Al_2O_3 tunnel barrier and poly-crystalline ferromagnetic electrode. We discuss the origin of the observed in-plane anisotropy and the role of the crystalline Si electrode and the contribution from coherent tunneling.

The thesis ends with a summary in chapter 8, the publications list and an acknowledgement.

Chapter 2

Principle of spin injection and detection in semiconductors using ferromagnetic tunnel contacts

This chapter provides an overview of the electrical methods that can be employed for the creation of a non-equilibrium spin polarization in a non-magnetic material. In particular, our focus will be on an all electrical scheme for injection and detection of the spins in silicon that employs ferromagnetic tunnel contacts. We describe the concept of spin injection into silicon by tunneling and also provide a detailed discussion about spin detection via Hanle effect. We discuss the measurement methods, i.e., three-terminal and two-terminal geometries for spin injection and detection. A discussion on spin detection in presence of vertical spin diffusion is also included. At the end of the chapter, we emphasize the importance of a control experiment to rule out the presence of spurious signal.

2.1 Introduction

Two of the fundamental requirements for realizing spin-functionality in semiconductor (SC) devices are the creation and detection of the spin polarization. Spin polarization can be created in a SC by optical methods, that is, by optical orientation [16, 34, 35]. By shining circularly polarized light on a SC, the momentum of the absorbed photons is transferred to the medium and electrons with different popula-

tion of opposite spin are created. These photo-excited spin-polarized carriers give rise to polarized radiation (luminescence) after recombination. By measuring the circular polarization of the luminescence the important quantities such as spin lifetime, the recombination time of the carriers and their spin polarization can be evaluated [36, 37]. Due to its direct band-gap, GaAs has been widely employed to study the electron spin dynamics with this technique [14, 16, 34, 35, 38–41]. An alternative to the above approach is to electrically induce the spin polarization into a SC and detect the emitted circularly polarized light as done in spin light-emitting diode (spin-LED) [27, 42]. This method has been successfully used not only in GaAs [43, 44] but also in devices with Si [26, 45]. However, the indirect band-gap in Si limits the efficient use of the optical techniques for creating and detecting spin polarization in Si.

In this thesis, we focus on an all-electrical scheme compatible with existing semiconductor technology. This would enable the integration of the spin and charge based devices on the same platform. Recently, magnetic tunnel devices with different SC (Si, Ge or GaAs) have been successfully employed for electrical injection and detection of the spin accumulation [29, 31, 32, 46, 47]. This has not only solved the fundamental problem of spin injection into a semiconductor, but also provided an opportunity to explore the various parameters that influence the spin transport in such spin-tunnel contacts. In this chapter, we therefore focus on silicon spintronic devices with ferromagnetic tunnel contacts. We start with a description of the physics that underlies their operation. We discuss spin injection through a tunnel barrier, and develop an expression for the spin accumulation induced in the semiconductor in terms of material parameters [48–51]. Next, we discuss the method of spin detection, i.e., the Hanle effect. This is followed by the description of the different measurement geometries. In particular, we focus on three-terminal method for creation and detection of the spin polarization and discuss its advantages over other measurement geometries. A two terminal geometry, which employs two contacts for both injection and detection of spins is also described. Finally, we emphasize the importance of doing a control experiment to rule out spurious signals and to establish that the signal that we observed is genuine and originates from spin polarized transport across the tunnel contacts.

2.2 Spin injection into silicon by tunneling

In a tunnel junction between a ferromagnet and a semiconductor, the tunnel current is spin-polarized because the tunnel conductance depends on spin. Majority ($\uparrow$) and minority ($\uparrow$) spin electrons with their magnetic moment, respectively, parallel and antiparallel to the magnetization of the ferromagnet have different tunnel conductances denoted by ($G^{\uparrow}$) and ($G^{\downarrow}$). Hence, one type of spin is injected into the semiconductor

at a higher rate than the other type, resulting in a net spin density in the semiconductor. This can be described by a spin splitting $\Delta\mu = \mu^{\uparrow} - \mu^{\downarrow}$ of the electrochemical potential, where $\Delta\mu$ is the spin accumulation. In the linear transport regime, the tunnel currents of majority and minority spin electrons, $I^{\uparrow}$ and $I^{\downarrow}$, respectively, are given by:

$$I^{\uparrow} = G^{\uparrow}\left(V - \frac{\Delta\mu}{2}\right) \tag{2.1}$$

$$I^{\downarrow} = G^{\downarrow}\left(V + \frac{\Delta\mu}{2}\right) \tag{2.2}$$

The voltage V is defined as $V_n - V_{fm}$, where V_n and V_{fm} are the spin-averaged potential of the non-magnetic (silicon) electrode and the ferromagnet, respectively (see Fig. 2.1). The total charge tunnel current $I = I^{\uparrow} + I^{\downarrow}$ and the spin tunnel current $I_s = I^{\uparrow} - I^{\downarrow}$ are then:

$$I = GV - P_{fm}G\left(\frac{\Delta\mu}{2}\right) \tag{2.3}$$

$$I_s = P_{fm}GV - G\left(\frac{\Delta\mu}{2}\right) \tag{2.4}$$

where $G = G^{\uparrow} + G^{\downarrow}$ is the total conductance and $P_{fm} = (G^{\uparrow} - G^{\downarrow})/(G^{\uparrow} + G^{\downarrow})$ is the tunnel spin polarization of the tunnel interface between a FM and an insulator.

The feedback of $\Delta\mu$ on the spin/charge tunnel current implies that another (independent) relation between $\Delta\mu$ and I_s is required to obtain a solution. This is provided by the requirement of a steady-state condition of the spin accumulation in the non-magnetic material, which is obtained when the spin current I_s injected by tunneling is balanced by the spin current due to spin relaxation in the material, integrated over the relevant volume. The spin current associated with spin relaxation is proportional to the spin accumulation and their relation can be expressed in terms of material parameters [22, 52, 53]. However, to illustrate the general features of spin injection and detection, it is more transparent to define a phenomenological parameter, the spin resistance r_s of the non-magnetic material, via:

$$\Delta\mu = 2I_s r_s \tag{2.5}$$

The r_s describes the conversion of the spin current I_s that is injected by tunneling, into a spin accumulation $\Delta\mu$, where $\Delta\mu$ denotes the value of the spin accumulation right at the tunnel interface, as relevant for the tunneling process. This definition of r_s is general and makes no specific assumptions about the spatial profile of the spin

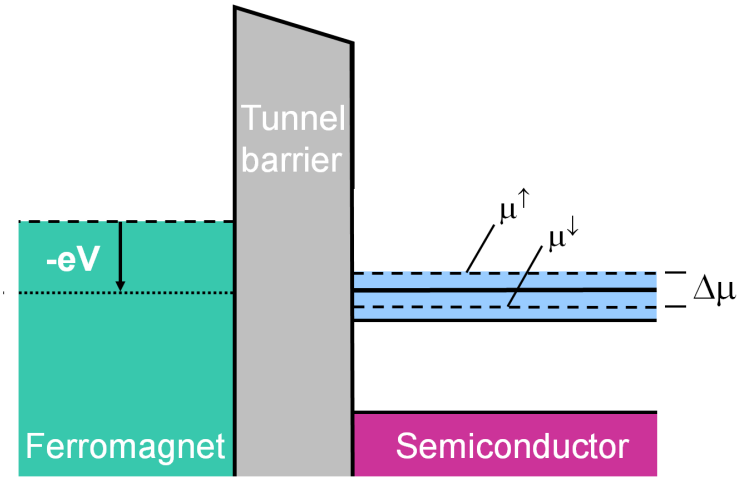

Figure 2.1: *Energy band diagram of a ferromagnet/insulator/semiconductor tunnel junction. In the semiconductor there is a spin accumulation, described by a spin splitting $\Delta\mu = \mu^{\uparrow} - \mu^{\downarrow}$ of the electrochemical potential. The applied bias voltage V is referenced to the spin-average potentials. For illustration purposes a degenerately doped semiconductor is chosen and band bending at the interface between the semiconductor and the tunnel barrier is omitted.*

accumulation in the non-magnetic material, or the formalism used to compute it. If we use the spin-diffusion equation and a spin accumulation that decays exponentially with distance from the injection interface with the spin-diffusion length L_{sd}, then the spin resistance of a unit contact area is $\rho_n L_{sd}$, where ρ_n is the resistivity of the non-magnetic material [22, 51–53] The solutions for the spin accumulation and spin current are:

$$\Delta\mu = \frac{2r_s R_{tun}}{R_{tun} + (1 - P_{fm}^2)r_s} P_{fm} I \tag{2.6}$$

$$I_s = \frac{R_{tun}}{R_{tun} + (1 - P_{fm}^2)r_s} P_{fm} I \tag{2.7}$$

where $R_{tun} = 1/G$. We identify two regimes. When $R_{tun} >> r_s$, the spin accumulation remains small and has negligible effect on the spin/charge current. We then have $I_s \approx P_{fm} I$, while $\Delta\mu$ is linearly proportional to the spin resistance of the non-magnetic electrode, and $\Delta\mu/I$ is independent of R_{tun}. In contrast, when $R_{tun} << r_s$, the spin current is reduced by the built-up of a large spin accumulation. The $\Delta\mu$ is then independent of r_s, but instead limited by R_{tun}.

2.3 Spin detection by the Hanle effect

The Hanle effect refers to depolarization of an oriented ensemble of spins by the application of transverse magnetic field. The effect was discovered by Wood and Ellett [54] in 1924 while studying the effect of a magnetic field on the polarization of the resonance radiation of the vapours of mercury and sodium. Initially they observed a high degree of polarization of the mercury vapour fluorescence that was later found to be diminished in a separate experiment. It was noticed that the apparatus was oriented in a different direction compared to the first configuration. By turning the apparatus by 90°, again they found the high value of polarization. The physical interpretation of this phenomenon was later provided by Hanle [55] and the effect is therefore referred to as the Hanle effect. It is considered as a standard test to prove or disprove the existence of spins inside a non-magnetic material. In the present work, we will make use of this effect to study the spin injection into silicon and various other parameters that influence the spin transport across a ferromagnetic tunnel contact.

Observation of a Hanle effect in a magnetic tunnel contact with silicon (or any other semiconductor or non-magnetic metal) involves three significant aspects. The first is the electrical injection of spin polarized carriers into the silicon. As pointed out in sec. 2.2, a bias voltage across a magnetic tunnel contact with silicon produces a non-equilibrium spin accumulation, $\Delta\mu = \mu^{\uparrow} - \mu^{\downarrow}$. The orientation of the spin accumulation is determined by the magnetization direction of the ferromagnet, which is parallel to the tunnel interface (that is, in-plane). The spin accumulation is greatest directly underneath the contact and decays exponentially with increasing distance from the interface with the spin-diffusion length , L_{sd}.

The second feature is the controlled reduction of the induced spin accumulation in an applied magnetic field. When a transverse magnetic field (B_Z) is applied, the spins precess with the Larmor frequency $\omega_L = g\mu_B B/\hbar$. Here g is the Landé g-factor, μ_B is the Bohr magneton and $\hbar$ is the Plank's constant divided by 2π. This results in a controlled reduction of the spin accumulation by means of the Hanle effect. As a result, the spin accumulation decays as a function of B with an approximately Lorentzian line shape [see Fig. 2.2]

$$\Delta\mu(B) = \frac{\Delta\mu(0)}{1 + (\omega_L \tau_s)^2)} \tag{2.8}$$

where τ_s is the spin lifetime and $\Delta\mu(0)$ is the spin accumulation at zero field.

At small B, the Larmor frequency is much smaller than $1/\tau_s$ and the spins precess only over a small angle during the time τ_s. In this case, the precession has little influence on the spin accumulation. For large B-field, the Larmor frequency becomes much larger than $1/\tau_s$ and spins make several complete cycles of coherent precession during the time τ_s. Since we are performing a DC measurement without moving

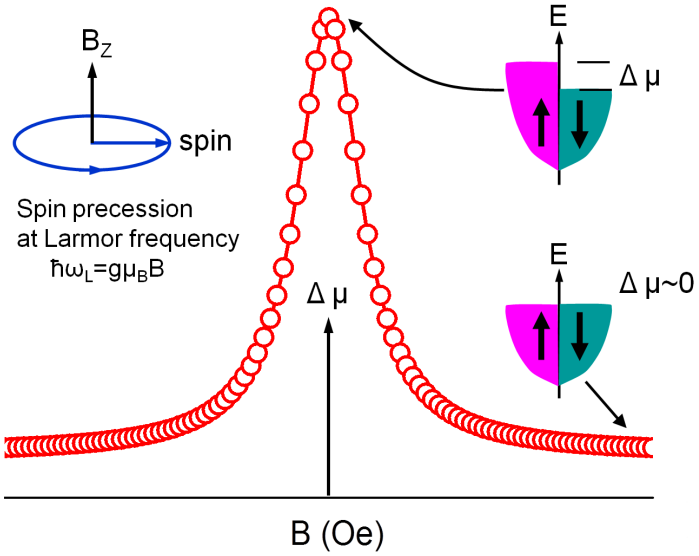

Figure 2.2: *Schematic illustration of the Hanle effect that allows the manipulation of the spin polarization in a semiconductor by an application of a transverse magnetic field. The spin accumulation gradually reduces to zero with increasing magnetic field strength, as indicated by the red curve. The line width at half maximum gives the effective spin lifetime.*

the spins in space (3-terminal geometry, using the same contact for injection and detection), the coherent precession causes the time average of the spin accumulation to gradually reduce to zero with increasing B. The spin accumulation is reduced to half of its initial value when $\omega_L = 1/\tau_s$. The half width of the Lorentzian Hanle curve thus allows extraction of the spin lifetime τ_s (at least, in principle: any deviations from the ideal behavior will modify the Hanle curve, such that we should consider the extracted time constant as a lower bound for the spin lifetime).

The third important feature is the electrical detection of the voltage signal due to the change in spin accumulation caused by the applied magnetic field. A spin accumulation can be detected electrically with a ferromagnetic tunnel contact, since the total charge current of the contact depends on the value of $\Delta\mu$. This is easily seen by rewriting eqn. 2.3:

$$V = R_{tun} I + \left(\frac{P_{fm}}{2}\right) \Delta\mu \tag{2.9}$$

From Eqns. (2.9) and (2.8) the amplitude of the Hanle signal, i.e., $V|_{\omega_L=0} - V|_{\omega_L\tau_s>>1}$, can be obtained and is given below:

$$\Delta V_{Hanle} = \left(\frac{P_{fm}}{2}\right) \Delta\mu^0 \tag{2.10}$$

Note that in order to observe a voltage signal, all the three features described above have to be simultaneously present. Hence, the successful observation of a Hanle signal proves spin injection, coherent spin precession, as well as spin detection in a single measurement.

From the Hanle measurement one can extract τ_s, since line width of the Hanle curve is inversely proportional to the spin lifetime, or strictly speaking, to the spin dephasing time. For delocalized carriers in bulk material and at room temperature, spin dephasing and longitudinal spin relaxation are controlled by the same microscopic scattering processes[34, 35], and we will simply use the term spin lifetime in this thesis.

It is important to keep in mind that deviations from a Lorentzian line shape can occur. If the semiconductor is thick compared to L_{sd}, spin diffusion perpendicular to the tunnel interface modifies the Hanle curve (see the supplement in ref. [29] as well as sec. 2.3.2), and the extracted spin lifetime can increase by about 50% compared to that obtained from a Lorentzian fit. Secondly, local magnetostatic fringe fields due to roughness can cause artificial broadening of the Hanle curve without a change of τ_s (see Ref. [56] and Chapter 3). Care should thus be taken, and in general the extracted values should be considered as a lower limit for the spin lifetime.

2.4 Measurement geometries

In this section, we will describe the three-terminal and two-terminal techniques of spin injection and detection. The non-local method of spin detection will not be considered here and details can be found elsewhere in the literature [57, 58].

2.4.1 Spin detection via three-terminal geometry

For detecting the non-equilibrium spin accumulation in magnetic tunnel contacts to Si we use the three-terminal (3T) geometry [29, 47, 59]. The 3T geometry (see Fig. 2.3) employs two non-magnetic reference contacts, and a third contact that acts as an injector as well as a detector of spins. For $V > 0$ (< 0), spin-polarized electrons are injected (extracted) into (from) Si, thus, creating a spin accumulation $\Delta\mu$ at the tunnel interface. This method probes the spin accumulation just at the tunnel interface, where it is largest. The spin accumulation $\Delta\mu$ gives rise to a voltage signal, which is given by eqn. 2.10. Spin detection in a 3T geometry relies on the controlled

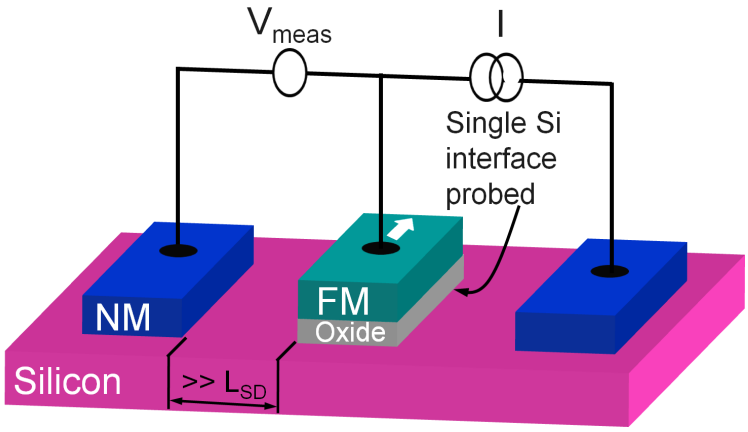

Figure 2.3: *Schematic illustration of the three-terminal device geometry for injection and detection of spin polarization in Si under a single contact (middle) consisting of an oxide insulator and a ferromagnetic metal electrode. Contacts used to source current (right) and detect the voltage (left) are placed away from the active interface by more than several spin-diffusion lengths.*

manipulation of the $\Delta\mu$ by an external transverse magnetic field (Hanle effect) and recording the resulting change in the voltage across the tunnel contact at constant bias current I. The advantages of employing three terminal geometry are:

(1) Nano-fabrication is not required. Standard optical lithography can be used to fabricate the test structure.

(2) This geometry allows the contact area to be chosen arbitrarily large so as to adjust the overall device resistance and thereby ensure a better signal to noise ratio.

(3) Relatively larger signal makes the spin detection easier.

The measured voltage signal can be described by an approximate Lorentzian line shape given by eqn. 2.8. But strictly speaking, eqn. 2.8 applies when spin-diffusion length is much smaller than the contact area (i.e., L_{sd} $<<$contact dimensions) and there is no drift. In general, when the current density in the semiconductor is low, the drift can be neglected. However, the effect of diffusion of the spins must be taken into account. A more detailed expression that consider vertical one-dimensional diffusion of the spin is discussed below. It is based on Ref.[34], but see also the supplement of Ref.[29].

The spins injected into the semiconductor from a ferromagnetic tunnel contact diffuse laterally as well as vertically from the point of injection. In most previous

experiments on electrical detection of the Hanle effect (see for instance [59, 60]), one uses the following expression for the spin dynamics including 1-dimensional (1-D) lateral diffusion (parallel to the injection interface):

$$S(x_1, x_2, t) = \frac{1}{\sqrt{4\pi Dt}} e^{-[(x_2 - x_1 - v_d t)^2/4Dt]} e^{-t/\tau_s} sin(\omega_L t) \tag{2.11}$$

It describes the spin polarization at detection point x_2 at a time t after the injection at point x_1 at t=0 for spins moving with drift velocity v_d and diffusion constant D. Integration of the above equation over time yields a steady state solution. When the same tunnel contact is used for injection and detection, one needs to integrate both x_1 and x_2 over the lateral dimension of the contact. This produces a Lorentzian if the contact is much larger than the spin diffusion length which applies to the measurements described in this thesis.

The case of 1-D diffusion perpendicular to the tunnel interface (along the z-axis) is mathematically equivalent to the case evaluated explicitly in the review by Fabian et al. [34]. Specifically, equation II.239 on page 617 of Ref[34] also applies to 1-D diffusion perpendicular to the interface with the B-field also along the z-axis:

$$S_y(z) \propto exp\left(\frac{-z\alpha_1}{L_{SD}}\right)\left[\frac{\alpha_1}{\alpha_1^2+\alpha_2^2} cos(z\alpha_2/L_{SD}) - \frac{\alpha_2}{\alpha_1^2+\alpha_2^2} sin(z\alpha_2/L_{SD})\right] \tag{2.12}$$

where $S_y(z)$ is the spin component along the magnetization direction (y-axes) of the ferromagnet at a distance z from the tunnel interface, and

$$\alpha_1 = \frac{1}{\sqrt{2}}\sqrt{1+\sqrt{1+(\omega_L.\tau_s)^2}}, \tag{2.13}$$

$$\alpha_2 = sgn(\omega_L).\frac{1}{\sqrt{2}}\sqrt{-1+\sqrt{1+(\omega_L.\tau_s)^2}}. \tag{2.14}$$

When single tunnel contact is used for injection and detection, the solution of eqn. (2.12) at z=0 is relevant:

$$S_y(z) \propto \frac{\alpha_1}{\alpha_1^2+\alpha_2^2} = \frac{1}{\sqrt{2}}\sqrt{\frac{1+\sqrt{1+(\omega_L.\tau_s)^2}}{1+(\omega_L.\tau_s)^2}} \tag{2.15}$$

Note that this expression is derived with fixed boundary conditions for the spin current injected from the tunnel contact at z = 0. In reality the modification of the

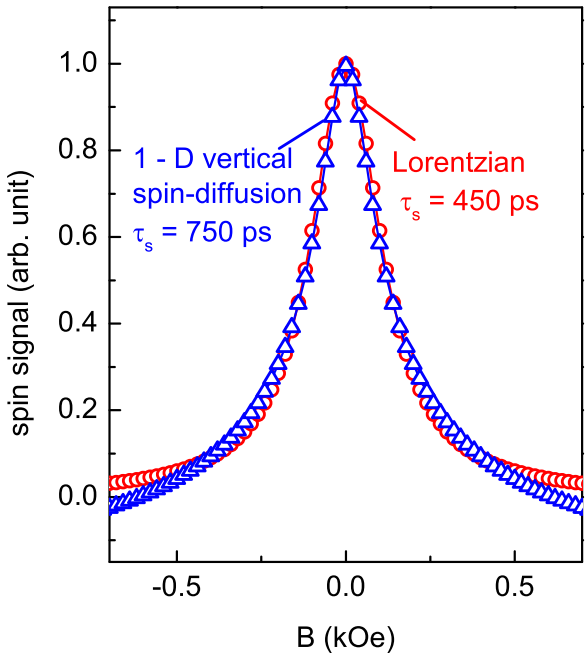

Figure 2.4: *Comparison between a pure Lorentzian (circular symbol) and to the case of eqn. 2.15 with 1-D diffusion perpendicular to the interface (triangular symbol), with the extracted values of the spin lifetime indicated. Approximately for the same line width, the latter approach results in a higher effective spin life time.*

spin accumulation by spin precession has a back-effect on the spin-polarized tunnel current [61], particularly if the spin accumulation is large. Also note that the above description does not include the effect of spatial inhomogeneity of the injected spin-polarized tunnel current, and assumes that the spin-relaxation time is homogeneous in the z-direction. Hence, a possibly shorter spin-relaxation time at the tunnel interface compared to the semiconductor bulk is not incorporated. A comparison between a pure Lorentzian and Eqn. 2.15 that takes into account the spin diffusion perpendicular to the tunnel interface is shown in Fig. 2.4. For the same line width the latter approach predicts a larger spin lifetime. A Lorentzian is thus likely to underestimate the spin lifetime and the extracted time constant should be considered as a lower bound. Since the diffusion can occur in all directions (perpendicular as well as parallel to the interface), we decided to stay on the safe side and use a Lorentzian to extract the spin lifetime.

2.4.2 Two-terminal geometry with large contact separation

Here, we describe another geometry that requires only two tunnel contacts which are separated by a distance larger than the spin-diffusion length L_{sd}. In such a case, there will be no contribution to the measured spin signal due to spin transport. A schematic diagram for spin detection using two terminal geometry is shown in Fig. 2.5. The method differs from spin-valve measurements in a sense that magnetization of the magnetic layers in both contacts is held fixed and points in the same direction. By applying a fixed current I, change in voltage is measured when a transverse magnetic field is applied. In this configuration, one of the terminals is biased in electron injection mode and the other one extraction mode. Individual contact produces a spin signal whose amplitude can be determined from Eqn. 2.10. Since contacts are separated by a distance larger than L_{sd}, signal due to spin transport across these contacts will be absent.

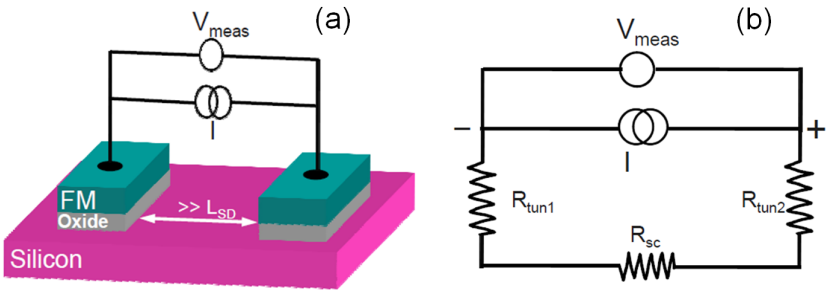

Figure 2.5: **Two terminal *Hanle* measurement.** **(a)** *Schematic illustration of the two-terminal Hanle geometry. The same contacts are used for applying current and measuring the change in voltage.* **(b)** *Equivalent circuit diagram for the geometry in* **(a)**.

Fig. 2.5(b) shows equivalent circuit for two terminal geometry. For a current I through the circuit, one may write:

$$V = \left[R_{tun1}I + \frac{P_{fm1}}{2}\Delta\mu_1\right] + \left[R_{tun2}I - \frac{P_{fm2}}{2}\Delta\mu_2\right] + R_{sc}I \tag{2.16}$$

where R_{tuni}, P_{fmi} and $\Delta\mu_i$ (i=1 or 2) represent the tunnel resistance, tunnel spin polarization and spin accumulation for contact one or two, respectively, and R_{sc} is the resistance of the semiconductor channel between the two contacts. It should be noted that process of spin injection (extraction) involves preferential injection (extraction) of majority spins (in magnetic tunnel contacts with Al_2O_3 as a tunnel barrier). Therefore, the spin accumulation $\Delta\mu$ under injection and detection will have opposite sign.

For that reason a negative sign appears in the second term. Assuming the contacts to be identical (i.e., $R_{tun1} = R_{tun2}$ and $P_{fm1} = P_{fm2}$), one can write for the Hanle signal:

$$\Delta V_{Hanle} = \frac{P_{fm}}{2} \left[|\Delta\mu_1| + |\Delta\mu_2| \right] \tag{2.17}$$

where $\Delta\mu_1$ and $\Delta\mu_2$ is the spin accumulation created under the contact one and two, respectively. Thus, even if spins injected at one contact are completely depolarized before reaching the other contact one can measure a spin signal originating from the spin accumulation underneath both the contact.

2.5 Control experiment

The spin-transport devices contain thin ferromagnetic layers either in direct contact with the SC or separated from the SC by an oxide layer. Such thin ferromagnetic layers produces fringe magnetic field, leading to local Hall voltage, magnetoresistance and even local change in carrier transport parameters [62]. These spurious signals may interfere with the real spin signal, thereby complicating the device behaviour. Therefore in spin-transport experiments, it is extremely important to carry out a proper control experiment to rule out all spurious signals.

In 3T geometry, a single ferromagnetic tunnel contact is used to create and detect the spins via Hanle effect. Since the Hanle effect is the primary experimental probe of the spin accumulation in 3T devices, another, independent control experiment is required. Replacing the ferromagnetic electrode with a non-magnetic metal does not solve the issue, as it removes both the magnetic fringe field as well as the source of spin-polarized transport. In such a case, both spin signal as well as any artefacts will be absent.

A novel and conclusive control experiment was introduced [29, 63] that can be used to prove or disprove the spin injection and detection in semiconductor devices with ferromagnetic tunnel contacts. It makes use of the extreme interface sensitivity of spin-polarized tunneling. By inserting a few nm of, a non-magnetic material at the interface between the tunnel barrier and the ferromagnetic electrode, the tunnel spin polarization can be suppressed to negligible values (see Fig. 2.6), without removing the magnetic materials or the external magnetic field and the associated spurious effects. In such a control device, true spin signals should be absent because $P_{fm} = 0$, while any artefacts still remain. The control experiment can also be performed in non-local devices, in which artefacts are not always automatically excluded. Strictly speaking, the method is not limited to semiconductor based devices but can be applied to any spintronic device that contains magnetic tunnel contacts.

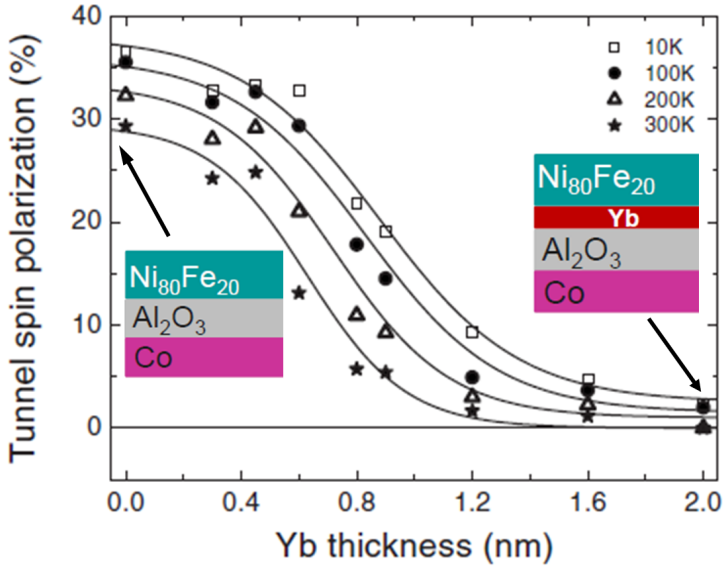

Figure 2.6: *Tunnel spin polarization of Al_2O_3/Yb/$Ni_{80}Fe_{20}$ interfaces vs. thickness of the Yb nanolayer measured at different temperatures. A 2 nm layer of Yb reduces the tunnel spin polarization to a negligible value. Data taken from Ref. [63].*

2.6 Summary

In this chapter, we described the principle of injection and detection of spin polarization induced in a semiconductor. We described the Hanle effect, which is considered as a standard test to prove or disprove the existence of the spin accumulation in a non-magnetic material. We pointed out the differences in analysing the data with a pure Lorentzian and another approach that takes into account the vertical spin-diffusion.

We also discussed the three and two-terminal methods for electrical creation and detection of spin accumulation. At the end of this chapter, we emphasize the importance of doing a control experiment to rule out spurious signals. In the next chapters, we will use three-terminal method to study the spin transport in magnetic-tunnel contacts to Si, with different ferromagnets and tunnel barriers.

Chapter 3

Electrical creation of spin polarization in Si at 300 K

In the previous chapter, we described the principle of spin injection and detection in a magnetic tunnel contacts to a semiconductor. In this chapter, we will demonstrate first all-electrical spin injection and detection by using magnetic tunnel contacts to n-type as well as p-type Si at 300 K. We discuss the variation of the spin signal with voltage, current density and temperature. Exceptionally large spin signal obtained in experiment is compared with theory. The possibly of signal enhancement by spin accumulation in localised states is ruled out by introducing Cs at interface between semiconductor and tunnel barrier. A control experiment is presented to rule out the spurious signals and establish the spin polarized transport and hence creation of spin polarization in Si. Further, we talk about the spin lifetime in Si obtained from Hanle linewidth. The influence of type of ferromagnet on Hanle line width is described. A model is presented to describe the influence of magneto-static fields (arising from the interface roughness) on Hanle line width. These magneto-static fields lead to spin precession in absence of external field. An inverted Hanle effect is presented as an experimental signature of the interface roughness. The magnitude of the magneto-static fields is influenced by the type of the ferromagnet. As a result the Hanle line width is found to scale linearly with the magnetization of the ferromagnetic electrode and the time constant extracted from Hanle line width is considered as a lower bound.

Part of this chapter has previously been published in
S. P. Dash, S. Sharma, R. S. Patel, M. P. de Jong, and R. Jansen, Nature **462**, 491 (2009).
S. P. Dash, S. Sharma, J. C. Le Breton, J. Peiro, H. Jaffrès, J. M. George, A. Lemaître, and R. Jansen, Phys. Rev. B **84**, 054410 (2011).
R. Jansen, S. P. Dash, S. Sharma and B. C. Min, Semicond. Sci. Technol. **27**, 083001 (2012).

3.1 Introduction and motivation

The injection of spin polarization in silicon from a ferromagnetic tunnel contact was first achieved in combination with optical detection in a spin-LED [26, 45, 64–66], but only at low temperature (5 - 80 K). Quantification of the spin polarization of the injected electrons in the silicon became possible with calculations of the spin-dependent phonon-assisted optical transitions in Si by Dery and coworkers [67]. Based on this, the measured light polarization [26] could be converted into an electron spin polarization of 27% in the Si-LED [67]. Spin injection in silicon spin-LEDs at low temperature was subsequently observed with different tunnel contacts [26, 45, 64–66]. This included SiO_2, following Park et al. [68], who first suggested that spin injection into silicon via SiO_2 should be feasible because for an interface of a ferromagnet on top of SiO_2, the tunnel spin polarization was found to be only slightly smaller than with Al_2O_3.

Fully electrical spin injection and detection in Si with magnetic tunnel contacts was also first observed at low temperature, using non-local devices [28, 30, 69–74]. The injection, detection and precession of spin in silicon were demonstrated using Fe/Al_2O_3 and Fe/MgO contacts, and the decay of the detected spin accumulation as a function of temperature [70] and distance between injector and detector [71, 72] was studied. Different measurement configurations and biasing conditions were also compared [72–74], all at low temperature (8 - 125 K). The electrical injection and detection of spin in silicon at room temperature, however, remained elusive until 2009. This forms the main motive of the present work.

In this chapter, we will demonstrate an all-electrical spin injection and detection into Si (n-type as well as p-type) at room temperature by using Si/Al_2O_3/ferromagnetic tunnel contacts. We will show the variation of the spin signal with voltage, current density and temperature. Spin signal enhancement by localized states is ruled out by an experiment that uses a Cs interlayer between Si and tunnel insulator. We also present the results of the control experiment which proves the spin polarized transport across magnetic tunnel contacts to silicon. The Hanle measurements are also performed by using two-terminal geometry which uses two tunnel contacts separated by a distance larger than spin-diffusion length. The effect of interface roughness on spin precession and effective spin lifetime is evaluated. The interface roughness results in magnetostatic fields that cause spin precession in absence of external field and leads to Hanle line width broadening. An inverted Hanle effect is presented as an experimental signature of the spin precession in presence of magneto-static fields due to roughness. The variation of the Hanle line width with different ferromagnets is investigated.

3.2 Device fabrication

The Si/Al_2O_3/ferromagnetic spin-tunnel contacts were prepared on n-type and p-type Si (100) substrates, referred to as n-Si and p-Si, respectively. The n-type silicon-on-insulator (SOI) wafer has a 5μm thick As doped active Si layer with a resistivity of 3 mΩcm and carrier density of 1.8×10^{19} cm^{-3} measured at 300 K. The p-type SOI wafer has a 3μm thick Boron doped active Si layer with resistivity of 11 mΩcm and carrier density of 4.8×10^{18} cm^{-3} measured at 300 K. Initially 300 nm of SiO_2 was grown at 1150° C on the SOI wafers. The oxide was patterned using standard optical lithography followed by wet etching to define contact holes of various sizes in the SiO_2. The substrates were introduced into the load-lock chamber in which, if desired, these were exposed to Cs using a Cs alkali-metal dispenser (SAES Getters). The current through the dispenser was increased in steps to 6A in 15 min and kept at 6A for another 15 min, and the pressure was constant at 10^{-7} Torr. The substrates were transferred into the ultra-high-vacuum chamber, where Al_2O_3 was deposited by electron beam (e-beam) evaporation from a single crystal Al_2O_3 source, followed by plasma oxidation for 2.5 min. Plasma oxidation is believed to compensate for oxygen vacancies occurred during e-beam evaporation. Subsequently the ferromagnetic metal and gold cap layers were deposited at a pressure better than 5×10^{-10} Torr. This was followed by ion beam etching to define the FM electrode, and finally the Cr/Au metal contacts were deposited by sputtering at a base pressure of 1.2×10^{-7} Torr.

3.3 Spin polarization in silicon at room temperature

Creating spin polarization in Si at room temperature has remained a long-standing goal in the area of semiconductor spintronics. Earlier attempts in this direction have been successful only at low temperature. Spin injection into Si at room temperature was realized in 2009, when we demonstrated the electrical injection of spin polarization into n-type and p-type Si from a ferromagnetic tunnel contact, the Hanle effect due to spin precession in the Si, and the electrical detection of the induced spin accumulation, at room temperature [29]. A three-terminal device with a single ferromagnetic tunnel contact (Fig. 2.3) was used for spin injection as well as detection, probing $\Delta\mu$ at the injection interface, where it is largest. The spin accumulation was created by applying a tunnel current across a Si/Al_2O_3/$Ni_{80}Fe_{20}$ contact with in-plane magnetization of the ferromagnet, injecting in-plane oriented spins. The spin polarization is manipulated with a perpendicular magnetic field B, transverse to the spin direction. For a constant tunnel current, the voltage across the junction is reduced with increasing B as spin precession gradually reduces $\Delta\mu$ to zero due to

Hanle effect (Chapter-2). First, we begin with the results on spin injection into n-Si and then we will show the similar data obtained on tunnel contacts to p-type silicon.

3.3.1 FM/Al_2O_3/Si spin-tunnel contact to n-type Si

In Fig. 3.1(a), we show a detected Hanle signal at a current I = 734 μA, corresponding to V = +172 mV at B=0 for a magnetic tunnel contact to n-Si. The signal is approximately Lorentzian in shape (solid black line). Similar data was obtained over the full temperature range, with a larger ΔV_{Hanle} at low temperature (Fig. 3.1b). This data demonstrates the electrical injection, detection and precession of spin polarization in silicon, since these three ingredients are simultaneously required in order to observe a voltage signal [29].

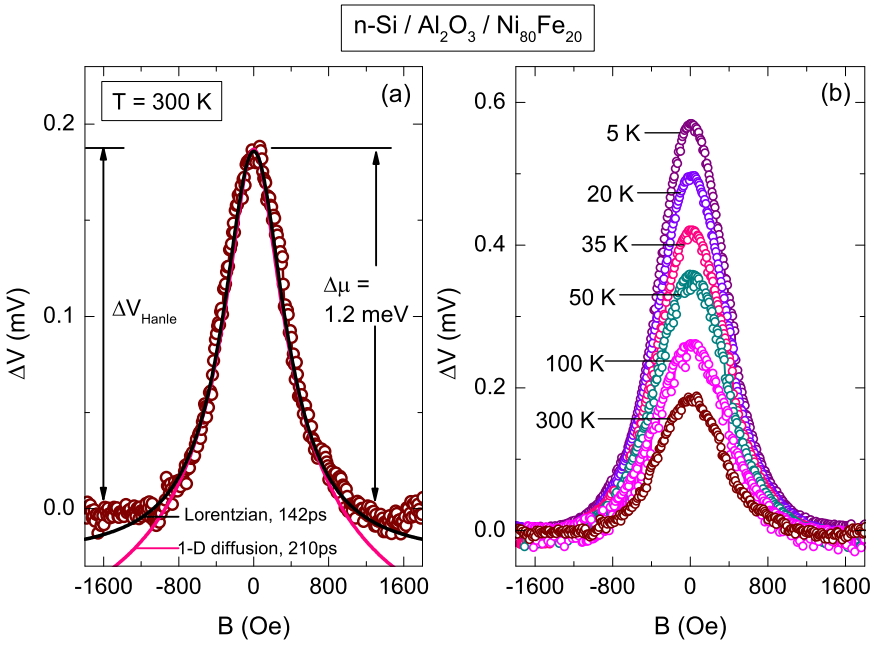

Figure 3.1: **Electrical injection and detection of a large spin accumulation in n-type Si at 300 K. a,** *Detected Hanle signal across an n-Si/Al_2O_3-$Ni_{80}Fe_{20}$(5 nm)-Co(20 nm) tunnel contact at T = 300 K, as a function of magnetic field perpendicular to the interface. Data are taken with a constant source current of 734 μA, corresponding to V = +172 mV at B=0. The black solid line is a Lorentzian fit with τ_s=142 ps. The pink solid line is a fit with τ_s=210 ps using Eqn. 2.15, that takes into account the 1-D spin diffusion perpendicular to the tunnel interface.* **b,** *Detected ΔV for various T, as indicated, for the same contact (all curves with V = +172 mV at B=0; the source current varied from 250 μA (5 K) to 734 μA (300 K)).*

From the amplitude of the Hanle signal ($\Delta V_{Hanle} \sim 0.2$ mV) a spin accumulation $\Delta\mu$ of 1.2 meV was determined, using eqn. (2.10) and $P_{fm} \sim 0.3$ for the Al_2O_3/$Ni_{80}Fe_{20}$ interface, as previously determined [75]. Thus, a sizable spin accumulation is induced in the Si at room temperature. From the width of the Hanle curve, a spin lifetime of τ_s = 140 ps was extracted, using a fit with a Lorentzian. However, it was noted that this should be treated as a lower bound, and fitting with an expression that takes account of vertical diffusion yields a larger value of 210 ps (see the supplement of Ref. [29] as well as the remarks at the end of sec. 2.4.1).

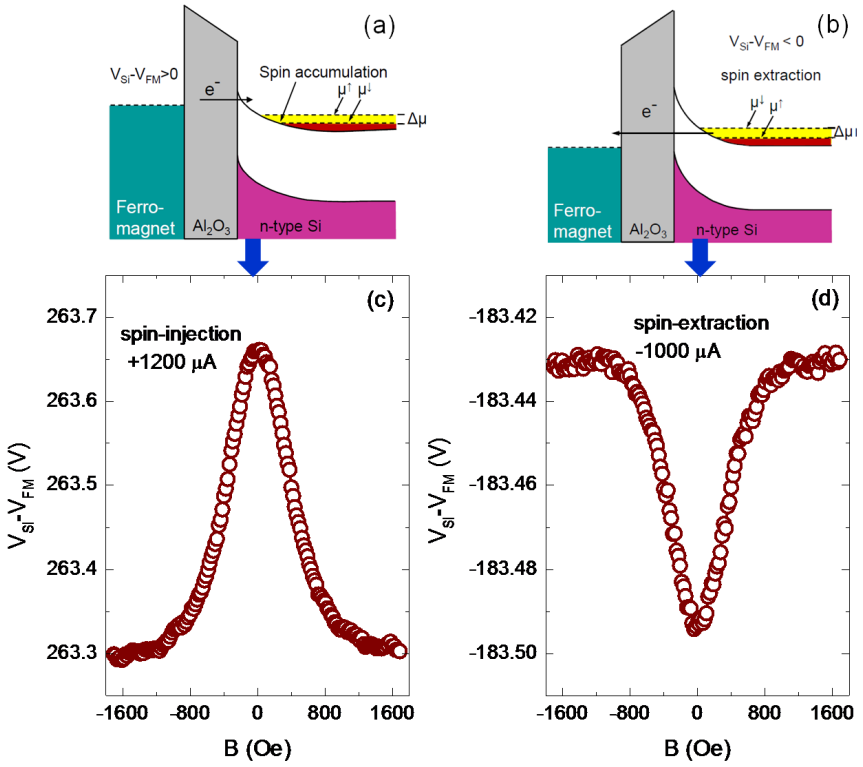

Figure 3.2: **Energy band diagram of magnetic tunnel contact with n-Si illustrating the concept of spin injection and extraction.** *Energy band profile of the contact to n-type silicon, consisting of an oxide insulator and a ferromagnetic-metal electrode (FM; green). In* **a**, *the reverse bias (V=V_{Si}-V_{FM} <0, spin injection into Si) across the tunnel contact, forms a depletion region in the Si that acts as a second part of the tunnel barrier.* **b**, *for V>0, spin are extracted from the conduction band of silicon.* **c** *&* **d**, *respectively, represent the measured Hanle signal for electron spin injection (extraction) into (from) n-type silicon at 300 K.*

An important aspect that enabled the room temperature spin observations was

the use of heavily doped Si with effective carrier density of 1.8×10^{19} cm^{-3} at 300 K. Carrier depletion in such heavily doped Si is negligible. Electrons can therefore tunnel directly into the silicon conduction band, and the Al_2O_3 dominates the tunneling transport. The high quality Al_2O_3 barrier (1 - 2 nm thick) provides a tunnel spin polarization that persists up to high temperature. It is important to mention that spin polarization in Si can also be created by preferential extraction of the spins from bulk bands of silicon. Figs. 3.2 (a) and (b) illustrates the basic concept of the electron spin injection and extraction, respectively. For V>0, the spin polarized electrons are injected into conduction band of Si, whereas, for V<0, the preferential extraction of spins (majority in present case) from bulk bands of Si occurs and leave behind the spin accumulation due to minority spins. Figs. 3.2 c and d display the measured Hanle curve for the case of electron spin injection and extraction. Thus, it demonstrates that spin polarization in Si can be created by injection as well as by extraction of spin polarized carriers. The reproducible and robust creation of spin polarization in silicon allowed a detailed investigation of the parameters that determine the spin accumulation. This includes the variation with bias voltage and current density, temperature, and the role of electrode material. Moreover, we showed that it is possible to induce spin polarization in p-type silicon. These topics are discussed in the following paragraphs.

3.3.1.1 Scaling with voltage and current density

An important question is how the magnitude of $\Delta\mu$ varies with bias voltage and current direction. Fig. 3.3 shows data for tunnel contacts on n-type Si with different ferromagnets. As expected, the spin accumulation increases at larger current density. Secondly, a spin accumulation can be created not only by injection of spin-polarized carriers from the ferromagnet into the Si (V>0), but also by spin extraction from the Si (V<0). For transition metal ferromagnets on Al_2O_3 the tunnel conductance is larger for majority spins (P_{fm} is positive [76]). Spin injection thus produces a net excess of electrons with majority spin in the Si. For the opposite current polarity a spin accumulation is also induced, but of opposite sign due to the preferential extraction of majority spin electrons.

For contacts with $Ni_{80}Fe_{20}$ electrodes, we found that the spin signal is asymmetric with respect to voltage/current polarity[29]. For electron injection (I>0), the Hanle signal increases rapidly with current density in an approximately linear fashion, whereas the spin signal is smaller for electron extraction (3.3a, bottom panel). Consequently, the spin-RA product (=($\Delta V_{Hanle}/I)\times$ area) decays at negative bias, whereas it is approximately constant at positive bias (3.3a, middle panel). For injection, the largest ΔV_{Hanle} of 0.43 mV is obtained, corresponding to $\Delta\mu \sim 2.9$ meV (with P_{fm} = 0.3).

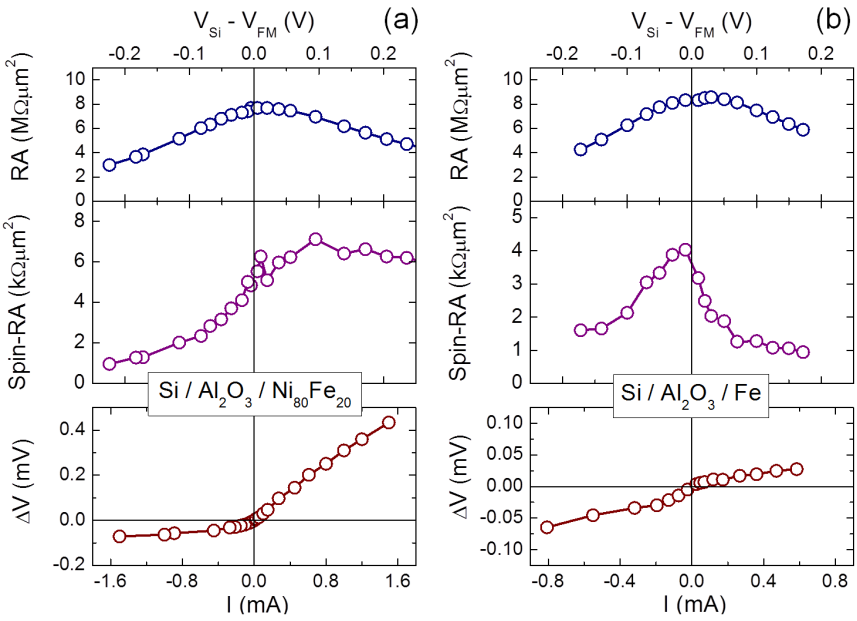

Figure 3.3: **Variation of spin signals with bias voltage and current density. (a),** *Data at 300 K for a Si/Al_2O_3/$Ni_{80}Fe_{20}$ contact on n-type Si, as in Fig. 3.1.* **(b),** *The same, but now with an Fe electrode. The top two panels show the resistance area (RA) product of the tunnel junction, and the spin-RA product (=(Δ V_{Hanle}/I) $\times$ area), versus bias voltage. The bottom panels display the Hanle spin signal (ΔV_{Hanle}) versus tunnel current for a junction area of 100$\times$ 200 μm^2. Positive voltage/current corresponds to electron injection into the Si.*

The bias asymmetry is not universal. For an Fe electrode in an otherwise identical junction, the spin-RA product decays for both bias polarities without a strong asymmetry (Fig. 3.3b). The spin-RA product at negative bias is similar, even in magnitude, but at positive bias it is distinctly different, even though the tunnel resistance (top panels) is similar for both electrodes. A different variation with bias voltage was also observed for devices on heavily doped n-type Si with MgO/CoFe contacts by Jeon et al. [31, 77]. The electronic structure of the ferromagnet/insulator interface thus plays a role. Indeed, the injected spin current depends on bias voltage because the tunnel spin polarization depends on the energy of the tunneling electrons [76, 78]. For positive bias, states below the Fermi energy of the ferromagnetic electrode contribute to the tunnel current, whereas at negative bias, electrons tunnel from the Si into empty states above the Fermi energy of the ferromagnet. The tunnel spin polarization for those states is different than at the Fermi energy. For Al_2O_3/ferromagnet interfaces, it was reported that P_{fm} decays asymmetrically [76, 78], and more rapidly

for states above the Fermi energy (as relevant for spin extraction).

Not only the spin current (which creates the spin accumulation) varies with bias, but also the efficiency of spin detection depends on the voltage. In the 3T geometry, the injection polarization and the detection efficiency together determine how the detected ΔV_{Hanle} varies with bias. The detection efficiency was invoked by Hamaya and coworkers to explain the rather different bias dependence of spin signals in Si devices with Schottky tunnel contacts [79, 80].

3.3.1.2 Spin accumulation at low temperature

The spin accumulation is expected to vary with temperature (T) because the tunnel spin polarization P_{fm} and the spin resistance 'r_s' of the semiconductor depend on T (for instance because the spin lifetime does).

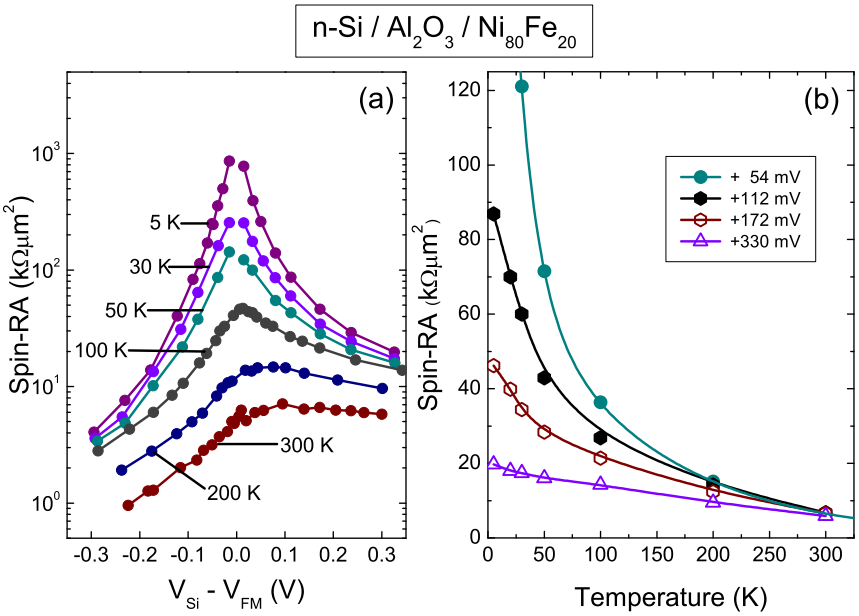

Figure 3.4: **Variation of spin signals with applied bias voltage and temperature. (a),** *Spin-RA product as a function of applied bias V at different temperatures, as indicated.* **(b),** *spin-RA product as a function of temperature at different bias voltage.*

For metal-based magnetic tunnel junctions, it is known that P_{fm} varies with T according to $P_{fm} \propto (1 - \alpha T^{3/2})$ with α = 3 - 5 $\times$ 10^{-5} $K^{-3/2}$ for Al_2O_3/$Ni_{80}Fe_{20}$ interfaces [81]. Since the Hanle signal is proportional to (P_{fm}^2), this contributes an

increase of the spin signal by a factor of 2.5 at low temperature. With regards to r_s, it is given by ρL_{sd} in the standard theory for spin injection and spin diffusion [22, 52, 53]. For heavily doped Si one does not expect r_s to have a strong variation with T, since both ρ and L_{sd} depend only weakly on temperature [29]. Assuming spin relaxation due to the Elliott-Yafet mechanism, the spin lifetime τ_s is expected to scale as $\tau_k/4\langle b^2\rangle$ where $\tau_k$is the momentum scattering time, and the parameter $\langle b^2\rangle$ was calculated [82] to decrease by 30 - 50$\%$ from room temperature to low T. Since for heavily doped Si also the mobility (directly proportional to τ_k) changes very little with T, the spin lifetime is expected to vary by only a factor of two or so.

The variation of the measured spin-RA product with T is shown in Fig. 3.4 for n-type Si/Al_2O_3/$Ni_{80}Fe_{20}$ tunnel devices [29]. As expected, the spin signal increases at low temperature. At large bias, the increase is about a factor of 3 to 4, which is reasonable given the variation that is expected from the factor $(P_{fm})^2$ and the increase of τ_s. However, at small bias voltage the signal increases much more rapidly, by up to two orders of magnitude, resulting in very large spin signals of about $10^3 k\Omega\mu m^2$. Similar behavior was observed for devices with heavily doped n-type Si with MgO/CoFe contacts by Jeon et al. [31]. Jonker and co-workers [33] observed very weak variation of the spin-RA product with temperature in devices with SiO_2 barrier, for measurements at much larger bias ($\sim$ 1 V), consistent with the trend shown in Fig. 3.4.

3.3.2 FM/Al_2O_3/Si spin-tunnel contact to p-type Si

The electrical injection of spins in p-type semiconductors had not been examined until 2009, when we reported the creation of spin polarization in p-type Si at room temperature[29] . Spins are injected by tunneling from a ferromagnetic contact (Al_2O_3/$Ni_{80}Fe_{20}$) into the valence band of the Si, in which holes are the electronic carriers. Results are shown in Fig. 3.5 for boron doped p-type Si with a measured hole density of $4.8\times10^{18} cm^{-3}$ at 300 K. Clear Hanle signals are observed for positive and negative currents (Fig. 3.5a), demonstrating electrically-induced spin polarization of holes in the valence band of p-type silicon, the spin precession of the holes, and the electrical detection of the spin accumulation of holes [29].

From the Hanle curve, a hole spin lifetime τ_s of 270 ps at 300 K was determined, which is larger than that of electrons in n-type Si. The free electron value of the g-factor (g=2) was used for valence band holes, in the absence of unique and accurate data [83]. If the g-factor for holes is different, the value of τ_s has to be adjusted correspondingly. The quoted spin lifetime is a lower bound, as already noted in the discussion of the data on n-type Si. Together with the measured hole mobility of 117 cm^2/Vs (diffusion constant D = 3.6 cm^2/s), a hole spin-diffusion length L_{sd} of 310 nm was determined [29]. Fig. 3.5b shows the variation of the spin-RA product with bias voltage. Interestingly, just as for n-type Si with Al_2O_3/$Ni_{80}Fe_{20}$ contacts, the

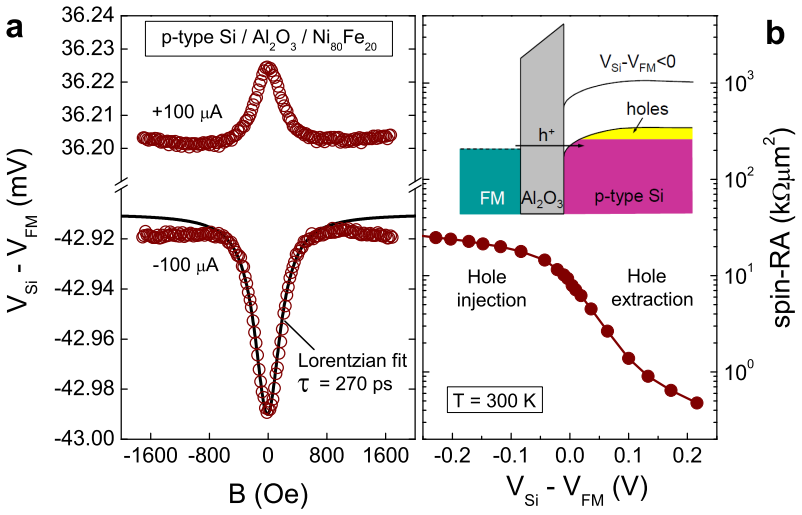

Figure 3.5: **Spin accumulation of holes in p-type Si at 300 K. (a),** *Detected Hanle signal across a p-Si/Al_2O_3/$Ni_{80}Fe_{20}$ tunnel contact at T=300 K, as a function of external field, B. Data for the two curves are taken with a constant current of either -100 μA or +100 μA. The solid line is a Lorentzian fit with τ_{eff} = 270 ps.* **b,** *Spin-RA product versus applied bias voltage at 300 K. Inset, energy band diagram for V<0, in which spin-polarized holes (h^+) tunnel from the FM into the valence band of the Si, where they are added to the pre-existing holes (yellow). This is equivalent to electrons tunneling from filled states (purple) in the Si valence band into empty states in the FM.*

spin-RA product is nearly constant when (hole) carriers are injected into the Si (V<0 in this case), whereas it exhibits a faster decay when the spin accumulation is created by extracting (hole) carriers from the Si (V>0).

3.4 Two terminal Hanle measurements

In this section, we demonstrate that one can measure a Hanle effect in two-terminal geometry where contacts are separated by a distance larger than the spin-diffusion length. In such a configuration the spin signal is dominated by the spin accumulation below individual contacts, rather than by spin transport from one contact to the other through the semiconductor channel. For such measurement a p-Si device with multiple magnetic tunnel contacts was taken. The contacts were separated by a distance of 100 μm, which is much larger than the spin-diffusion length in silicon. First,

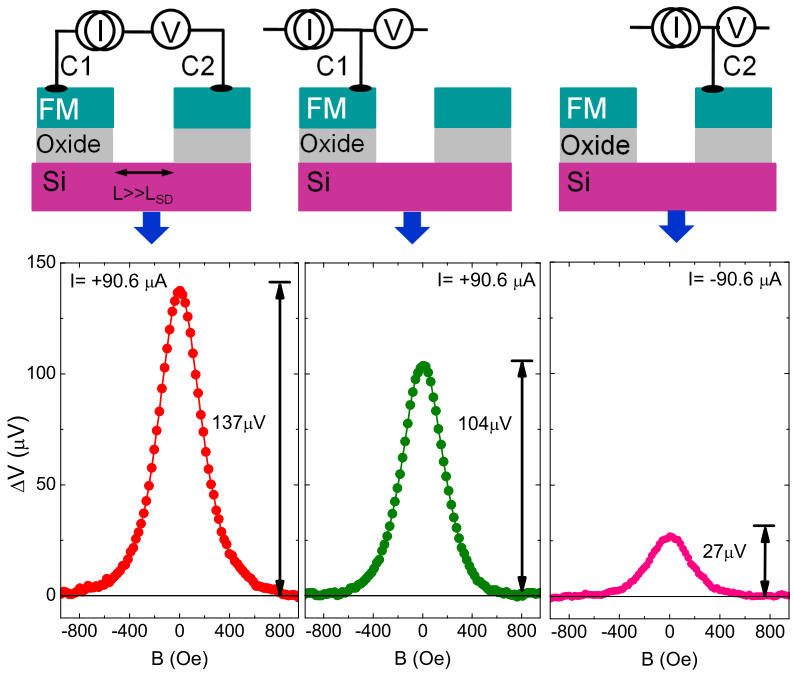

Figure 3.6: **Two-terminal *Hanle* measurements.** *Electrical Hanle measurements on p-type $Si/Al_2O_3/Ni_{80}Fe_{20}$ tunnel contacts in two-terminal geometry (left), and in the 3T geometry for each of the two contacts separately (middle and right). The contacts are separated by a distance (100 μm) larger than the spin diffusion length. (Left) 2T Hanle measurement at a source current of +90.6 μA, producing a Hanle signal of ΔV = 137 μV. The current direction is such that contact c1 is under positive bias (hole injection) and contact c2 is under negative bias (hole extraction). (Middle panel) 3T Hanle measurement of contact c1 with source current of +90.6 μA (hole injection, same current direction as in the 2T measurement), giving rise to spin signal of 104 μV. (Right panel) 3T Hanle measurement of contact c2 with source current of -90.6 μA (hole extraction, same current direction as in the 2T measurement), producing a spin signal of 27 μV. All data are taken at 300 K.*

consider a 2T Hanle measurement where both contacts c1 and c2 are involved. A source current of +90.6 μA gives rise to a spin-signal ΔV = 137 μV, as shown in left panel of Fig. 3.6. In this case, the contact c1 is under positive bias (hole-injection) and contact c2 is under negative bias (hole-extraction). Since the tunnel contacts are separated by a distance larger than the expected spin-diffusion length in Si, the observed spin signal is solely due to spin accumulation under the individual contacts. The middle panel of Fig. 3.6 shows a spin signal of 104 μV (+90.6 μA), obtained in 3T geometry under similar bias condition (hole-injection) for contact c1 as it was in the 2T method. The right panel in Fig. 3.6 shows similar 3T measurement for contact

c2 with a source current of -90.6 μA (hole-extraction). A spin signal of 27 μV is obtained. It is to be noted that a linear, field independent background voltage has been subtracted from the data and absolute value of the ΔV are plotted. As the measurement confirms, the signal from 2T measurement 137 μV is almost equal to the sum of the signals from the single contact measurements (104 μV + 27 μV). The small difference is only due to the uncertainty in determining the value of the background voltage, which is subtracted from the measured data.

This implies that, even if we place two magnetic contacts close enough so that spin transport is feasible, the large spin accumulation under individual contact will likely dominate over the signal due to spin transport from one contact to the other. This has consequences for the interpretation of the Hanle data in two-terminal devices. This also implies that a control experiment other than the Hanle effect is needed to prove spin transport for a two-terminal device geometry. In the next section we will present the results on such a control samples having a non-magnetic nanolayer between the ferromagnet and tunnel barrier.

3.5 Control experiment

In the previous chapter, we emphasized the importance of a control experiment to rule out any spurious signal due to the presence of a thin magnetic layer. Since the Hanle effect is the primary experimental probe of spin accumulation in 3T devices, another, independent control experiment is required. Here, we present the results of such a control experiment that can be used to prove or disprove the spin injection and detection in a semiconductor device. In control devices we inserted a few nm thick non-magnetic material at the interface between tunnel barrier and the feromagnetic electrode. It suppresses the tunnel spin polarization to a negligible value [63], without removing the magnetic materials or the external field and the associated spurious effects. In such a control device, true spin signals should be absent because $P_{fm} = 0$, while any artifacts still remain.

Fig. 3.7 displays the results of Hanle measurements for such control devices with the insertion of a non-magnetic nanolayer of Yb or Au for n-type Si, and a nanolayer of Au for p-type Si. All other device and measurement parameters are kept the same as for the "standard" Si/Al_2O_3/$Ni_{80}Fe_{20}$ junctions, for which data is included for comparison. Indeed, a Hanle signal is absent for all the control devices. These control experiments unambiguously prove that the Hanle signals observed in the standard junctions [29] are bona fide and represent spin accumulation induced by injection of a spin-polarized tunnel current.

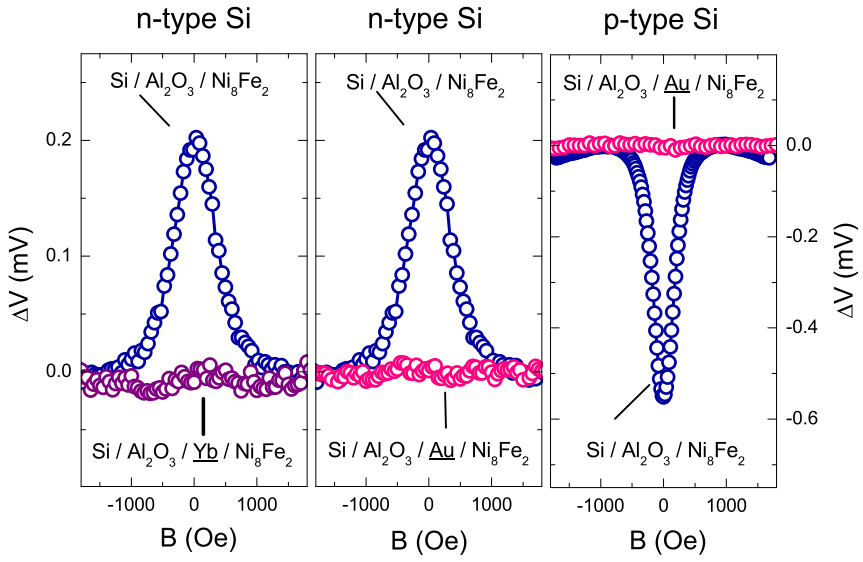

Figure 3.7: **Control experiment.** *Control experiments with devices having a non-magnetic nanolayer inserted between the ferromagnetic electrode and the tunnel barrier, which suppresses the tunnel spin polarization to zero. Hanle curves are shown for $Si/Al_2O_3/Ni_{80}Fe_{20}$ devices with and without nanolayer of Yb (2 nm) or Au (3 nm) for n-type Si, and Au (10 nm) for p-type Si. All data was taken at room temperature.*

3.6 Spin lifetime in Si

The spin lifetime determines how fast an induced non-equilibrium spin polarization decays without supply of fresh new spins, and how large the steady-state spin polarization is under continuous injection conditions. Spin relaxation of conduction electrons is relatively slow in silicon for the following three reasons. Firstly, the crystal has inversion symmetry. Hence, spin relaxation mediated by intrinsic internal electric fields (D'yakonov-Perel mechanism [34, 35]) is absent. Secondly, whereas spin relaxation via hyperfine interaction is important for localized electrons at low temperature, it is negligible for delocalized conduction electrons in the temperature range around room temperature. In addition, the ^{28}Si and ^{30}Si isotopes with relative abundances of 92% and 3% have no nuclear spin. Thirdly, the Elliott-Yafet spin-relaxation mechanism, which is dominant in silicon [34, 84, 85], arises from the combined action of momentum scattering (by phonons or impurities) and spin-orbit (SO) interaction, and SO interaction is small in silicon.

3.6.1 Spin lifetime in n-type Si

We have used Lorentzian expression to extract the effective spin lifetime in silicon. For the magnetic tunnel contacts on n-Si with $Ni_{80}Fe_{20}$ as a magnetic electrode, the spin lifetime is found to be 142 ps.

A detailed review of the spin lifetimes in n-type Si (with different dopant elements) extracted from Hanle data in ferromagnetic tunnel devices has been recently reported [51]. It is found that in 3T devices with As or Sb doping, τ_s is typically 0.1 to 0.3 ns. Such values are smaller than the electron spin resonance (ESR) values for bulk Si by about a factor of 6, to more than an order of magnitude. Again, this indicates that the spin lifetime is reduced by extrinsic factors that are related to the tunnel contact. This is also suggested by the fact that on average, the NL devices exhibit larger spin lifetimes than the 3T devices. In NL devices, the Hanle measurement probes spin precession dominated by the Si channel, and values closer to the bulk spin lifetime may be expected. On the other hand, 3T devices probe spins accumulating directly under the ferromagnetic tunnel contact, and it was suggested that the spin lifetime is reduced by the proximity of the tunnel oxide and/or the ferromagnetic electrode [29]. In the next section, we discuss the influence of the interface roughness and type of the ferromagnet on effective spin lifetime.

3.6.2 Interface roughness and spin precession in a semiconductor

In previous sections, we found that magnetic tunnel contacts with silicon provide a robust method to create spin polarization in Si. Because these spintronic nanostructures combine different materials, (ferromagnet with semiconductor or nonmagnetic metal) a key question is to what extent the proximity to interfaces influences the spin accumulation and the spin dynamics. Dipolar fields from magnetic domain walls in a demagnetized Ni film have been reported to reduce the spin-dephasing time of optically excited carriers in GaAs, [86] but the associated increase of the Hanle linewidth ($\sim$1Oe) is small. Spin precession is also known to be affected by nuclear hyperfine fields [87, 88]. These are not related to the ferromagnetic interface and are typically relevant only at low temperature. In contrast, we demonstrate here a much more general mechanism (present even at room temperature and for homogeneously magnetized ferromagnetic electrodes) that has a surprisingly dramatic effect on spin accumulation and spin dynamics of carriers in a nonmagnetic medium near a magnetic interface. Specifically, inhomogeneous magnetostatic fields arising from finite interface roughness are shown to alter precession of spins in a semiconductor near the magnetic interface, dominate spin dynamics up to surprisingly large external fields as large as 1 kOe, and reduce the spin accumulation up to tenfold. We focus here on spin polarization created in semiconductors by injection of spins from a fer-

romagnetic tunnel contact. However, the phenomena described here should occur irrespective of the type of nonmagnetic material or the method used to create the spin accumulation, although the extent of the effect depends on the details of the system.

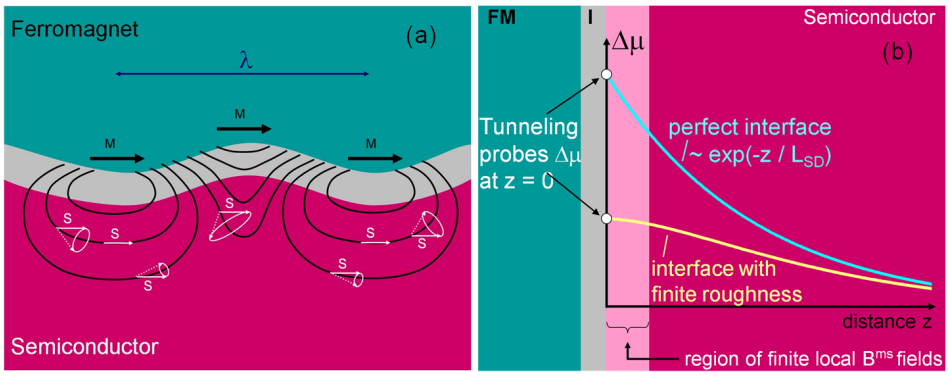

Figure 3.8: **Illustration of local interface magnetic fields and there effect on spin precession in a semiconductor. (a),** *The inhomogeneous magnetostatic field near a ferromagnetic interface with finite roughness, sketched for a sinusoidal interface profile with period λ. Field lines are in black; the magnetization of the ferromagnet (black arrows) points strictly along the global interface plane everywhere. Spins are injected into the semiconductor with spin initially aligned with the magnetization of the ferromagnet (solid white arrows). In the local fields, the spins are precessing on different trajectories represented by dotted arrows and white ellipses. Also the strength of the local field and hence the precession frequency is spatially inhomogeneous.* **(b)** *Decay of the spin accumulation $\Delta\mu$ as a function of distance z from the oxide/semiconductor interface for (i) a perfectly smooth interface (exponential decay with spin-diffusion length L_{SD}) and (ii) an interface with finite roughness. For the latter, the region in which the local magnetostatic fields B_{ms} have an appreciable value is given in pink. Note that tunneling probes the value of $\Delta\mu$ at z = 0.*

The magnetostatic fields near a ferromagnetic interface with finite roughness are sketched in Fig. 3.8 for the case of a sinusoidal interface profile with period λ. The magnetization of the ferromagnet is taken to lie in plane and point strictly along the global interface everywhere. This is a valid approximation for the soft magnetic thin films without significant interface anisotropy that we use here, as their magnetization can easily be saturated in a small in-plane magnetic field. While for an extended and perfectly flat, in-plane magnetized film the magnetostatic field would be zero outside the ferromagnet, in the presence of finite roughness there are local magnetostatic fields that penetrate into the nonmagnetic medium and influence the spins. Note that this is not only determined by the ferromagnet/tunnel barrier interface, but for thin films also by the roughness of the top surface of the ferromagnet, due to the long-range nature of magnetic fields. The magnetostatic fields are inhomogeneous in

magnitude and direction, and change sign periodically. The magnitude of the fields scales with the roughness amplitude, and is linearly proportional to the magnetization M_s of the ferromagnet. The strength of the field decays with distance z from the interface on a length scale that, for periodic roughness, is set [89] by the lateral roughness period λ. In the absence of roughness, a spin accumulation $\Delta\mu$ decays exponentially as a function of distance z from the injection interface [Fig. 1(a)], with a spin-diffusion length L_{sd}. However, for finite roughness spin precession is altered significantly in the region between z = 0 and z = λ where appreciable local magnetostatic fields exist, strongly reducing $\Delta\mu$. Even if λ is shorter than L_{sd}, interfacial depolarization reduces $\Delta\mu$ over the full depth range [Fig. 1(b)] because spin diffusion connects all spins and dictates that spatial variations in spin density cannot exist on a length scale much smaller than L_{sd}. Hence, interfacial magnetostatic fields affect the spins to an effective depth of L_{sd}. Also note that by spin-polarized tunneling into the ferromagnet one probes the value of $\Delta\mu$ at z = 0, where the reduction is strongest, as the spin accumulation right at the interface is most directly affected by the local magnetostatic fields.

3.6.3 Influence of type of ferromagnet on Hanle line width

When spin-polarized electrons tunnel from the ferromagnet into the semiconductor, the injected spins initially point along the magnetization direction of the ferromagnet, taken to be along x. Ideally, in the absence of an external applied magnetic field B^{ext} there is no Larmor spin precession, and a static, nonequilibrium spin accumulation is induced. The local magnetostatic fields B^{ms}(x,y,z) modify this simple picture. The spins are precessing in the total magnetic field that is composed of B^{ext} and B^{ms}(x,y,z). Since the latter is spatially inhomogeneous in direction and amplitude, the axis of spin precession and the precession frequency become spatially inhomogeneous. A full account of the consequences is given in sec. 3.6.5, after description of the experimental data.

The spin accumulation is probed by using 3T method as described in sec. 2.4.1. Since [53] the tunnel resistance is directly proportional to $\Delta\mu$ (i.e.,$\Delta V = P_{fm}\Delta\mu/2$ with P_{fm} the tunnel spin polarization associated with the Al_2O_3/FM interface) and $\Delta\mu$ is reduced by spin precession, the value of ΔV and its variation with B^{ext} provide information about the spin dynamics. We start with n-type Si and conventional Hanle measurements (Fig. 3.9, left panel), with B^{ext} applied along the z axis (perpendicular to the interface and to the injected spins). A typical Hanle curve is observed, with a maximum voltage (and hence $\Delta\mu$) at B^{ext} = 0, and a gradual reduction with increasing external field due to spin precession. This is similar to Hanle data obtained previously (Fig. 3.1), establishing that a non-equilibrium spin accumulation in the Si is induced by the injection of the spin-polarized tunnel current. We observe spin

signals for different ferromagnets in the range of 1-10 k$\Omega\mu$m^2 and thus larger than expected from theory, as noted before in sec. 3.7. Therefore we will not discuss here the factors that determine the overall magnitude of $\Delta\mu$, and show only normalized data.

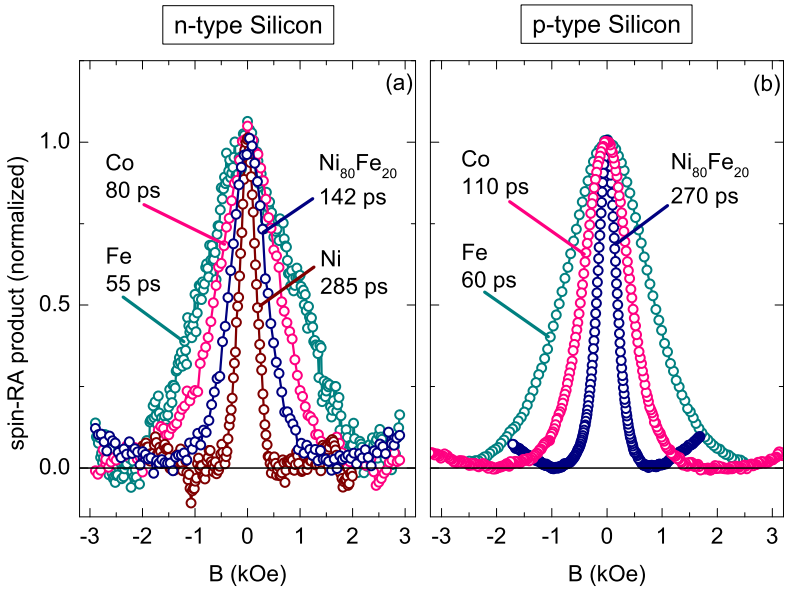

***Figure 3.9: Hanle* effect in tunnel contacts to Si with different ferromagnet.** **(a)** *Room temperature data for n-Si/Al_2O_3/ferromagnet contacts with Ni, $Ni_{80}Fe_{20}$, Co or Fe electrode.* **(b)** *Similar data for p-Si/Al_2O_3/ferromagnet contacts with $Ni_{80}Fe_{20}$, Co or Fe electrode. Hanle curves for different ferromagnets are normalized for better comparison of the linewidth.*

Let us now focus on the features that are due to the proximity of the interface with the ferromagnet. We find that the width of the Hanle curve depends on the ferromagnet used, i.e., the width increases from Ni, to $Ni_{80}Fe_{20}$, to Co, to Fe, with a half width at half maximum (HWHM) of 200, 400, 710, and 1030 Oe, respectively. Conventionally, the Hanle curves are described [29, 34] by a Lorentzian given by $\Delta\mu(B)$= $\Delta\mu(0)$/[1 +$(\omega_L\tau_s)^2$], where τ_s is the spin lifetime and ω_L is the Larmor frequency (ω_L=gμ_BB/$\hbar$, where g is the Lande g factor, μ_B the Bohr magneton, and $\hbar$ Planck's constant divided by 2π). The width of the Hanle curve is then set solely by parameters of the semiconductor (τ_s and g), which is inconsistent with our data. We attribute the experimental trend to modification of the spin dynamics near the FM interface due to local magnetostatic fields that arise for finite roughness. As shown in Sec. 3.6.5, this produces an artificial broadening of the Hanle curve that depends on the direction and magnitude of B^{ms}, which in turn is proportional to the

magnetization (M_s) of the FM. Indeed $\mu_0 M_s$ at room temperature increases from 0.6 T for Ni, to 0.9 T for $Ni_{80}Fe_{20}$, to 1.8 T for Co, and to 2.2 T for Fe.

Qualitatively similar results are obtained for tunnel contacts on p-type Si (Fig. 3.9b). For all ferromagnets, a Hanle signal is observed at room temperature, consistent with previous results on the creation of spin polarization in p-type Si (see fig. 3.5). For increasing M_s the width of the Hanle curve increases, with HWHM of 200 Oe (Ni), 210 Oe ($Ni_{80}Fe_{20}$), 515 Oe (Co), and 950 Oe (Fe), although the difference between $Ni_{80}Fe_{20}$ and pure Ni is small. For all devices an inverted Hanle curve is observed too, with a width and saturation field that increase systematically for FM electrodes with larger M_s . The induced $\Delta\mu$ at B^{ext} = 0 is about 27% of the ideal value, but with less variation compared to the data for n-type Si.

In principle one can still fit the Hanle curves with a Lorentzian and extract a time constant (given as labels in the Fig. 3.9). However, it should be treated as an effective time or a lower limit to the spin lifetime in the semiconductor, because interface magnetostatic fields are present and cause artificial broadening of the Hanle curve. Experimentally this situation is easily recognized if an inverted Hanle effect (see next section) is observed. Nevertheless, the lower bound for the spin lifetime in the n-type Si we obtain (285 ps, Ni electrode) is already an improvement by a factor of 2 compared to previously extracted value (Fig. 3.1) with $Ni_{80}Fe_{20}$ electrodes [29], and the true spin lifetime is expected to be larger.

3.6.4 Inverted Hanle effect

The above interpretation is proved by the following phenomenon, hereafter referred to as the inverted Hanle effect. It denotes the increase of the spin polarization in an applied (longitudinal) magnetic field [in analogy with the term Hanle effect, which gives a reduction of the spin polarization in an applied (transverse) magnetic field]. If B^{ext} = 0, the spin accumulation will be reduced by precession in the y and z components of the local magnetostatic fields, which are orthogonal to the injected spins for a ferromagnet with magnetization along x. If now a nonzero B_x^{ext} along x is added and increased, the total magnetic field (vector sum of B^{ms} and B_x^{ext}) rotates into the direction of the magnetization, thus reducing the angle between the injected spins and the axis of precession.

The precession is suppressed, and an increase in the spin accumulation is expected as a function of B_x^{ext}. Indeed, the data in Figs. 3.10 and 3.11 show exactly this inverted Hanle effect for all FM electrodes. The smallest voltage (and hence $\Delta\mu$) is obtained for B_x^{ext}=0, while at large B_x^{ext} the voltage across the contact saturates as spin precession in the local magnetostatic fields is fully eliminated. The saturation occurs at a larger field value for the ferromagnet with larger M_s , consistent with the outlined scenario.We conclude that application of an external in-plane magnetic field

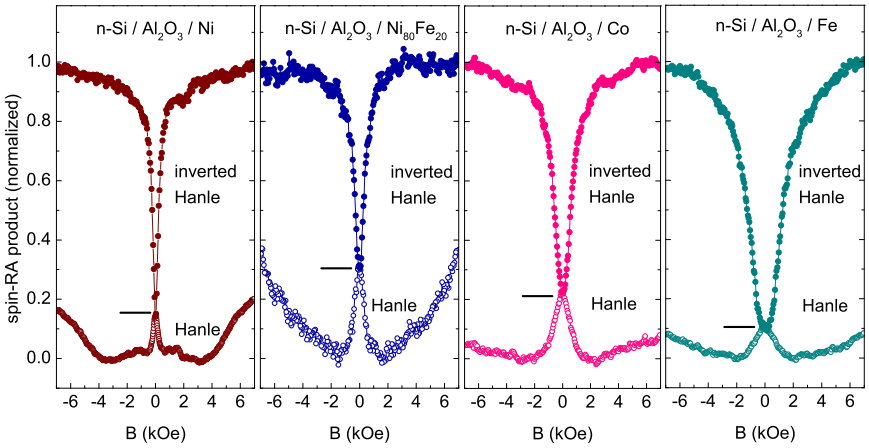

Figure 3.10: **Spin accumulation and precession in n-type silicon near a ferromagnetic interface.** *Room temperature data for n-Si/Al_2O_3/ferromagnet contacts with Ni, $Ni_{80}Fe_{20}$, Co or Fe electrode. The vertical axis gives the product of spin resistance and area (the spin-RA product), defined as $(\Delta V/I)\times$ area. The magnetic field is applied perpendicular to the interface plane (open symbols, Hanle), or parallel to the interface (solid symbols, inverted Hanle), with V_{Si}-V_{FM} = +172 mV (electron injection).*

leads to a recovery of the spin accumulation, reaching the ideal value (that would be obtained without any precession) for large enough B_x^{ext}. The "true" value of the spin accumulation is thus given by the difference between the saturation signal of the inverted Hanle curve (large B_x^{ext}) and the minimum of the signal of the conventional Hanle curve with B^{ext} along z. This difference has been normalized to 1 for all data presented. Importantly, the precession in local magnetostatic fields causes a significant reduction of the spin accumulation, with $\Delta\mu$ at B^{ext} = 0 varying from 10% to 31% of the ideal value.

Note that an inhomogeneous spin accumulation can in principle also arise if the interface magnetization does not point along the global interface plane everywhere, as this would lead to inhomogeneity in the orientation of the spins that are injected. However, the in-plane magnetic coercivity of the magnetic films used here is 5-30 Oe and the films do not have any significant interface anisotropy. Therefore, the ferromagnet is homogeneously and fully magnetized along the external in-plane field well below 100 Oe. Hence, the spin injection is homogeneous and does not change for fields between 100 Oe and several kOe where the signal variation due to the inverted Hanle effect is observed. Even if some slight deviation of the interface magnetization from strictly in plane were present, this cannot account for the strongly reduced

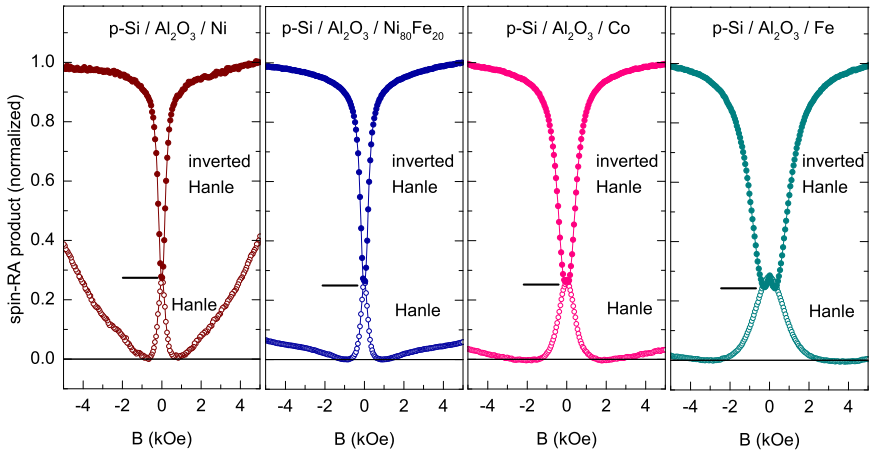

Figure 3.11: **Spin accumulation and precession in p-type silicon near a ferromagnetic interface.** *Room temperature data for p-Si/Al_2O_3/ferromagnet contacts with Ni, $Ni_{80}Fe_{20}$, Co or Fe electrode. The vertical axis gives the product of spin resistance and area (the spin-RA product), defined as $(\Delta V/I)\times$ area. The magnetic field is applied perpendicular to the interface plane (open symbols, Hanle), or parallel to the interface (solid symbols, inverted Hanle), with V_{Si}-V_{FM} = -172 mV (hole injection).*

spin accumulation that is observed. This would require injection of carriers with spin pointing almost along the interface normal. This is not plausible and is inconsistent with the magnetic behavior of magnetic tunnel junctions prepared from the same materials [75].

3.6.5 Hanle effect in local magnetostatic field

The experimental features mentioned above have been described in a model by Dash *et al.* [56]. We will consider here the salient features, more details can be found in ref.[56]. The model starts from the equation [3,44] for spin dynamics of an ensemble of spins in a nonmagnetic host:

$$\frac{\partial S}{\partial t} = S \times \omega_L + D\nabla^2 S - \frac{S}{\tau_s} \tag{3.1}$$

where S is the spin density function and $\omega_L = (\omega_x,\omega_y,\omega_z) = (g\mu_B/\hbar)\,(B_x, B_y, B_z)$. Terms on the right-hand side describe, respectively, spin precession, spin diffusion (D is the spin diffusion constant) and spin relaxation. We seek a solution for a homogeneous B^{ext} plus inhomogeneous magnetostatic fields near the FM interface: B_i =

B_i^{ext} + B_i^{ms}(x,y,z), with i = x,y,z.

In the limit where the spin-diffusion length L_{sd} is small compared to the roughness period λ, the spin-diffusion term in Eq. (3.1) can be neglected. This provides an analytical solution that is strictly correct when electrons are sufficiently localized for gradients in the spin density to be sustained on the length scale of λ. This applies to the case of spin accumulation in localized states (as in the GaAs devices [47]). It is not strictly valid for mobile electrons since spin diffusion tends to average out the inhomogeneity of the spin density (in our Si devices L_{sd} is [29] at least a few 100 nm, while λ is estimated to be 20-60 nm. see previous section). The net result is a more homogeneous spin density, but with a reduced value. Although a rigorous, but cumbersome, numerical treatment including spin diffusion can be done, we can expect that the value of the spin accumulation with spin diffusion is comparable to the spatial average of the inhomogeneous spin density that is calculated without spin diffusion. We therefore average the spin density over the x-y plane, finding that the basic experimental trends of the Si devices are reproduced. Without spin diffusion, the general steady state solution for the x, y, and z components of the spin density is [44]:

$$S_x = S_0 \left\{ \frac{\omega_x^2}{\omega_L^2} + \left(\frac{\omega_y^2 + \omega_z^2}{\omega_L^2} \right) \left(\frac{1}{1 + (\omega_L \tau_s)^2} \right) \right\}, \tag{3.2}$$

$$S_y = S_0 \left\{ \frac{\omega_x \omega_y}{\omega_L^2} - \left(\frac{\omega_x \omega_y}{\omega_L^2} + \omega_z \tau_s \right) \left(\frac{1}{1 + (\omega_L \tau_s)^2} \right) \right\}, \tag{3.3}$$

$$S_z = S_0 \left\{ \frac{\omega_x \omega_z}{\omega_L^2} - \left(\frac{\omega_x \omega_z}{\omega_L^2} - \omega_y \tau_s \right) \left(\frac{1}{1 + (\omega_L \tau_s)^2} \right) \right\}, \tag{3.4}$$

where ω_L^2 = ω_x^2 + ω_y^2 + ω_z^2 and ω_i = ω_i^{ext} + ω_i^{ms}(x,y,z). Importantly, as ω^{ms} is spatially inhomogeneous, the spin density is too. Second, while the injected tunnel electrons have spin along the x axis, for nonzero B^{ms}, the steady state spin density has x, y, and z components and is thus generally noncollinear with the magnetization of the ferromagnetic injector (pointing strictly along x). Third, without external field there is no suppression of the spin polarization if ω_y^{ms} = ω_z^{ms} = 0 (S_x=S_0 and S_y = S_z = 0), whereas S_x <S_0 in the presence of magnetostatic fields with components orthogonal to the injected spins (i.e., when $\omega_y^{ms} \neq 0$ and or $\omega_z^{ms} \neq 0$). Hereafter we shall focus on the S_x component, since in electrical detection using the same ferromagnetic tunnel contact only this component is relevant (the tunnel resistance is proportional to the projection of the spin accumulation onto the detector magnetization).

As described in Dash et al. [56], the magnetostatic field B^{ms} was evaluated considering two-dimensional square array of magnetic dipoles. Alternatively, for one-dimensional roughness and exact expression for B^{ms} in terms of roughness amplitude and M_s has been discussed in ref.[90]. From this and the measured roughness of our structures (sec. 3.6.6), we find that the strength of the magnetostatic fields can easily be in the range of 1 kOe to 100 Oe up to a distance of 10 nm from the interface.

The spin density was calculated using Eq. (3.2) by taking B^{ms} at a distance 5 nm away from a dipole array. For an external magnetic field along z (x) Hanle (inverted Hanle) curve is obtained. The variation of the average spin density as a function of B^{ext} is shown in Fig. 3.12 for two different cases with a dipole strength of 2 (10) T nm^3. By increasing the dipole strength, the Hanle linewidth increases. This qualitatively reproduces the experimental data: (i) the spin density at B^{ext} = 0 is reduced from its maximum, (ii) there is an inverted Hanle effect, (iii) the width of the conventional Hanle curve is broadened as compared to the situation without magnetostatic fields, which would produce a Lorentzian with τ_s = 1 ns (shown in green, with amplitude adjusted for easy comparison), and (iv) for increasing amplitude of B^{ms} (larger dipole moment, bottom panel), the width of the Hanle curve increases, and the inverted Hanle curve and the reduction of the spin density at B^{ext} = 0 become more pronounced. We conclude that, despite the neglect of spin diffusion, the model agrees well with the experimental observations and captures the basic physics.

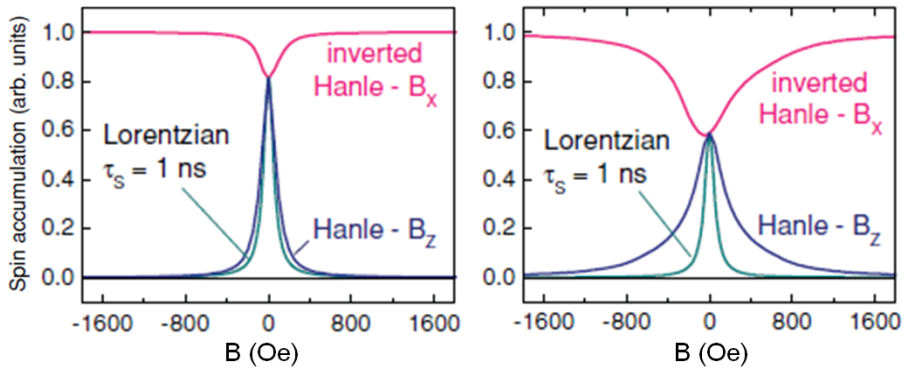

Figure 3.12: **Calculated spin accumulation near an interface with local magnetostatic fields.** *The magnetostatic fields were taken at 5 nm distance from a dipole array with λ = 20 nm. Fig. shows the resulting Hanle (blue) and inverted Hanle (pink) curves for external applied magnetic field along the z or x axis, respectively. The dipole strength is such that $\mu_0\mu/4\pi$ = 2 (left panel) or 10 T nm^3 (right panel). Also shown in green are pure Lorentzian line shapes for the same 1 ns spin lifetime, with the peak amplitude scaled for easy comparison.*

In the description above, the effect of B^{ms} on spin accumulation was calculated

by including B^{ms} only in ω_L of the precession term of Eq. (3.1), without changing τ_s in the last term. That is, we have modeled the phenomenon as being due to changes in the axis and frequency of the (locally) coherent precession of the ensemble spin polarization, modifying the measured time average of the spin density, and leading to artificial broadening of the Hanle curve and thereby an apparent shortening of the spin lifetime. In addition, the spatial inhomogeneity of the magnetostatic fields leads to decoherence and further broadening. Let us now consider whether the inhomogeneous magnetic fields have an effect on τ_s. For localized electrons there is no effect on τ_s. However, mobile electrons near a FM interface moving through a spatially inhomogeneous magnetostatic field experience this as a field fluctuating in time. This is distinct from D'yakonov-Perel' spin relaxation, where the fluctuation is due to changes of the momentum, rather than the location in real space that is relevant here. The associated time scale is given by $\tau^{ms} = \lambda/4v$, where v is the carrier velocity and $\lambda/4$ the length scale over which the field changes significantly. Since electrons with different trajectories acquire a different spin-precession phase and transport is random, this causes irreversible dephasing of the ensemble spin. Considering an electron moving parallel to the interface and typical parameters (λ <100 nm and v=10^5m/s for electrons in Si), τ^{ms} is below 1 ps and thus smaller than the spin-precession period for practical fields ($1/\omega_L \geq$5 ps for B$\leq$1 T). Hence, we are in the regime of motional narrowing[35] and the associated spin-dephasing time is given[35] by T_2^{ms}=$1/\Omega_{av}^2\tau^{ms}$, where B_{av}=$\hbar\Omega_{av}/g\mu_B$ is the average amplitude of the magnetostatic field. We thus have $1/T_2 = 1/T_2^{bulk} + 1/T_2^{ms}$, where T_2^{bulk} is the regular spin-dephasing time in the absence of local magnetostatic fields. For B_{av} $\leq$100 mT and τ_s = 1 ps we obtain T_2^{ms}=3 ns. This is larger than the spin lifetimes we observe, and we therefore described the spin dynamics with a single spin lifetime, including the magnetostatic fields only in the coherent precession term of Eq. (3.1). In other situations, especially when T_2^{bulk} is large, this source of dephasing may be of importance or even become limiting.

3.6.6 Roughness characterization of devices

Since the magnitude of the local magnetostatic field near a ferromagnetic interface depends on the amplitude and lateral period of the roughness, we performed characterization of the roughness using atomic force microscopy (AFM) under ambient conditions for some of the devices (Fig. 3.13). The top panel shows an AFM image of the surface of the Al_2O_3 tunnel barrier on p-type Si, prior to deposition of the metal electrode. The root-mean-square (rms) roughness is about 0.2 nm. An example of a cross-sectional height profile (right) reveals that the peak-to-peak roughness h is about 0.5 nm, while the lateral variation has two different length scales of about 20 and 60 nm, respectively. This roughness is then copied to the bottom surface of the

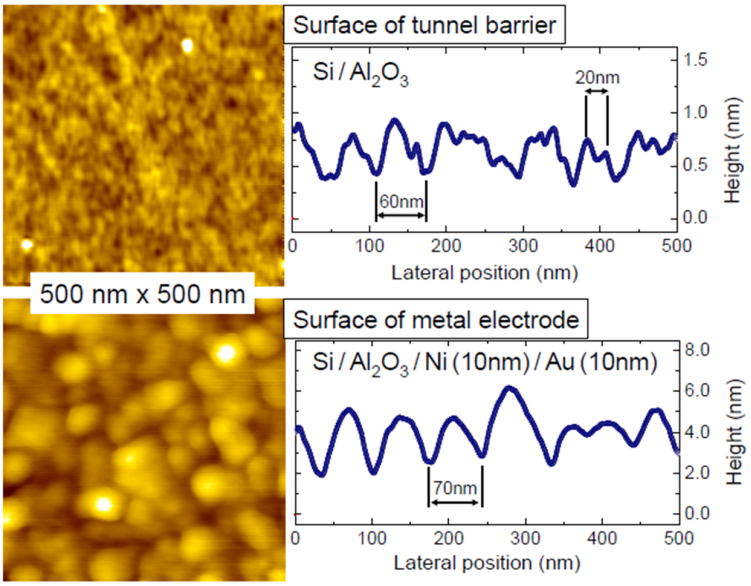

Figure 3.13: **Roughness characterization.** *Top panels: Atomic force image (500×500 nm^2) of the surface of the Al_2O_3 tunnel barrier on p-type Si, prior to metal electrode deposition, and a representative cross-sectional height profile. Bottom panels: the same, but now after deposition of the ferromagnetic metal electrode (Ni, 10 nm) and the Au cap layer (10 nm).*

ferromagnetic metal that is grown on top of the tunnel barrier. The observed roughness can certainly cause local magnetostatic fields in the range of 1 kOe to 100 Oe up to a distance of 10 nm away from the surface of the ferromagnet.

Because magnetostatic fields are long range and the ferromagnet is a thin film (thickness $\sim$10 nm), the local magnetostatic fields that penetrate into the semiconductor are determined not only by the roughness of the bottom interface of the ferromagnet with the Al_2O_3 tunnel barrier, but also by the roughness of the top surface of the ferromagnetic layer. Unfortunately, oxidation of the ferromagnet i.e., surface prevents a good *ex situ* measurement under ambient conditions, and hence no data on this are available. For the sake of completeness we did perform AFM analysis of the top of the complete metal electrode stack, consisting of 10 nm Ni and a 10 nm Au cap layer (bottom panels of Fig. 3.13), although this may not be representative of the roughness of the top surface of the FM. The roughness amplitude is significantly larger (rms roughness of 1.4 nm and a peak-to-peak amplitude of 3-4 nm) compared to the surface of the tunnel barrier, while there is no small-scale (20 nm) lateral roughness.

3.6.7 Spin lifetime in p-type Si

For p-type Si, we reported a τ_s of 270 ps from electrical Hanle measurements [29] on magnetic tunnel contact with $Ni_{80}Fe_{20}$. Such a large value, comparable to that of n-type Si with $Ni_{80}Fe_{20}$ as FM electrode, was unexpected. Part of this may be due to the use of a light dopant element (boron) [29] and the lower density of acceptor impurities in the p-type sample compared to the donor impurity density in the n-type samples. However, while SO interaction is weak in Si, the valence band is directly affected by it and contains states with mixed spin character. Spin relaxation on the time scale of momentum scattering may then be expected due to scattering between light hole and heavy holes states, although explicit calculations for p-type Si are unavailable. Interestingly, hole spin lifetimes of 9 ps and 94 ps were recently determined for heavily doped p-type Si in which spins are electrically injected by spin pumping [91, 92]. In addition, hole spin lifetimes of the order of 35 ps at low T, and around 10 ps at room temperature have been observed in spin-transport devices with heavily doped p-type Ge [32, 93, 94]. What determines τ_s in these p-type semiconductors is currently not understood and further work is necessary to elucidate the physics of holes spin relaxation in electrically spin-transport devices. Electrical injection may create a specific distribution of holes over the respective holes states. Another factor to take into account is that at high doping concentrations, most of the holes are not in the valence band but in a band of delocalized impurity states derived from randomly distributed dopants. For the concentrations used [29], the conduction in the impurity band is metallic in nature and the impurity band has not yet merged with the valence band [95]. Spin relaxation is then governed by impurity band holes, which has so far not been explored theoretically.

3.7 Magnitude of the spin accumulation

The standard theory predicts a spin signal ΔV_{Hanle}/J = $(P_{fm})^2 \rho L_{sd}$, where J is the charge tunnel current density [22, 52, 53]. The expected values are 0.001 to 0.01 k$\Omega\mu m^2$, based on P_{fm} = 30-50 %, L_{sd} = 0.3-1μm, and ρ = 2-20 mΩcm. We observed spin accumulation signals of 2 - 6 k$\Omega\mu$m^2 at 300 K in heavily doped n-type Si with Al_2O_3/$Ni_{80}Fe_{20}$ contacts, and thus several orders of magnitude larger than predicted, as noted [29]. Such large values have later on been reproduced by other research teams using a similar approach (heavily doped Si, three-terminal Hanle measurement, large contact area), but a different tunnel barrier: crystalline MgO in Ref. [31], and SiO_2 in Ref. [33]. The same conclusion applies to devices with somewhat lower doping density ($\sim 10^{18}$cm^3, see Refs. [33, 45]) and for devices on p-type Si [29]. Thus, spin signals several orders of magnitude larger than $(P_{fm})^2 \rho L_{sd}$ are consistently observed, irrespective of the type of tunnel oxide. The discrepancy between

experiment and theory is also observed for Ge [32, 93, 96–99] and with GaAs, for which it was actually first noted [47].

A different behavior was found by Suzuki et al., who observed a spin signal of about 10^{-5}k$\Omega\mu$m^2 in a non-local device [100]. In order to make this consistent with theory, it had to be assumed that P_{fm} is only 1-2 $\%$ for the Fe/MgO contacts used. Since Fe/MgO interfaces are famous [101, 102] for their extraordinary large P_{fm}, it would be reasonable to expect $P_{fm} > 50\%$. The expected signal is then about 10^{-2}k$\Omega\mu$m^2. Thus, in this case the measured signal is several orders of magnitude smaller than expected. It was confirmed that the small signal is not related to the non-local measurement geometry, because 3T and NL measurements on the same device show comparably small signals [73]. In non-local devices with a Ge channel an even smaller P_{fm} of 0.23$\%$ for the Fe/MgO contacts was reported [99].

Whether the failure to describe the magnitude of the spin accumulation in 3T and NL devices has a common origin is unclear. Understanding what controls the magnitude of the spin accumulation has a high priority, because spin injection and detection with a ferromagnetic tunnel contact are cornerstones of silicon spintronics. Although the discussion was sparked by data on 3T devices [47], the issue is not specific for the 3T geometry. It concerns the nature of spin transport across magnetic tunnel contacts on semiconductors, and may therefore play a role in any spin-transport device with tunnel contacts, including non-local devices and spin-LEDs.

3.7.1 Experiment versus theory

The possible causes of the discrepancy between experiment and theory are given below:

(i) Non-tunneling transport (thermionic emission) [103]

(ii) Lateral inhomogeneity of the tunnel current density [29].

(iii) Underestimation of the value of τ_s extracted from Hanle curves [29, 56].

(iv) Two-step tunneling via localised states [47].

The standard theory is based on direct tunneling in the linear regime. One cannot expect it to yield the correct magnitude of the spin accumulation for devices in which the dominant transport mechanism is not tunneling. Thermionic emission yields a completely different conversion of $\Delta\mu$ into a voltage signal [103]. It thus is not surprising that in devices in which transport is rectifying, diode-like and thermally activated, the spin signals do not match with $(P_{fm})^2\rho L_{sd}$. This applies to devices with a doping concentration around 10^{18}cm^3 or below.

In tunnel junctions the lateral current density may become inhomogeneous due to variation in thickness of the tunnel barrier. The real (local) tunnel current density is then significantly larger than the average current density calculated from geometric contact area [29]. The local spin accumulation is then enhanced, potentially by orders of magnitude.

The third factor could be related to the underestimation of the value of τ_s that is extracted from the Hanle curves, which are artificially broadened due to local magnetostatic fringe fields (see section. 3.6.2 and ref. [56]). The real values of τ_s and thus $L_{sd} \propto (\tau_s)^{1/2}$ are then larger than extracted from a Hanle curve, but the effect is far from sufficient to bring the theory and experiment into agreement.

Another possibility for spin signal enhancement was proposed by Tran et al., who considered spin transport via localized states at interface between a semiconductor and a tunnel barrier [47]. Although this can, in principle, enhance the spin signals by orders of magnitude, there are several requirements that need to be fulfilled [49]. Whether or not this plays a role is not at all obvious, and there is so far no experiment that directly proves the presence of a large spin accumulation in interface states. On the contrary, spin signal enhancement by two-step tunneling via interface states has been explicitly ruled out in some of the experiments (see Sec. 3.7.2), notably, those of Dash et al. [29], and systems with only a single tunnel barrier (MgO-based tunnel contacts on p-type Ge without Schottky barrier [32, 93]. Therefore, the exact origin of large spin signal observed in 3T Hanle measurement is still unclear.

3.7.2 Ruling out spin signal enhancement by localized states

Exceptionally large spin signals obtained in 3T measurements have attracted significant attention. We considered whether or not the discrepancy between experiment and standard theory can be explained by spin accumulation in localized interface states, and performed an experiment specifically targeted at testing this scenario [29]. We prepared devices in which the Si surface was treated with Cs prior to tunnel barrier deposition [45]. The Cs interlayer, produces states in the Si bandgap at about 0.1 eV below the bottom of the conduction band [45, 104]. This shifts the charge neutrality level at the Si interface and reduces the Schottky barrier height on n-type Si from 0.7-0.8 eV for the clean devices, to 0.2-0.25 eV for the devices with Cs. The width of the depletion region is also reduced, from $\sim$5 nm to about 3 nm. This reduces the associated value of the Schottky resistance (r_b) by 3 to 4 orders of magnitude. Therefore, if the large spin signals observed in the clean devices would be due to interface states, the spin accumulation in those states should be reduced drastically in the Cs treated devices. In contrast, we found that devices with and without Cs exhibit a comparable spin signal of the order of 2 - 6 k$\Omega\mu$m^2 at room temperature (Fig. 3.1 and Fig. 3.14a). This is not consistent with an interpretation of the large

spin signals in terms of spin accumulation in interface states. Moreover, a Schottky barrier of 0.2 - 0.25 eV has a narrow width due to the high doping level of the Si ($\sim 10^{19}$cm^3), and thus provides an efficient coupling between interface states and bulk bands (negligible r_b). This prevents the build up of a large spin accumulation in interface states.

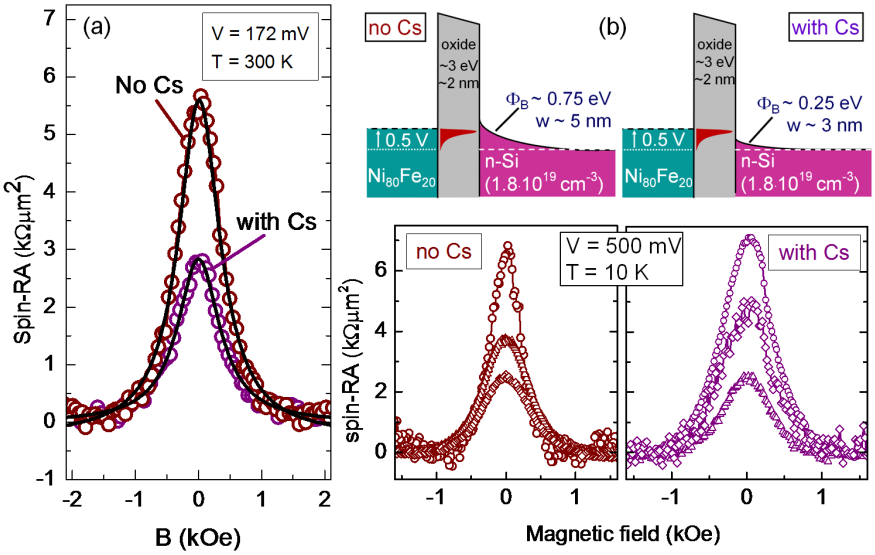

Figure 3.14: **Spin accumulation in n-type Si with the depletion region of Si removed by Cs. (a),** *Hanle-signals at 300 K for junctions without Cs and with Cs, displayed as the spin-RA product. Data are taken with a constant source current of 511 μA and 734 μA for the junction with and, respectively, without Cs, corresponding to about V = +172 mV at B=0. The solid lines are fit to the Lorentzian.* **b,** *Data for three different devices, but at 10 K and +500 mV. Also shown are the corresponding energy band diagrams (drawn to scale) with the values of the Schottky barrier height ϕ_B and depletion width w, and the width and height of the oxide tunnel barrier. The red shaded region indicates the energy distribution of the tunnel current, which is peaked near the Fermi level of the ferromagnet.*

Additional data taken at low temperature and higher injection bias (500 mV) are presented in Fig. 3.14b. Since the energy distribution of the tunnel electrons is peaked near the Fermi level of the ferromagnet, at large bias electrons can easily tunnel through the narrow top of a 0.75 eV barrier (no Cs), and they can go over a 0.25 eV barrier and directly into the semiconductor bulk bands (with Cs). We thus expect a negligible resistance of the Schottky barrier, consistent with the absence of any significant change in device resistance by the Cs (Fig. 3.14). Notably, the spin signal is comparable with and without Cs. Thus, two-step tunneling via interface states does

not explain the large spin signals. A more conclusive experimental evidence which rules out the two-step tunneling mechanism will be discussed in Chapter 5.

3.8 Conclusions

In this chapter, we described the successful implementation of the magnetic tunnel contacts to silicon to electrically create and detect the spin accumulation. We demonstrated the spin injection, detection and their manipulation via the Hanle effect, in both n-type as well as p-type Si at 300 K. From the τ_s of 3T devices and the diffusion constant, a spin-diffusion length in the range of 200 - 300 nm in Si was determined. Such values are comparable to the channel length of transistors in state-of-the-art electronic circuits. The observed spin signals differ by several order of magnitude from the standard theory. We also discussed the possible causes for the discrepancy between experiment and theory. The enhancement of the spin signal due to spin accumulation in localized states was ruled out in an experiment that uses Cs treatment of the silicon surface. Additional control experiments with a non-magnetic layer (Yb or Au) between a FM and tunnel barrier, confirm that the large room-temperature spin signal is genuine and originates from spin-polarized tunneling and spin accumulation in the Si.

The effective spin lifetime extracted from the Hanle curve is found to be smaller than obtained from electron spin resonance measurements. This indicates that spin lifetime is reduced by the extrinsic factors that are related to the tunnel contacts. We discussed that the process of spin tunneling into Si is sensitive to the interface roughness. The interface roughness gives rise to magnetostatic fields B^{ms}, whose magnitude depend upon the amplitude and period of the roughness. Due to these magnetostatic fields, the injected spins precess even in the absence of an external field. This produces an artificial broadening of the Hanle curve, that depends on the direction and the magnitude of B^{ms}, which in turn is proportional to the magnetization of the FM. As a result the width of the Hanle curve depends on the ferromagnet used, i.e., the width increases from Ni, to $Ni_{80}Fe_{20}$, to Co, to Fe as a FM electrode. An inverted Hanle effect is introduced as an experimental signature. It denotes the increase of spin accumulation in an applied (in-plane) magnetic field.

In conclusion, we successfully demonstrated the spin injection, detection and manipulation via Hanle effect using magnetic tunnel contacts to Si with amorphous Al_2O_3 as a tunnel barrier. In the next chapter, we will investigate the use of crystalline MgO instead of amorphous Al_2O_3 as a tunnel barrier.

Chapter 4

Spin polarization in Si using crystalline MgO/Fe tunnel contacts

In the previous chapter, the successful creation of spin polarization in silicon using Si/Al_2O_3/ferromagnet tunnel devices was shown. In this chapter, we examine whether crystalline MgO/Fe tunnel contacts are suitable for creating spin polarization in Si at room temperature. For this purpose, we investigate the Hanle and inverted Hanle effects in Si/MgO/Fe tunnel devices. We discuss the effect of the substrate preparation and growth conditions on the relative amplitude of the Hanle and inverted Hanle signals.

4.1 Introduction

As described in the previous chapter, we have developed spin-tunnel contacts to Si which contain amorphous Al_2O_3 as a tunnel barrier and a polycrystalline ferromagnetic electrode. Another materials of choice as a tunnel barrier could be SiO_2 or MgO. The SiO_2, due to its superior interface with Si, has been used as a gate oxide in semiconductor devices and successfully employed in magnetic tunnel junctions[68]. On the other hand, crystalline MgO, due to its spin filtering properties has been successfully implemented in metal-based spintronics devices.

Extensive theoretical work has predicted very high tunneling magnetoresistance

Part of this chapter has previously been published in
A. Spiesser, S. Sharma, H. Saito, R. Jansen, S. Yuasa and K. Ando, Proc. SPIE **8461**, 84610K (2012).

on crystalline Fe/MgO/Fe magnetic tunnel junctions (MTJs)[105–107]. The single-crystalline MgO barrier acts as a spin filter and allows tunneling of the states with well defined symmetry. This in turns give rise to a very high tunnel spin polarization. This is consistent with the experimentally observed high tunneling magneto resistance on epitaxial Fe/MgO/Fe magnetic tunnel junctions and very large ($\approx 85\%$) tunnel spin polarization for the tunneling current[101, 102]. Therefore, the use of crystalline MgO in metal-based spintronics device is well established. Similarly, one can expect crystalline MgO to acts as an effective spin filter in magnetic tunnel contacts to silicon. Here, we will examine the use of crystalline MgO/Fe tunnel contacts on Si as an efficient spin filter.

There has been a significant progress in making high quality crystalline tunnel contacts on Ge[94, 96, 108] and GaAs[109] with epitaxial growth of MgO/FM layers. These tunnel devices have been successfully used for creating and detecting the spin accumulation in a semiconductor. However, the development of the methods of crystalline growth of MgO/ferromagnet tunnel contacts on Si is very recent and further investigations are required. By using highly ordered CoFe/MgO tunnel contacts on n-type Si, Jeon et.al., obtained spin signals (2-3 $k\Omega\mu m^2$), which are comparable to that of a NiFe/Al_2O_3/n-Si tunnel devices[29]. It should be noted that for that latter case the tunnel barrier and ferromagnet are amorphous and poly-crystalline, respectivly. Suzuki et.al., on the other hand, contrary to the expectations reported a very small value of tunnel spin polarization (less than 2%) at room temperature for n-Si/MgO/Fe spin-tunnel devices[100]. Thus, it is important to investigate the relationship between crystal quality of the spin tunnel contacts to silicon and parameters like spin lifetime, spin diffusion length and amplitude of the spin accumulation.

In this chapter, we will investigate the influence of the substrate preparation on the quality of the tunnel contacts and efficiency of spin injection into silicon through highly ordered magnetic tunnel contacts. In Sec. 4.2, we describe the fabrication and structural characterization of the spin-tunnel contacts. Here, we discuss the influence of the starting Si surface on the growth of the MgO/Fe tunnel contact. In Sec. 4.3, we will describe the three terminal Hanle measurements at room temperature on magnetic tunnel contacts to n-type as well as p-type silicon. Our discussion will be focused on the amplitude of the spin signals obtained in crystalline Si/MgO/Fe tunnel devices. This section will include the basic results on electrically induced spin polarization into Si. A more detailed analysis of spin-resistance area product (spin-RA) and effective spin lifetime shall be presented in chapter 5.

4.2 Device fabrication and structural characterization

Fig. 4.1 depicts the cross-sectional diagram of a Si/MgO/Fe tunnel device. These devices were fabricated on n-type as well as on p-type silicon-on-insulator (SOI) wafers with (100) orientation. The carrier density measured at 300 K was found to be $1.8\times10^{19}\text{cm}^{-3}$ (As doped) and $4.8\times10^{18}\text{cm}^{-3}$ (B doped) for n-type and p-type Si, respectively. Initially, 300 nm of SiO_2 was grown at 1150°C on the SOI wafers. The oxide was then patterned using standard optical lithography followed by wet etching with buffered HF solution to define the contact holes of different area through SiO_2. Two devices with etching time 10 min (sample 1) and 5 min 30 sec (sample 2) were prepared to observe the influence of the starting Si surface on the quality of the tunnel interfaces and their impact on electrical parameters. It should be noted that etching of 300 nm of SiO_2 requires 5 min and 30 sec, which we call as optimum etching time. The over-etching after optimized etch time results in a rough Si surface. After etching, the silicon substrates were introduced into the MBE system with a base pressure better than 5×10^{-10} Torr. Then the silicon substrates were annealed at 700°C for 10 min. After annealing, MgO (0.7 nm to 3 nm) and Fe layers (10 nm) were deposited by electron-beam-evaporation at 300°C and 100°C, respectively. To avoid the oxidation of the magnetic layer, a 20 nm thick Au capping layer was deposited by using a conventional Knudsen-cell. Subsequently, the ferromagnetic electrode was patterned using Ar-ion-milling. This was followed by another lithography step and sputter deposition of Cr/Au contact metallization.

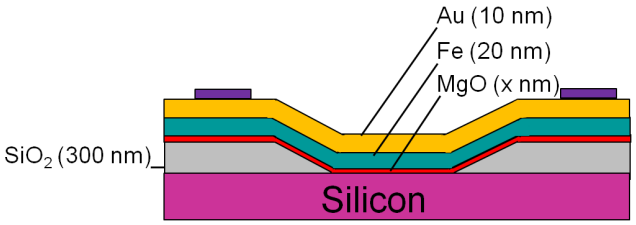

Figure 4.1: *Cross sectional diagram of a Fe/MgO/Silicon tunnel contact. The active area on Silicon is defined by wet etching of 300 nm thick SiO_2.*

Structural analysis was performed by in-situ reflection high-energy electron diffraction (RHEED). Fig. 4.2 (a) shows the RHEED patteren of the Si surface after annealing at 700°C for 10 min. A Si surface with a well-defined (2×1) reconstructions is obtained [110]. The RHEED image of MgO (Fig. 4.2 (b)) grown on Si at 300°C shows a spotty crystalline pattern corresponding to MgO(001). Finally, Fe deposition

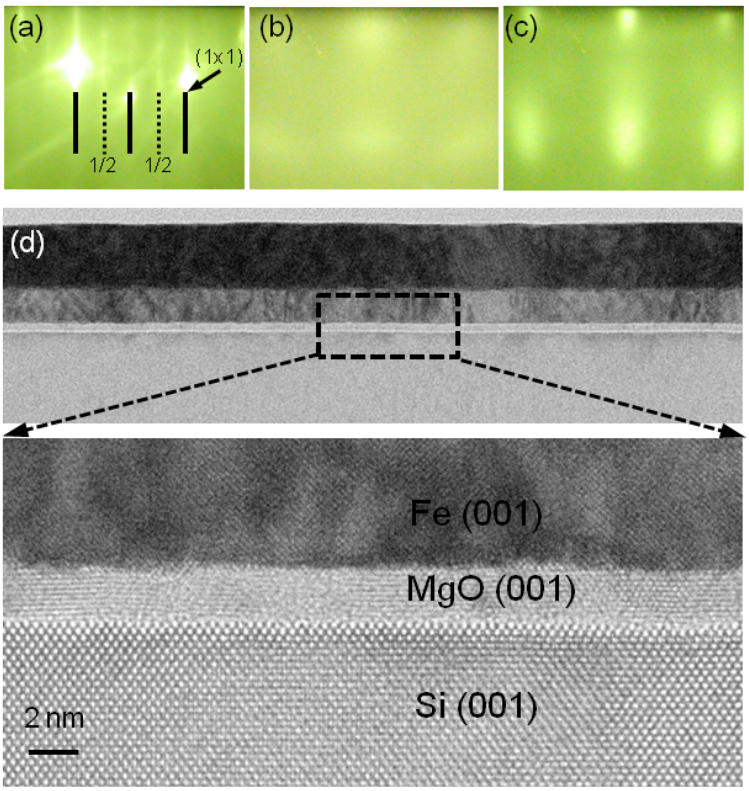

Figure 4.2: **Structural characterization of Fe/MgO/Si tunnel devices.** *In-situ RHEED patterens of* **(a)** *Si(001) surface after annealing at 700° C for 10 min,* **(b)** *after MgO deposition at 300° C* **(c)** *after Fe deposition at 100° C. The (1×1) and (2×1) patterns are indicated in* **(a)** *with solid and dotted black lines, respectively.* **(d)** *High-resolution TEM image of the sample for which the Si surface was prepared by etching of SiO_2 for optimized time of 5 min and 30 sec.*

on MgO results in a clear spotty (1×1) pattern without any rings in the RHEED image (Fig. 4.2 (c)) indicating crystalline Fe (001). For further analysis, we performed high-resolution transmission electron microscopy (HRTEM) analysis of the sample. Sharp interfaces without inter-diffusion and/or intermixing between Si, MgO and Fe are obtained. An atomically flat interface (roughness $\approx$ 2 monolayers) between Si and MgO with clear atomic planes in the MgO layer indicates an ordered crystalline tunnel barrier. More detailed analysis about crystallographic relationship has been presented in Ref. [110] where we showed that MgO(001) grows on Si(001) with a cube-on-cube relationship with top Fe cell rotated in the plane by 45° w.r.t the MgO and Si cells. We also showed that the crystal quality of the Fe/MgO layers

is quite sensitive to the surface condition of the Si substrate before deposition. We found that the Si surface with reconstructions (2×1) is essential for achieving epitaxial MgO(001) on Si, whereas MgO grown on (1×1) Si surface shows polycrystalline structure. Clear Hanle and inverted Hanle effects were observed at room temperature for polycrystalline as well as epitaxial Fe/MgO spin tunnel contacts by using standard three-terminal method. Thus demonstrating the electrically induced spin polarization in p-type silicon at 300 K. The device with epitaxial Fe/MgO contact exhibits longer spin lifetime and higher magnitude of the spin accumulation. We attributed the enhancement in the spin signal to the spin filtering effect of the epitaxial MgO(001), giving rise to higher tunnel spin polarization of the tunnel contact. Thus, we found that high quality MgO barrier is desireable to achieve efficient spin injection into Si.

4.3 Electrical spin injection and detection

We use the three-terminal geometry (Sec. 2.4) for performing electrical spin injection and detection across Si/MgO/Fe tunnel devices via Hanle effect. The tunnel contacts have dimensions of 100×200 μm^2 (p-type Si) and 50×200 μm^2 (n-type Si). The tunnel contacts are separated by a distance of 150 μm, which is much larger than the spin-diffusion length L_{sd} of spins in Si. Thus, we measure the spin accumulation directly underneath the tunnel contact and there is no spin signal due to transport between the tunnel contacts. Let us start with tunnel contacts on p-type Si.

4.3.1 Fe/MgO/Si spin-tunnel contact to p-type Si

Fig. 4.3(a) displays the Hanle measurements on p-Si/MgO/Fe tunnel device. The bias convention is the same as explained in Chapter 3, i.e., V = V_{Si}-$V_{FM} < 0$ corresponds to hole spin injection into valence band of Si. For a bias current of -97μA (-172 mV, lower curve in Fig. 4.3(a)), we obtain a maximum signal at zero field. With increase in transverse field, the measured voltage reduces and the line shape is Lorentzian . A similar signal (with opposite polarity) is obtained for a bias current of 389 μA (≈174 mV, upper curve) at 300 K. Thus, these measurements clearly establish the creation of spin polarization in Si using crystalline MgO/Fe magnetic tunnel contact. By taking g = 2, we extracted the effective spin lifetime τ_s = 190 ps for holes in Si. This is higher than the value (60 ps) found for p-Si/Al_2O_3/Fe tunnel contacts (see Sec. 3.6.3), but smaller than the 270 ps found for p-Si/Al_2O_3/$Ni_{80}Fe_{20}$ tunnel devices (Sec. 3.6.7 and Ref. [29]).

Fig. 4.3(b) shows the variation of spin-resistance area (spin-RA) product with voltage for the same tunnel contact. Here, the spin-resistance $\Delta R_{spin} = [\Delta V_{B_{\phi=0^\circ}} + \Delta V_{B_{\phi=90^\circ}}]/I$, where $\Delta V_{B_{\phi=0^\circ}}$ and $\Delta V_{B_{\phi=90^\circ}}$ are the Hanle and inverted Hanle signal

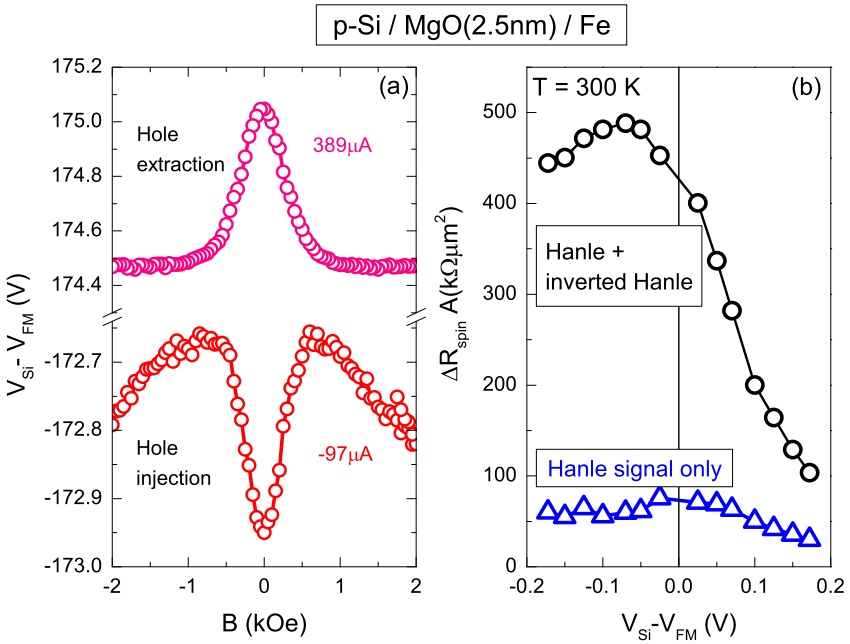

Figure 4.3: **Electrical injection and detection of spin accumulation in p-type Si at 300 K. (a)** *Detected Hanle signal across a p-Si/MgO/Fe(20nm) tunnel contact for hole injection (-97μA) and extraction (389μA) at T = 300 K, as a function of magnetic field perpendicular to the interface.* **(b)** *Spin-resistance* ΔR_{spin}=$[\Delta V_{B_{\phi=0^\circ}} + \Delta V_{B_{\phi=90^\circ}}]/I$, *where* $\Delta V_{B_{\phi=0^\circ}}$ *and* $\Delta V_{B_{\phi=90^\circ}}$ *are the Hanle and inverted Hanle signal amplitude, respectively, as defined in Chapter 3. From a Lorentzian fit to the data the effective spin lifetime* τ_s*=190 ps is obtained.*

amplitude as defined in Chapter 3. Here, the subscripts $B_{\phi=0^\circ}$ and $B_{\phi=90^\circ}$ signify the field direction perpendicular and parallel to the interface, respectively. Further, I is the constant bias current across the tunnel contact and A is the contact area. The lower curve represents the spin-RA corresponding to Hanle signal. The corresponding spin-RA ranges from 25-70 k$\Omega\mu$m^2, several orders of magnitude higher than expected from theory as noted earlier (see Ref.[29], Sec. 3.3.2 and Chapter 5). The Spin-resistance is almost constant for V < 0 and it decays linearly for V > 0. The upper curve in Fig. 4.3(b) represents the total spin-RA which includes the inverted Hanle signal. We observe that spin-RA reduces significantly for V > 0, while for V < 0 the change is less. Thus we see that magnetic tunnel contacts to Si with crystalline MgO/Fe can be employed successfully for creating spin polarization in Si at room temperature.

4.3.2 Influence of surface preparation

Here, we compare two devices fabricated under different surface processing conditions which result in a different starting Si surface onto which the MgO/Fe contact is grown.

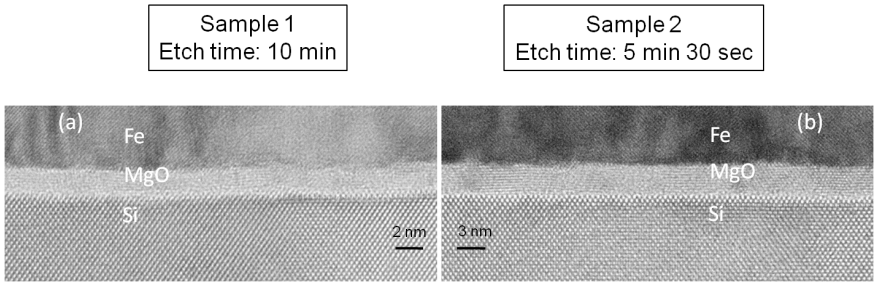

Figure 4.4: **Influence of over etching on tunnel interfaces**. **(a)** *TEM image of sample 1 (etching time 10 min) and* **(b)** *sample 2 (etching time 5 min 30 sec).*

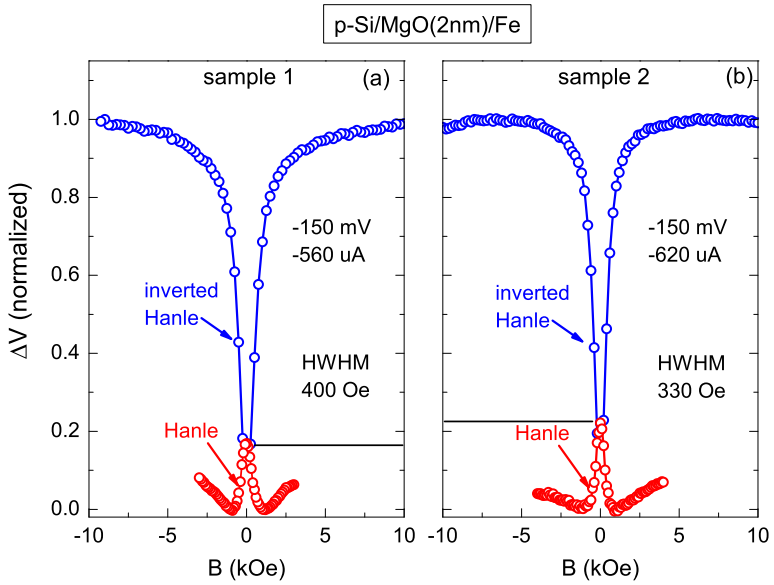

Figure 4.5: **Comparing relative amplitudes of Hanle and inverted Hanle signals**. *Electric Hanle and inverted Hanle measurements on* **(c)** *sample 1 (-150 mV, -560 μA) and* **(c)** *sample 2 (-150 mV, -620 μA).*

One of the device (sample 1, Fig. 4.4(a)) was prepared using an etching time of 10 min compared to sample 2 with an etch time of 5 min 30 sec (Fig. 4.4(b)) required for etching 300 nm of thermaly grown SiO_2. The tunnel barrier (MgO) thickness for these two samples was kept similar (2 nm) so that similar tunnel resistance can be obtained (as confirmed experimentally, see Fig. 4.6). It is clear from the TEM picture in Fig. 4.4 (a) that over etching results in a more rough interface between Si and MgO. For sample 2, (Fig. 4.4(b)) with an optimized etch time, a relatively smooth interface is obtained.

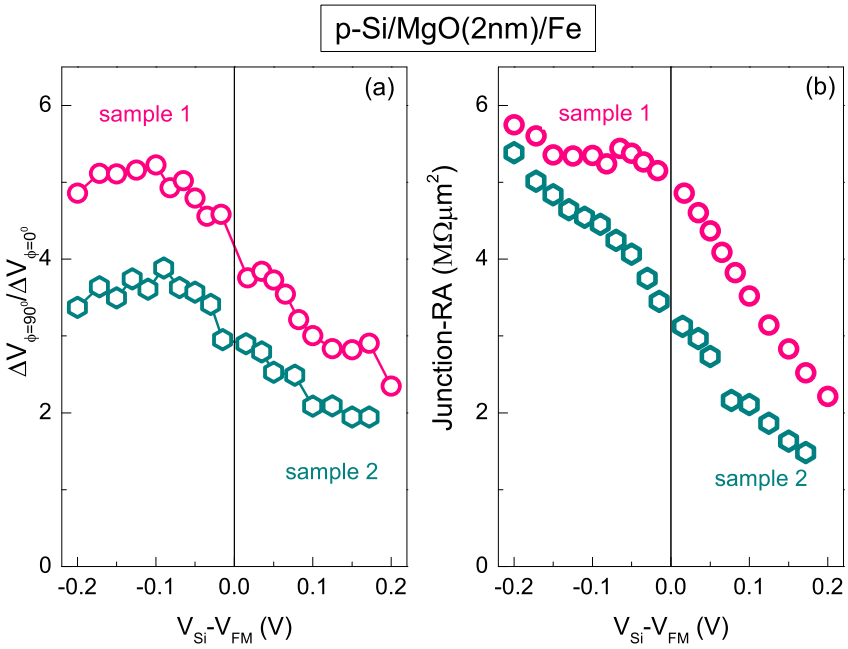

Figure 4.6: *Bias variation* **(a)** *of relative ratio of inverted Hanle and Hanle signal i.e.,* $\Delta V_{B_{\phi=90^\circ}}/\Delta V_{B_{\phi=0^\circ}}$ *for sample 1 and 2, where* $\Delta V_{B_{\phi=0^\circ}}$ *and* $\Delta V_{B_{\phi=90^\circ}}$ *are the Hanle and inverted Hanle signal amplitude as defined in Chapter 3. Here, the subscripts* $B_{\phi=0^\circ}$ *and* $B_{\phi=90^\circ}$ *signify the field direction perpendicular and parallel to the interface, respectively.* **(b)** *Bias voltage versus junction-RA product for the same devices with different growth conditions.*

Figs. 4.5 (a) and (b) display Hanle and inverted Hanle curves measured at a bias current of -560 μA (sample 1) and -620 μA (sample 2), corresponding to a voltage of about -150 mV. For both devices, a Lorentzian line shape due to Hanle spin precession is obtained. For an in-plane magnetic field, we obtain an inverted Hanle effect (see Chapter 3). Here, we show the normalized data for comparing the relative amplitude of Hanle and inverted Hanle signal. It is observed that sample 2 with a rel-

atively smooth interface has a larger Hanle signal compared to sample 1. Although the difference is not so large. Due to the larger interface roughness for sample 1, the stray magnetostatic fields [56] cause larger reduction of the spin accumulation as compared to sample 2, which has a relatively smooth interface. As a result sample 1 has a bit larger inverted Hanle signal compared to sample 2.

This becomes more clear in Fig. 4.6(a), where the bias variation of the ratio between inverted Hanle and Hanle signals ($\Delta V_{B_{\phi=90^\circ}}/\Delta V_{B_{\phi=0^\circ}}$) for samples 1 and 2 is shown. Both devices have same order of junction resistance area (Junction-RA) product (Fig. 4.6(b)). In Fig. 4.6(a), for V $<$ 0 the spin signal for sample 1 is dominated by a strong inverted Hanle signal. Whereas for V $>$ 0, the ratio between inverted Hanle and Hanle signal is still large but it reduces. For sample 2, a similar qualitative behavior is found but the ratio $\Delta V_{B_{\phi=90^\circ}}/\Delta V_{B_{\phi=0^\circ}}$ is lower compared to sample 1 for all bias voltages. This indicates that in sample 1 due to larger interface roughness, the net spin signal has a large contribution due to inverted Hanle signal compared to sample 2 with relatively smooth interface. Further, from the Lorentzian fit to the data, the line width is larger (400 Oe) for sample 1 compared to sample 2 (330 Oe). These results suggest that interface roughness give rise to larger inverted Hanle signal as well as Hanle line width broadening, as reported earlier for Al_2O_3 based devices [56].

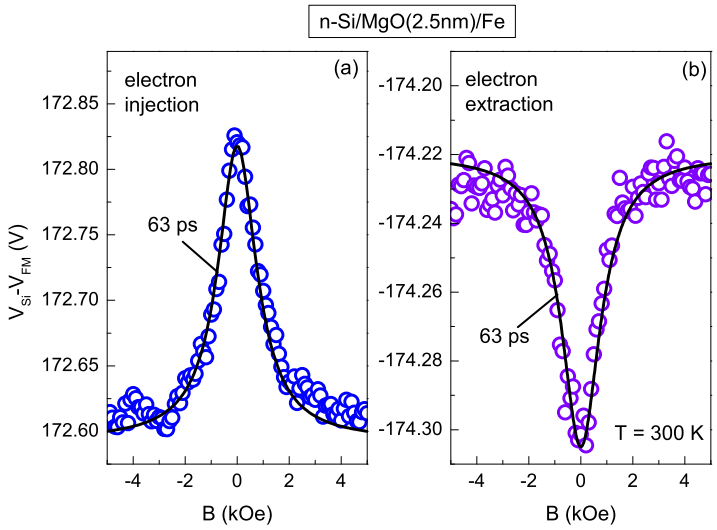

Figure 4.7: **Electrical injection and detection of spin accumulation in n-type Si at 300 K.** **(a)** *Detected Hanle signal across an n-Si/MgO/Fe(20nm) tunnel contact for electron injection (460μA) and* **(b)** *extraction (-405μA) at T = 300 K, as a function of magnetic field perpendicular to the interface. Solid black lines represent the Lorentzian fits with τ_s = 63 ps.*

4.3.3 Fe/MgO/Si spin-tunnel contact to n-type Si

Now, let us consider three terminal Hanle measurements on tunnel contacts to n-Si with MgO/Fe layers. As shown in Fig. 4.7(a), we observe a Hanle signal for a bias current of 460 μA (172 mV) corresponding to electron spin injection into conduction band of silicon. A Similar Hanle signal (but of opposite polarity) is obtained for electron spin extraction from Si conduction band at a current of -405 μA (-174 mV). A lower bound of 63 ps for the spin lifetime is obtained from a Lorentzian fit to the data. Thus, the observation of Hanle effect (for injection as well as extraction of spins) establish successful creation of spin polarization in bulk bands of n-type Si with MgO/Fe contacts and again prove that magnetic tunnel contacts to Si serve as robust system to study the spin transport.

4.4 Conclusions

In this chapter, Si/MgO/Fe tunnel contacts were investigated for realizing spin polarization in Si at 300 K. From the structural characterization (RHEED and HR-TEM) we found that highly ordered crystalline tunnel contacts can be obtained on Si with optimum etching conditions of SiO_2 which give rise to a smoother interface between Si and MgO and subsequent annealing of Si surface to obtain a (2×1) reconstructed Si (001) surface. Subsequent deposition of MgO and Fe at 300°C and 100°C, respectively, results in crystalline tunnel contacts and successful spin injection was observed into n-type as well as p-type Si at 300 K.

We also evaluated the influence of the starting Si surface on spin injection into Si. The properties of Si surface were changed by varying the etching time of SiO_2. The tunnel contacts with over-etching display a more rough Si/MgO interface. Electrical measurements reveal that for both devices, the inverted Hanle signal is larger compared to the Hanle signal. However, for the device with more rough interface, the inverted Hanle signal is larger compared to other with relatively smooth interface. Thus, we conclude that the magnetostatic fields arising from the rough interface (due to over etching) produce stronger inverted Hanle signal and a broadening of the Hanle curve.

Chapter 5

Scaling of spin accumulation with tunnel resistance

In previous chapters, we described the creation and detection of the spin polarization in Si via the Hanle effect. We investigated the magnetic tunnel contacts to Si with different tunnel barriers and ferromagnets. A common feature shown by these devices is the exceptionally large spin signal, orders of magnitude larger than predicted by the standard theory of spin injection and diffusion. Here, in this chapter, we investigate the variation of spin-signal obtained in a Hanle measurement with the thickness of the tunnel barrier (Al_2O_3 and crystalline MgO). We compare the experimental data with the available theoretical models which consider the direct tunneling, two-step tunneling and direct as well as two-step tunneling in parallel. To rule out spin signal enhancement by two-step tunneling via localized interface states, we present measurements on control devices in which the semiconductor is replaced by a non-magnetic metal (Ru) electrode.

5.1 Introduction

Mainstream semiconductors such as silicon and germanium play a key role in the development of a spintronics information technology in which spin is used to represent digital data [14, 50, 51, 111]. To create and detect spin-polarized carriers in non-magnetic materials, the use of ferromagnetic tunnel contacts has proven to be a

The content of this chapter has appeared at
S. Sharma, A. Spiesser, S. P. Dash, S. Iba, S. Watanabe, B.J. van Wees, H. Saito, S. Yuasa and R. Jansen, http://arxiv.org/abs/1211.4460

robust and technologically viable approach that is widely used in spin-based devices, including those with Si and Ge [26, 28, 29, 31, 32, 70, 79, 94, 97, 98, 100, 112, 113]. As recently reviewed [50, 51], controversy has arisen because in many semiconductor spintronic devices, the magnitude of the observed spin voltage differs by several orders of magnitude from what is expected based on the available theory for spin injection and diffusion [22, 53, 114, 115]. A common feature of all theories is that the injected spin current produces a spin accumulation $\Delta\mu$, i.e., a spin splitting in the electrochemical potential and thus a spin-dependent occupation of the electronic states in the non-magnetic material. Conservation of spin-angular momentum requires the injected spin current to be balanced by spin relaxation, from which the steady-state non-equilibrium spin accumulation is evaluated. Consequently, the spin accumulation is predicted to be proportional to the injected spin current.

A powerful way to test the predictions is to vary the thickness of the tunnel barrier, which changes the current density J exponentially. The spin accumulation is expected to exhibit a similar exponential variation, so that $\Delta\mu/J$ remains constant. Here we present an extensive set of spin-transport data on Si and Ge based magnetic tunnel devices with different tunnel oxides. The scaling of the detected spin voltage with tunnel oxide thickness violates the expected proportionality of spin voltage and injected spin current. The data is shown to be incompatible with any of the known theories, including those based on direct tunneling [22, 53, 114, 115] or two-step tunneling via localized states [47, 49].

5.2 Device fabrication

The device fabrication is similar to as described in chapter 3 and chapter 4 for Si/Al_2O_3 /FM and Si/MgO/Fe tunnel devices, respectively. In this chapter, we will show only the experimental results obtained on these devices.

To probe the spin accumulation over a large range of the tunnel barrier thickness, we employ three-terminal devices [29] in which a single ferromagnetic tunnel contact is used to inject the spin accumulation, and to detect it. This geometry, unlike 4-terminal non-local devices [28, 100], allows the contact area to be chosen arbitrarily large so as to adjust the overall device resistance and thereby ensure a sufficient signal to noise ratio. Here, the tunnel junction area is between 10×10 μm^2 and 100×200 μm^2. Positive voltage corresponds to electrons tunneling from ferromagnet to semiconductor.

5.3 Scaling with tunnel barrier thickness

To illustrate the generic nature of the observed scaling, we use devices with heavily doped Si (p-type and n-type), with an amorphous Al_2O_3 tunnel barrier and $Ni_{80}Fe_{20}$ ferromagnet, or with epitaxial, crystalline MgO/Fe contacts.

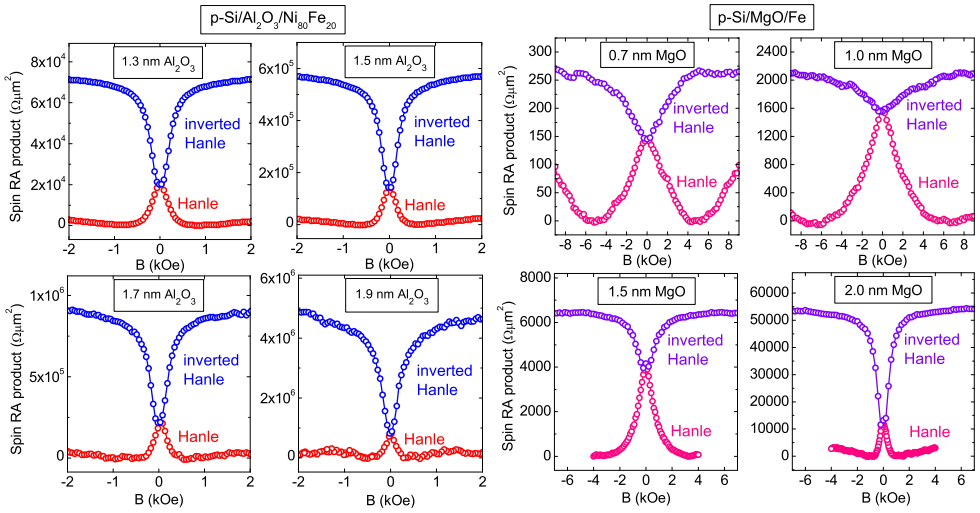

Figure 5.1: **Hanle detection of spin accumulation in semiconductor/oxide/ferromagnet tunnel devices.** *Shown are representative Hanle and inverted Hanle curves for magnetic field B applied, respectively, perpendicular or parallel to the magnetization of the ferromagnet. Data is shown for p-type Si/Al_2O_3/$Ni_{80}Fe_{20}$ and p-type Si/MgO/Fe devices with different thickness of the tunnel barrier, all at 300 K. The vertical axis gives the spin-RA product, defined as $\Delta V_{Hanle}/J$.*

In all devices, voltage signals corresponding to the Hanle and inverted Hanle effect [56] were detected when a magnetic field is applied perpendicular or parallel to the tunnel interface, respectively, at constant tunnel current (Fig. 5.1). The Hanle (inverted Hanle) signal originates from the suppression (recovery) of the spin accumulation due to spin precession (or the reduction thereof), and is the signature of the presence of a spin accumulation [29, 56]. The most striking observation is that the amplitude of the spin signal (the spin RA product, defined as $\Delta V_{Hanle}/J$, the spin voltage signal per unit of J) increases by orders of magnitude when the thickness of the tunnel barrier is increased. The width of the Hanle curve and the ratio of the Hanle and inverted Hanle amplitudes are also not constant.

The tunnel resistance exhibits the expected exponential variation with thickness of the tunnel oxide (Fig. 5.2a). From the slope we extract an effective tunnel bar-

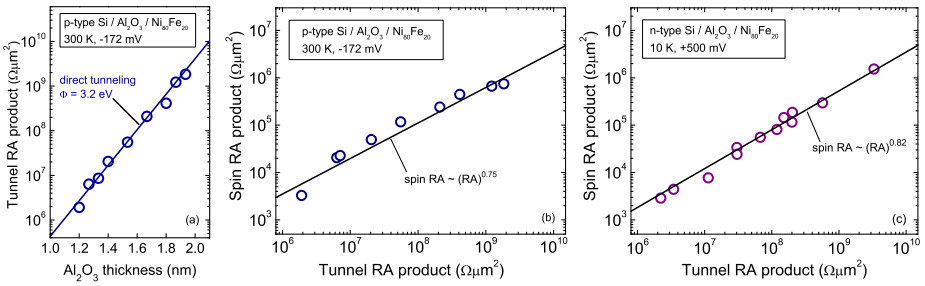

Figure 5.2: **Scaling of Hanle spin signals in Si tunnel devices with amorphous Al_2O_3 barrier.** **a,** *tunnel resistance-area (RA) product versus tunnel oxide thickness for p-type Si/Al_2O_3/$Ni_{80}Fe_{20}$ devices at 300 K. The extracted tunnel barrier height is 3.2 eV.* **b**, *the corresponding spin RA product versus tunnel RA product. The solid line corresponds to a power law with exponent 0.75.* **c**, *data for similar devices but with n-type Si at 10 K. The solid line corresponds to a power law with exponent 0.82. The spin RA value is derived from the Hanle signal only, instead of the sum of the Hanle and inverted Hanle signals. See Fig. 5.7 for additional data with different oxidation time (p-type) and Cs treated surfaces (n-type).*

rier height Φ_{eff} of 0.8 eV. Taking into account the effective electron mass in Al_2O_3 (about 0.2 - 0.3 times the free electron mass), this translates into a real barrier height of $\Phi = 3.2 \pm 0.8$ eV. This is a reasonable value [116] for Al_2O_3 on p-type Si, showing that direct tunneling from the ferromagnet into the Si is the dominant transport process (for multi-step tunneling via localized states within the oxide [117], the extracted barrier height would be 4 times larger, which is unrealistic). More importantly, the data implies that the contact resistance is dominated by the Al_2O_3, and that the depletion region associated with the Schottky barrier in the Si contributes little to the resistance, as expected for heavily doped Si. The spin RA product also displays an exponential variation with thickness of the tunnel oxide, and a power law is revealed when the spin RA product is plotted against tunnel resistance (Figs. 5.2b and c). The associated scaling exponent is about 0.75 and 0.82, respectively, for Si/Al_2O_3/$Ni_{80}Fe_{20}$ devices with p-type and n-type Si. For devices with crystalline MgO/Fe contacts, a similar exponential variation of spin RA product with MgO thickness is obtained (Fig. 5.3a). The contact resistance is dominated by tunneling through the MgO at larger thickness, but for small MgO thickness a transition occurs to the regime where the contact resistance is limited by the Schottky barrier and becomes constant. Interestingly, the spin RA product displays no transition. It scales with the MgO thickness even in the low thickness regime, suggesting that the spin signal is determined by the tunneling across the MgO. The spin RA products for p-type Si with MgO/Fe and Al_2O_3/$Ni_{80}Fe_{20}$ contacts display similar scaling as a

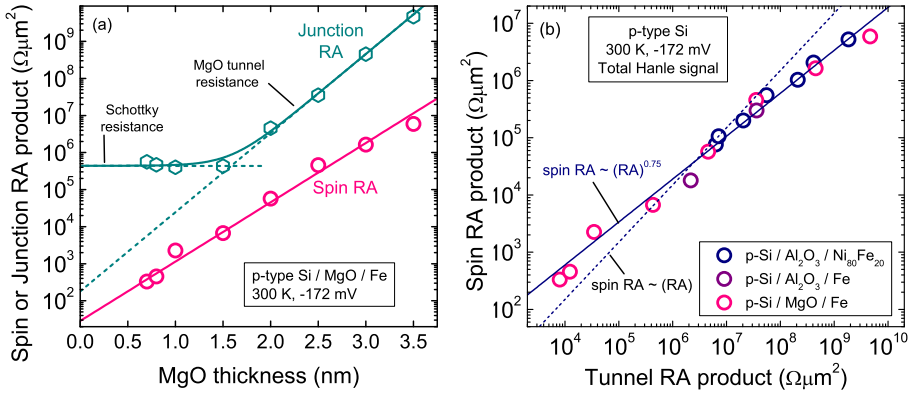

Figure 5.3: **Scaling of Hanle spin signals for devices with MgO and p-type Si or Ge. a,** *spin RA product and tunnel RA product versus MgO thickness for p-type Si/MgO/Fe devices at 300 K.* **b**, *corresponding spin RA product versus tunnel RA product for the same devices (pink symbols), together with data for p-type Si/Al_2O_3/$Ni_{80}Fe_{20}$ (blue symbols). For the 3 devices with the thinnest MgO barrier, the tunnel RA product is determined by extrapolation from the high thickness regime (dashed green line in a) to remove the Schottky resistance. The solid line corresponds to a power law with exponent 0.75. The spin RA product is the sum of the Hanle and inverted Hanle signal.*

function of resistance of the tunnel oxide (Fig. 5.3b), with an exponent (0.75) smaller than 1. Note that a similar scaling was recently reported by Uemura *et al.* for n-type Si/MgO/$Co_{50}Fe_{50}$ devices [118] , although a direct comparison cannot be made because their data was taken with the same bias current for each oxide thickness, and hence with a different tunnel voltage. This, in turn, changes the tunnel spin polarization, which is known to vary with the energy of the tunnel electrons [76, 78]. This additional source of variation of the spin signal with tunnel oxide thickness is not present in our data, which was obtained using the same bias voltage for each oxide thickness. Our collection of data leads to the striking and unexpected conclusion that $\Delta V_{Hanle}/J$ is not a constant but scales with R_{tun}, and up to values larger than 10^9 $\Omega\mu m^2$. This behavior is generic, as it is observed for devices with different semiconductors, tunnel oxides, and ferromagnetic electrodes. Below we explain that this behavior is incompatible with any of the known theories for the injection, accumulation and diffusion of spins in ferromagnetic tunnel devices.

5.4 Comparison with existing theory

5.4.1 Direct tunneling

In the standard theory, the spin accumulation gives rise to a Hanle spin signal $\Delta V_{Hanle} = [P_{fm}^2]\, r_s\, J$, where P_{fm} is the tunnel spin polarization associated with the oxide/ferromagnet interface, and r_s is the spin resistance of the semiconductor [34, 51] that describes the relation between spin current and spin accumulation in nonmagnetic materials. Thus, $\Delta V_{Hanle}/J$ is constant and independent of the resistance R_{tun} of the tunnel contact. This applies when R_{tun} is larger than r_s. If $R_{tun} < r_s$, back flow of the spins into the ferromagnet limits the spin signal [34, 51], which is then proportional to the tunnel resistance: $\Delta V_{Hanle}/J = [P_{fm}^2/(1 - P_{fm}^2)]\, R_{tun}$. Although this produces a scaling with tunnel resistance, the experimentally observed scaling extends to tunnel RA values beyond 10^9 $\Omega\mu m^2$, and a value of r_s larger than this would be required for back flow to be active. This is unreasonable, since r_s is typically around 10-100 $\Omega\mu m^2$ for the semiconductors used [51]. The standard description thus predicts that $\Delta V_{Hanle}/J$ is independent of R_{tun} (and up to 7 orders of magnitude smaller than observed) and cannot describe the data.

5.4.2 Two-step tunneling

Two-step tunneling via localized states near the oxide/semiconductor interface can produce an enhanced spin signal due to spin accumulation in those states [47], provided that certain conditions are satisfied [51]. To obtain a spin resistance of 10^9 $\Omega\mu m^2$, localized states with a spin lifetime of at least 10 μs are needed for a reasonable density of interface states ($> 10^{12}$ states$/eVcm^2$). While this cannot be excluded a priori, there exists ample experimental evidence that shows that this mechanism is not the origin of the large spin signals observed, as recently reviewed [50, 51]. The scaling data presented here provides additional and conclusive proof that two-step tunneling via interface states cannot be responsible, as it leads to a fundamental inconsistency. The scaling of the contact resistance with oxide thickness (Fig. 5.2a) implies that the resistance is dominated by the oxide tunnel barrier, and that any resistance r_b of the Schottky barrier in the semiconductor is much smaller. For two-step tunneling, the effective spin resistance r_s^{eff} of the interface states cannot be larger than the resistance r_b that couples the states to the bulk semiconductor [47, 51]. Taken together this would mean $r_s^{eff} < r_b < R_{tun}$. However, in order to obtain a scaling of the spin RA with tunnel resistance (due to back flow from the interface states into the ferromagnet), one needs the opposite, namely, $R_{tun} < r_s^{eff}$. These requirements cannot be satisfied simultaneously, whatever the parameters chosen. Thus, Tran's model [47] for spin accumulation in interface states is inconsistent with the simul-

taneous exponential scaling of contact resistance and spin signal with tunnel barrier thickness.

5.4.3 Two-step and direct tunneling in parallel

The model introduced by Tran et al. [47] for two-step tunneling via localized states assumes that *all* the current goes via the localized states and, as just noted, this cannot describe the experimental data. However, Tran's model has recently been extended [49] by including charge and spin transport by direct tunneling, in parallel with two-step tunneling. It is therefore important to examine whether this extended transport model can describe the experimental data. Depending on the details of the system, the spin accumulation created in localized states due to two-step tunneling can be much larger than that induced in the semiconductor bands by direct tunneling. If as a function of some parameter (e.g. the tunnel barrier thickness) the relative contribution of two-step and direct tunneling is changed, then a transition from a small signal (direct tunneling dominant) to a large signal (two-step tunneling dominant) or vice versa, can be produced. In this paragraph we examine whether this can explain the observed scaling of the spin RA product with tunnel barrier thickness, and show that this is not possible.

We start by attempting to fit the experimental data for the p-type Si/MgO/Fe devices by setting the direct tunnel current to zero. That is, we consider transport by two-step tunneling, where the first step is by tunneling across the MgO from ferromagnet into interface states, and the second step is by tunneling through the Schottky barrier from interface states into the bulk semiconductor. The result is shown in the left two panels of Fig. 5.4, for which the spin resistance of the localized states was set to infinity, so that the spin signal is not limited by spin relaxation in the localized states. A good fit (thick solid lines) is obtained for the junction resistance. For small MgO thickness, the junction resistance is limited by the resistance of the Schottky barrier, whereas at large MgO thickness it is limited by tunneling across the MgO. According to the model, this should be accompanied by a transition in the behavior of the spin RA product, which first increases with MgO thickness, but becomes constant as soon as the junction resistance is determined by the MgO. This corroborates the statement made in the previous paragraph that the junction resistance and spin resistance cannot simultaneously exhibit a scaling with MgO thickness if transport is by two-step tunneling via localized interface states. Note that in the regime of small MgO thickness, the magnitude of the spin signal is determined by the tunnel spin polarization P_{fm} associated with the Fe/MgO interface, and a value of 20% is needed to obtain a match with the data in this regime. With a value of 75%, which is more reasonable [119], the data cannot be described, not even in the regime of small MgO thickness.

The two middle panels show the result if transport is purely by direct tunneling, setting the two-step tunnel current to zero. In principle the data can be described, however, the required spin resistance r_s^{Si} of the silicon is of the order of 10^8 $\Omega\mu$m^2. This is unreasonable considering that is expected to be in the range of 10 - 100 $\Omega\mu$m^2 at best, for which one would obtain a spin RA product that is independent of the tunnel oxide thickness and orders of magnitude smaller than experimentally observed.

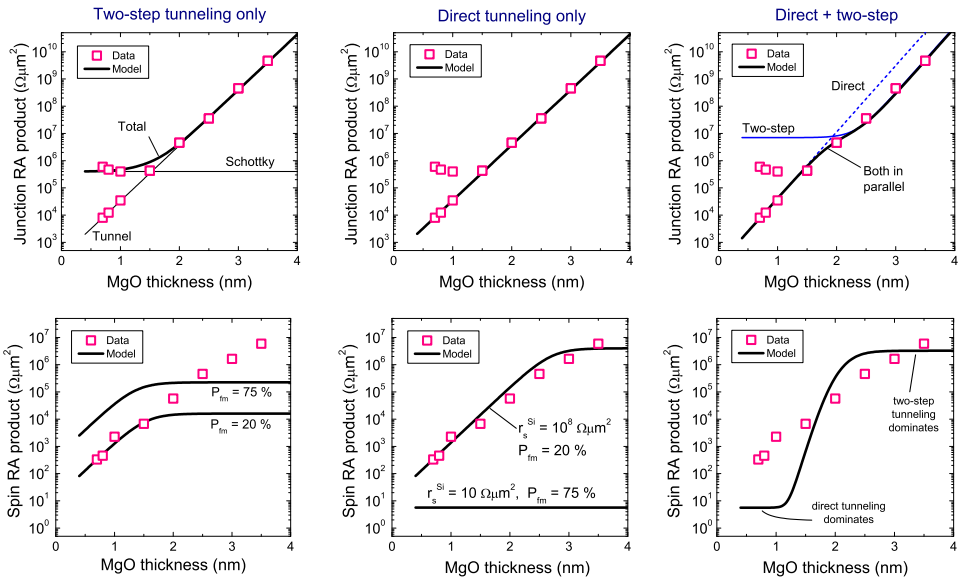

Figure 5.4: *Attempts to fit the data by direct and two-step tunneling in parallel. The experimental data (symbols) for the junction resistance and spin RA product of p-type Si/MgO/Fe devices is compared with the model (solid lines) for three cases: (i) two-step tunneling only, (ii) direct tunneling only, and (iii) two-step tunneling and direct tunneling in parallel. In the top panels, two data points are given for the junction RA product of the three junctions with smallest MgO thickness; the larger value corresponds to the measured junction RA product, whereas the smaller value is obtained when the resistance of the Schottky barrier is subtracted.*

Next, we attempt to describe the data by direct and two-step tunneling in parallel, using the equations given in Ref.[49]. As already eluded to above, in order to obtain an increase of the spin RA product as a function of MgO thickness, one needs to have a transition from transport dominated by direct tunneling to transport dominated by two-step tunneling via interface states. Such a situation is depicted in the two right panels of Fig. At large MgO thickness, transport is determined by tunneling across the MgO, and we have chosen the parameters such that in this regime the resistance associated with two-step tunneling is smaller than that for direct tunneling.

At small MgO thickness, the two-step tunnel current is limited by the resistance of the Schottky barrier. As a result, the transport at small MgO thickness is dominated by direct tunneling. This change in transport process can reasonably well describe the observed scaling of the junction resistance, but not the scaling of the spin signal. A transition from a small spin RA product, governed by direct tunneling, to an enhanced spin RA product due to two-step tunneling is indeed created, but the model does not reproduce the experimental data. It does not reproduce the observed exponential increase of the spin RA with MgO thickness, and deviates from the data in almost the entire range. We conclude that a transition in transport from direct to two-step tunneling does not describe the experimental data.

5.4.4 Inhomogeneous tunnel current density

It has previously been pointed out that an enlarged spin signal can be produced in three-terminal devices if the tunnel current density is not homogeneous across the contact area[29]. In that case the local current density, and thereby the spin accumulation, can be significantly larger that what is expected from the applied current and the lateral dimensions of the tunnel contact. In previous work[29] the spin signal was larger than expected by 2-3 orders of magnitude and in principle this could be due to lateral inhomogeneity of the tunnel current. However, the new data presented here exhibit a scaling with tunnel barrier resistance that is not readily understandable with an explanation in terms of current inhomogeneity. Moreover, for devices with the thickest tunnel barrier, the observed spin signals are larger than expected by up to 6 orders magnitude, and this cannot be explained by inhomogeneous tunnel current. It would require that all the tunnel current goes via an area that is 10^6 times smaller than the geometric contact area of 100×200 μm^2. This translates into an effective tunnel area on only 100×200 nm^2 or so, which is unreasonable. We conclude that inhomogeneity of the tunnel current is not responsible for the experimental observations.

5.5 Control devices

5.5.1 Devices with metal instead of semiconductor

The argument used in the previous section to rule out two-step tunneling via localized interface states was based on the assumption that the states are located at the oxide/semiconductor interface, and decoupled from the semiconductor bulk bands by a Schottky barrier with resistance r_b. In principle, it is possible that the relevant localized states are present *within* the oxide tunnel barrier, and that a large spin accumulation is induced in those states by two-step tunneling. In this case the value

of r_b that couples the localized states to the semiconductor bands is no longer determined by the Schottky barrier, but by the resistance of part of the tunnel oxide. It is known that two-step tunneling is more efficient for states near the center of the tunnel barrier [117]. Hence, the associated value of r_b is determined by half of the tunnel oxide and would systematically increase with the thickness of the tunnel oxide. Depending on the parameters of the system, this could produce a spin accumulation that increases with tunnel barrier thickness, and thereby a scaling of the spin RA product with tunnel resistance.

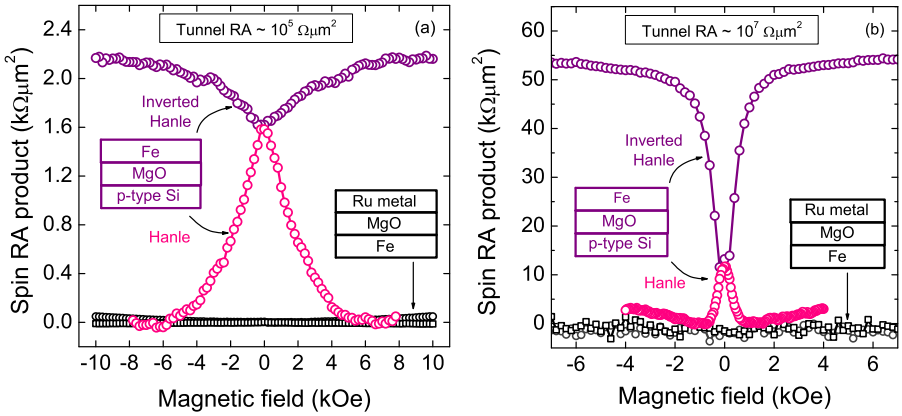

Figure 5.5: **Absence of spin accumulation in control tunnel devices with the Si replaced by non-magnetic Ru metal.** *Shown are the Hanle and inverted Hanle signal for p-type Si/MgO/Fe devices, together with similar data on control devices with Fe/MgO/Ru structure (black circles and squares). Measurements were done at 300 K, and devices with similar tunnel RA product are compared ($10^5 \Omega\mu m^2$ and $10^7 \Omega\mu m^2$ for the left and right panel, respectively). The absence of any spin signal in the metallic control devices proves the absence of spin accumulation in localized states within the MgO tunnel barrier.*

In order to exclude this possibility, we fabricated control devices in which the semiconductor is replaced by a nonmagnetic metal (Ru) electrode. If the large spin RA product originates from spin accumulation in states within the tunnel oxide, the spin accumulation does not depend on the spin resistance of the non-magnetic electrode, and a similarly large spin accumulation should be observed with a Ru metal electrode. However, in control devices with the structure Fe/MgO/Ru, no spin signal could be observed, neither Hanle nor inverted Hanle (see Fig. 5.5). Therefore, we conclude that the spin signal does not originate from spin accumulation in localized states in the tunnel oxide. This control experiment also rules out the recent proposal [118] of spin accumulation in states localized in the tunnel barrier close to the oxide/ferromagnet interface, in which a large spin accumulation is not expected to exist

anyway because the strong coupling with the ferromagnet would easily deplete the spin accumulation.

5.5.2 Devices with zero tunnel spin polarization

Given that the experimental data deviates fundamentally from the theory, it is of the utmost importance to convincingly establish that the observed spin signals are genuine and originate from spin accumulation, rather than some kind of measurement artifact. Such potential artifacts can arise from (anisotropic) magnetoresistance effects related to the current through the ferromagnetic electrode itself, or from the effect of magnetic fields on charge transport in the semiconductor (Hall voltages etc.). A powerful way to exclude these artifacts is to introduce a thin non-magnetic

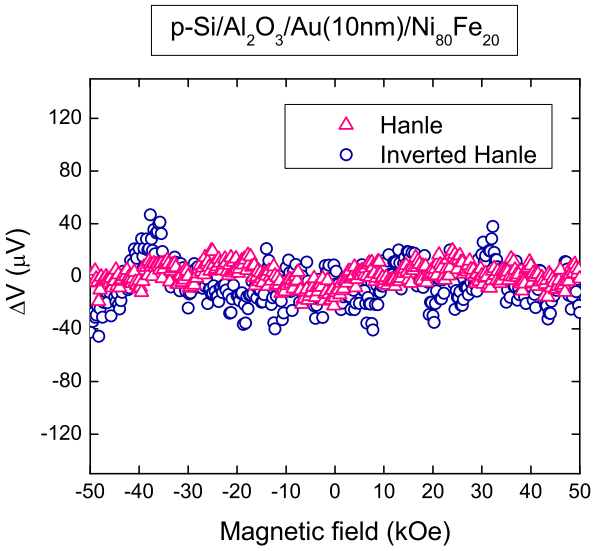

Figure 5.6: *Absence of spin signals in control tunnel devices with zero tunnel spin polarization. Shown are the Hanle and inverted Hanle signal for a control device with structure p-type Si/Al_2O_3/Au(10nm)/$Ni_{80}Fe_{20}$, in which the non-magnetic Au interlayer causes the tunnel spin polarization to be zero. Measurements are done at room temperature with a constant current of -195μA (hole injection condition). A constant bias voltage of about -172mV was subtracted from the data.*

layer at the interface between the tunnel oxide and the ferromagnet, without removing the ferromagnet [63]. The method relies on the extreme interface sensitivity of (spin-polarized) tunneling, such that insertion of a thin non-magnetic layer causes the tunnel spin polarization to vanish, and hence the spin accumulation. Genuine spin signals should then disappear, whereas any signals due to artifacts, if present,

would still remain. This approach was previously used to rule out artifacts in the experiments by Dash et al. [29, 120], although only the signal for out-of plane magnetic field (Hanle curve) was investigated, and only in the range of small field. In Fig. 5.6, a more complete characterization is presented, showing measurements on a control device in the Hanle as well as the inverted Hanle geometry, and for fields up to 50 kOe. No spin signals are observed. This implies that the signals (Hanle and inverted Hanle) observed in the regular devices (without the non-magnetic interlayer) are not due to an artifact but originate from spin-polarized tunneling and the spin accumulation this produces. This result corroborates previous experiments on spin injection from similar ferromagnetic tunnel contacts into a silicon light emitting diode [26, 45], from which the presence of spin-polarized carriers inside the silicon was unambiguously established.

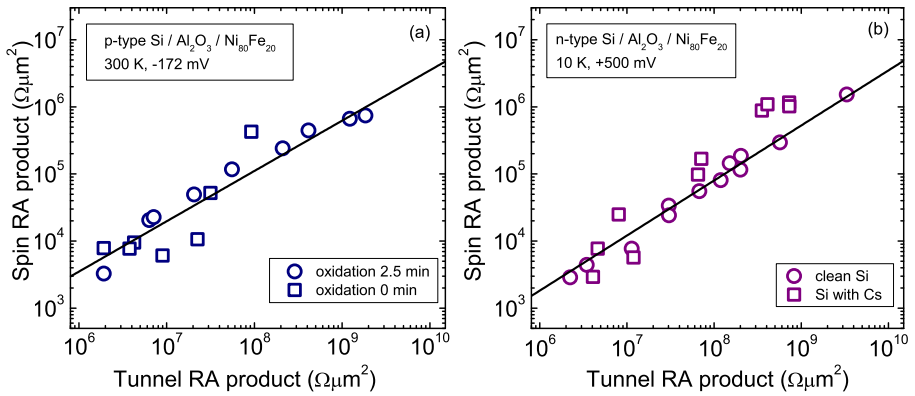

***Figure 5.7:* Additional data on scaling of Hanle spin signals in tunnel devices with n-type and p-type Si.** *The open circles are the same data as in Fig. 5.2 b and 5.2 c, whereas squares are additional data for devices with different oxidation time (p-type, left panel) and with Cs treated surfaces (n-type, right panel).*

5.5.3 Devices with oxygen vacancies

To investigate the effect of localized states produced by oxygen vacancies within the oxide tunnel barrier, we fabricated devices with p-type Si and Al_2O_3 tunnel barrier, but without the plasma oxidation step. Since the Al_2O_3 is grown by electron-beam deposition, the deposited oxide is oxygen deficient. We found that there is no effect on the spin signal, i.e., junctions with and without the plasma oxidation have the same spin RA product at the same tunnel resistance (Fig. 5.7, left panel). This suggests that two-step tunneling via localized states within the tunnel barrier plays no major role

in the spin transport, consistent with the result of the control devices with Ru metal.

In order to investigate the effect of the resistance r_b of the depletion region in the Si, the Schottky barrier height was reduced (and with it r_b) using the procedure with a Cs treatment of the Si surface that was previously developed[29, 45]. Here we present similar data as in Ref.[29] for n-type Si/Al_2O_3/$Ni_{80}Fe_{20}$ devices with and without Cs, as a function of tunnel RA (Fig. 5.7, right panel). The Cs treatment produces no change of the spin RA product, and it scales to values of $10^6 \Omega \mu m^2$. This is not compatible with a description in terms of two-step tunneling via localized states at the oxide/Si interface. Owing to the small value of r_b for the devices treated with Cs, a large spin accumulation cannot built up in the interface states because spins will leak away efficiently into the silicon.

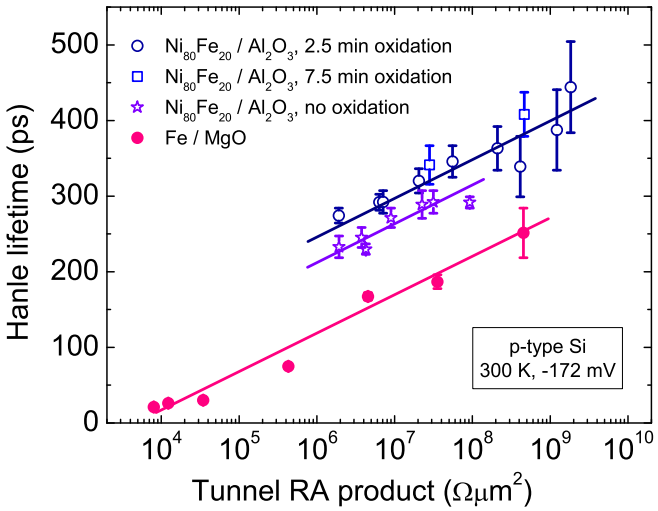

Figure 5.8: *Hanle line width versus tunnel resistance. The Hanle line width is characterized by an effective lifetime obtained from a fit of the Hanle curve using a Lorentzian. This time constant is a lower bound to the spin lifetime, as previously discussed[29, 51, 56]. The solid lines are guides to the eye.*

5.6 Hanle line width versus barrier thickness

Fig. 5.8 shows that the effective spin lifetime, extracted from the width of the Hanle curves, increases as a function of the tunnel resistance. For devices with an Al_2O_3 tunnel barrier, the line width is slightly dependent on the oxidation time. The spin lifetime for devices with MgO/Fe contacts is smaller than with Al_2O_3/$Ni_{80}Fe_{20}$ con-

tacts. This is attributed to broadening of the Hanle curve by inhomogeneous magnetostatic fields, which is more pronounced for Fe owing to its larger magnetization[56].

5.7 Discussion and conclusions

It has previously been noted that the magnitude of the spin accumulation signal observed in magnetic tunnel devices on semiconductors is significantly different than that predicted by the theory of spin injection, diffusion and detection, first for GaAs based devices [47], and subsequently also for Si and Ge based devices [29, 50]. The results presented here provide an even larger discrepancy (of up to 7 orders of magnitude), and perhaps more importantly, reveal that the scaling with tunnel barrier resistance deviates universally from theory in a fundamental way. The scaling extends over a wide range of tunnel resistance, down to the lowest tunnel RA values of about 10 k$\Omega\mu$m^2. It would certainly be of interest to extend the measurements to devices with even lower tunnel resistance. Although it was recently proposed that ferromagnetic tunnel contacts on Si with a single layer of graphene as the tunnel barrier may be ideal for this purpose the obtained tunnel RA product (6 k$\Omega\mu$m^2) was not much different from what was already achievable with oxide tunnel contacts. For instance, in silicon-based non-local devices, Fe/MgO contacts with a tunnel RA product of 4.6 k$\Omega\mu$m^2 have been successfully used for spin injection and detection by Suzuki et al. [100]. However, unlike the case of graphene, the oxide tunnel barriers can still be made thinner and thus appear more promising to reach even lower RA product.

Care has to be taken when in a particular device the observed magnitude of the spin signal is found to be in agreement with theory, because this could be accidental. For instance, the scaling trend predicts that at small junction RA product there must be a point where experiment and theory are in agreement, but a more detailed investigation varying the tunnel barrier thickness would reveal a discrepancy. This point of "accidental agreement" will shift to larger junction RA product when the thickness of the semiconductor channel is reduced, because the theory predicts a larger spin signal when the volume of semiconductor into which spins are injected is decreased. An experiment to explicitly confirm the predicted enhancement (for instance by studying devices with different channel thickness) would be helpful, but is still lacking. Clearly, one needs to look beyond the magnitude of the spin signal in order to (in)validate the theory.

While the above results are obtained with three-terminal devices and the observed signal is larger than predicted, in silicon-based non-local devices [100] the observed signal deviates in the opposite direction, i.e., it is about two orders of magnitude smaller than expected, as recently noted [50]. Although in the latter case there can be several other reasons, the results presented here suggest that the difference between

experiment and theory in three-terminal and non-local devices has a common origin, namely, a missing ingredient in the existing theoretical descriptions. Several explanations for the discrepancy had so far been proposed. These include two-step tunneling via localized states near the semiconductor/oxide interface [47], lateral inhomogeneity of the tunnel current density [29], two-step tunneling in parallel with direct tunneling [49], or two-step tunneling via localized states near the oxide/ferromagnet interface [118]. The scaling results presented here, together with the control experiments, show unambiguously that none of these proposals can explain the results. It is unclear whether the discrepancy arises from an incorrect description of the magnitude of the spin accumulation that is induced by spin injection, or from the description of the conversion of the induced spin accumulation into a voltage signal in a Hanle measurement. Obviously, resolving this puzzle is of crucial importance for application of magnetic tunnel contacts in semiconductor spintronic devices.

Chapter 6

Tunneling anisotropy in Si/Al_2O_3/ferromagnet devices

It has been shown in previous chapters, that spin polarization in Si can be created by using amorphous or crystalline tunnel barrier. We observed that effective spin lifetime is controlled by extrinsic factors, and the spin accumulation in Si is reduced significantly by the magnetostatic fields arising from interface roughness. Here, in this chapter we will study another parameter, the tunneling anisotropy, which can also play a role in the interpretation of the spin signal. The anisotropy in the measured signals may have different origins. For correct interpretation of the spin signal it is essential to distinguish between different contributions. Indeed, here we show that by using the magnetic tunnel contacts on n-type as well as p-type Si with different ferromagnets (Fe and Ni), different contributions can be distinguished. We discuss the various sources of anisotropic spin accumulation in Si. We also describe the fitting equation along with the strategy adopted for interpretation of the experimental results.

6.1 Introduction

In a magnetic tunnel junction (MTJ) with two ferromagnetic (FM) electrodes, a large change in resistance can be produced when the relative alignment of the magnetization of the two magnetic layers is switched[121]. The resulting tunneling mag-

The content of this chapter has previously been published in
S. Sharma, S. P. Dash, H. Saito, S. Yuasa, B.J. van Wees and R. Jansen, Phys. Rev. B **86**, 165308 (2012).

netoresistance (TMR) depends on the tunnel spin polarization (TSP)[34]. Also, it has been observed that in a tunnel junction with a single FM layer[122], a change in tunnel resistance occurs when the magnetization of the magnetic layer is rotated and the absolute orientation of the magnetization changes. This phenomena is called tunneling anisotropic magnetoresistance (TAMR). Depending upon the device configuration, TAMR can be classified as *in-plane* and *out-of-plane* TAMR. The *in-plane*[122–126] TAMR refers to the change in tunnel resistance when the magnetization is rotated in the plane of the magnetic layer. On the other hand, *out-of-plane* [32, 34, 124, 127, 128] TAMR refers to the change in tunneling resistance when the magnetization is rotated from in-plane to out-of-plane.

Theoretical investigations reveal [129] that the TAMR phenomenon is generic in transition metal FMs including Co-Pt multilayers. For Co, these calculations predict an anisotropy in tunneling density of states (DOS) ranging from $0.3\% \sim 1.3\%$. This is supported by the relatively small TAMR value (below 0.5 $\%$) in MTJs with one transition metal electrode[123], consistent with the weak spin-orbit coupling (SOC) in Fe or CoFe. One may expect that engineering the interface adjacent to tunnel barrier can improve the TAMR. For CoPt film the anisotropy in tunneling DOS was predicted[129] to be $>12\%$. This was confirmed [127] by exploiting the enhanced SOC at the interface with CoPt based electrodes giving rise to large TAMR of 15%. Although the TAMR effect may be small in magnitude in tunnel contacts with transition metal FMs, it may influence the spin injection from a FM into a semiconductor (SC). Therefore, to correctly interpret the results of spin injection into a SC[32, 126], it is essential to investigate the TAMR effect in tunnel contacts with a SC.

The recent breakthrough[29, 50] in electrical injection and detection of the spin-polarized carriers in Si at 300 K has given a boost to the research activities in silicon spintronics [30, 31, 46]. Several control experiments[45, 120] have proven unambiguously that the large room-temperature spin signal is genuine and originates from the spin-polarized tunneling and the spin accumulation in the Si bands. This now enables the systematic study of the various parameters that influence the spin injection into silicon[56], of which our understanding is still rather limited. A feature that provides more insight is the anisotropy of the tunnel conductance, which may have various sources, including the TAMR. Previous reports on TAMR concluded that the change in tunnel resistance is due to the anisotropy in DOS[122–124, 127–130] at the tunnel interface between a FM and an insulating barrier. As the magnetization direction is rotated, it faces different DOS, thereby changing the transport across the tunnel contact. This leads to the change in resistance of the tunnel contact. Other sources of the anisotropy include the anisotropic tunnel spin polarization (TASP) associated with the ferromagnet/tunnel barrier interface[131, 132] and/or anisotropic spin relaxation time τ_s inside the non-magnetic SC. Such an anisotropic spin relax-

ation has been invoked to describe experiments with graphene[133], where it was argued that there is 20% decrease in spin-relaxation time for electrons with spin perpendicular to the graphene layer compared to the spins oriented parallel to the layer. Assuming the TSP to be isotropic, the anisotropy in τ_s will results in anisotropic spin accumulation $\Delta\mu$ inside the semiconductor. On the other hand, the anisotropic TSP of the magnetic tunnel contact will also create different spin accumulation levels inside the SC, irrespective of the anisotropy in τ_s. The anisotropic spin accumulation in a SC, caused by either the anisotropy of TSP or by the anisotropic spin relaxation time in a SC, makes the measured signal to be anisotropic. Distinguishing between these different sources of the anisotropy is essential for the correct interpretation of the data.

In this chapter, we describe that by using tunnel contacts made on n-type as well as on p-type Si with Fe or Ni electrodes, we have been able to separate the different sources of the tunneling anisotropy. Rotation of the magnetization of the ferromagnet in a plane perpendicular to the magnetic layer results in an out-of-plane tunneling anisotropy that depends on the type of ferromagnet and on the doping of the Si (n, p-type). Analysis reveals that different contributions to the tunneling anisotropy coexist. In addition to regular TAMR, we identify a contribution due to anisotropy of the TSP. This causes the injected spin accumulation in Si to be dependent on the absolute orientation of the magnetization of the ferromagnet. Further, we observed that due to magnetic shape anisotropy of the magnetic layer, the magnetization makes an angle θ with the external field. This angular separation between the magnetization and the field is larger for Fe (saturation magnetization (M_S = 2.15T) compared to Ni (M_S = 0.6T). The misalignment between the magnetization and the external field results in Hanle spin precession[16], and it is more pronounced in the tunnel contacts with Fe compared to Ni. The relative strength of the different contributions to the anisotropy is found to depend on bias voltage. As a result, a significant change in the angular variation of the signal with bias voltage is observed, particularly for the tunnel contacts with Fe, while in the tunnel contacts with Ni, the measured signal retains its shape irrespective of the bias voltage.

This chapter is organized as follows. Sec. 6.2 describes the experimental technique used for characterizing the anisotropy of the tunnel resistance. This section also provides a brief introduction to the different components in the measured signal. The device fabrication is similar as described in chapter 3. In Sec. 6.3 and 6.4, a detailed description of the experimental results obtained on the tunnel contacts with different ferromagnetic electrodes and different Si (n-type and p-type) is given. This is followed by Sec. 6.5, describing the anisotropy of the spin accumulation in Si. This section includes detailed discussion about the Hanle spin precession, which arises from the misalignment between the magnetization and the external field. We

also describe the fitting equation along with the strategy adopted for interpretation of the experimental results. A Summary shall be presented in Sec. 6.6.

6.2 Measurement principle

The magneto-transport measurements have been carried out at 300 K in a system equipped with a sample rotator and a superconducting magnet. Two types of measurements, namely the field scan and the angle scan, were performed. The field scan measurements are obtained by fixing the angle ϕ between the applied field and the surface normal (see Fig. 6.1) and varying the field strength. The ϕ values of 0°, 180° and 360° correspond to the magnetic field perpendicular to the film plane, whereas 90° and 270° represent the field in the plane of the FM layer. The easy axis of the magnetization lies in-plane of the magnetic layer, i.e., along the X direction in Fig. 6.1. Sweeping the magnetic field with direction perpendicular to the tunnel interface (i.e. ϕ=0°, 180° and 360°) and the magnetization lying along the easy axis, give rise to a Hanle curve[29]. On the other hand, sweeping the magnetic field with direction parallel to the tunnel interface and magnetization still lying along the easy axis (i.e. ϕ=90° and 270°) results in an inverted Hanle curve[56].

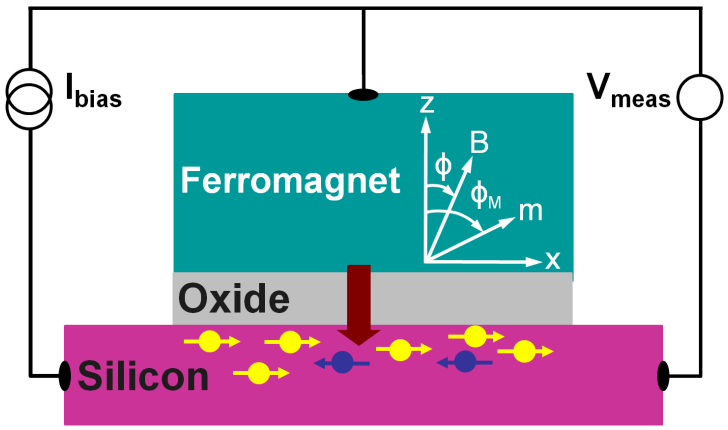

***Figure 6.1:* Schematic of three-terminal geometry used for measuring the anisotropy in tunneling resistance**. *A constant current I, across the tunnel junction produces a voltage that changes when the magnetization of the magnetic layer is rotated out-of-plane. Here ϕ represents the angle between a surface normal and the external field whereas ϕ_M is the angle between a surface normal and the magnetization direction $\vec{m}$. Here X and Z denote the in-plane and surface normal direction respectively. The measured voltage V_{meas}, and therefore the tunnel resistance R(ϕ) (=V_{meas}/I) depends on the magnetization direction.*

In the angle scan, the sample is rotated i.e., changing ϕ at a fixed external magnetic field B of 50 kOe. This is equivalent to rotating the magnetization from in-plane to out-of-plane. The experimental geometry is shown in Fig. 6.1. A constant current I is sourced across the tunnel contact and the resulting voltage change (or dc resistance change) is measured as a function of angle ϕ when the magnetization of the magnetic layer is rotated. Due to a shape anisotropy (see Sec. 6.5 for details) the magnetization of the magnetic layer makes an angle $\theta = (\phi_M - \phi)$ with applied field as shown in Fig. 6.1. Here ϕ_M is the angle between the magnetization direction ($\vec{m}$) and the normal to the surface (the Z axis).

In three-terminal configuration a fixed source current across the junction results in a bias voltage $V = V_{Si}$-V_{FM} such that for $V > 0$ (< 0) spin polarized electrons are injected in to (extracted from) the Si. The total voltage across the contact at constant current is given by $V_{meas} = V_0 + V_{TAMR}(\phi) + V_{ASA}(\Delta\mu(\phi))$, where V_0 is a constant voltage independent of the field and the other two terms describe the changes of the voltage produced when the magnetization of the magnetic layer is rotated. The second term V_{TAMR} is due to the tunneling anisotropic magnetoresistance[34] that comes from an anisotropy in spin tunneling due to Bychkov-Rashba [134] (BR) type spin-orbit interaction at the tunnel interfaces and/or intrinsic SOC in the ferromagnet [122, 123, 129]. The third term V_{ASA} is due to an anisotropic spin accumulation (ASA) in the Si, i.e., a spin accumulation $\Delta\mu$ that depends on ϕ. This, in turn causes an angular dependence of V_{meas} across the junction, because V_{meas} is proportional to $\Delta\mu$ [29, 50, 56]. An ASA may results from an anisotropic spin-relaxation time (τ_s) in the Si, from Hanle precession of spins in Si (due to the fact that the magnetization makes an angle θ with the external field) or due to tunneling anisotropic spin polarization[34, 131, 132].

6.3 Tunneling anisotropy

To investigate the anisotropy in the tunnel resistance, we performed 3T measurements on devices made on n-type as well as on p-type Si with different FM electrodes (Fe and Ni). Let us start with the experimental data obtained on tunnel contacts with Fe.

6.3.1 Tunnel contacts on n-type and p-type Si with Fe

Figs. 6.2 (a) and (b) show the field scan and the angle scan data for a p-Si/Al_2O_3/Fe tunnel contact taken at a constant current of -91.3μA (hole injection into Si). A constant voltage V_0 = -172 mV was subtracted from the data. The red (blue) curve is obtained for $\phi = 0^\circ$ (90°) so that the external field is perpendicular (parallel) to the tunnel interface.

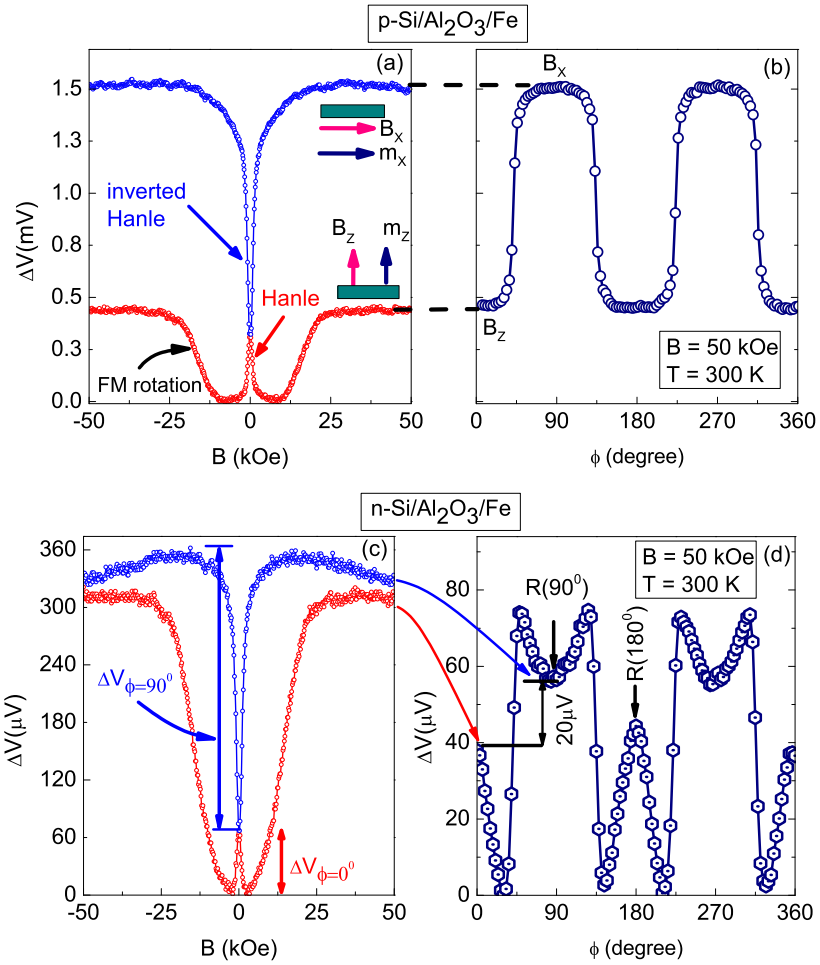

Figure 6.2: *Experimental data for p-Si/Al_2O_3/Fe junction (a) with field perpendicular (Hanle, red) and parallel to the tunnel interface (Inverted Hanle, Blue) and (b) the angular dependence of the measured signal at same bias voltage. Data is shown after subtracting an offset signal of V_0= -172 mV (I = -91.3 μA). Labels B_X and B_Z in (b) represent the situations when the external field is parallel or perpendicular to the tunnel interface. Similar data set with n-Si/Al_2O_3/Fe tunnel contacts for (c) Hanle (ϕ=0°, red), inverted Hanle (ϕ=90°, blue) and (d) angle scan measurements at a bias voltage of -172 mV (-807 μA). In figure (c) $\Delta V_{\phi=0^\circ}$ and $\Delta V_{\phi=90^\circ}$ are the signal amplitude obtained in Hanle and inverted Hanle measurements respectively. In Figure (d) R(ϕ) is the resistance (V_{meas}/I) at respective ϕ value. All the measurements have been performed at 300 K. Note that (c) and (d) have different vertical scales.*

For the red curve, the symmetric peak around zero field is the signature of the Hanle effect [29, 50]. At zero external field there is no spin precession and the spin accumulation is maximum. With increasing external field, spins start to precess and the spin signal reduces to zero. At a field around 10 kOe the curve (red) rises and after reaching a maximum above a field of $\approx$ 22 kOe, it saturates at this level. The rise in the signal is due to the rotation of the magnetization of the FM. Above a field of $\approx$ 22 kOe, corresponding to the saturation magnetization of the Fe, the magnetization of the magnetic layer is aligned with the transverse field. The spins injected into Si are then oriented parallel to the external field, and thus there is no precession. Due to this complete alignment, the spin signal reaches a maximum and saturates.

The blue curve is obtained for ϕ = 90° so that the external field is parallel to the tunnel interface. In this case, the spins injected into silicon will have orientation parallel to the external field and ideally there is no spin precession. Based on this we expect a constant signal (no variation with B-field) under steady state conditions. However, we see that there is a dip in blue curve around zero field. The spin signal has a minimum at zero field, and as the external field is increased, the signal rises to the maximum value. This is referred as an inverted Hanle effect [56]. The suppression of the signal around zero field is attributed to the spin precession in magneto static fields, arising from roughness of the magnetic layer [56].

We find that at sufficiently large field (>22 kOe) when the external field and the magnetization of the FM are aligned with each other, the Hanle and inverted Hanle curves [Fig. 6.2 (a)] do not saturate at same level. This indicates that the tunnel resistance (R(ϕ)=V_{meas}/I) depends on the absolute orientation of the magnetization of the FM electrode. To explore this fact in more details we have carried out angular dependence study of the tunneling resistance. Fig. 6.2 (b) shows such a measurement for p-Si/Al_2O_3/Fe junction at V = -172 mV (hole injection into p-Si). By keeping the current fixed and changing the field angle ϕ, the curve in Fig. 6.2 (b) is obtained. Comparison between Figs. 6.2 (a) and (b) reveals that the angle scan reproduces the anisotropy observed between the two measurements of the Hanle and inverted Hanle effect. Defining the zero of the signal at ϕ = 0°, it raises to a value set by the in-plane (ϕ = 90°) signal, resulting in the two-fold symmetry. Note that the curve is not sinusoidal.

Figs. 6.2 (c) and (d) show a similar data set for Si/Al_2O_3/Fe tunnel contacts with n-type Si at a bias of -172 mV (-807 μA). Similar to p-Si in Fig. 6.2 (a), we obtain a symmetric Hanle and inverted Hanle curves around the zero field. For the Hanle curve, the signal reduces with increasing field. Then due to rotation of the magnetization of the FM, the signal rises until the external field reaches the saturation magnetization of the Fe. Beyond that the signal stays almost constant, as there is no spin precession in the silicon. In Fig. 6.2 (c), $\Delta V_{\phi=0^\circ}$ and $\Delta V_{\phi=90^\circ}$ represent the

signal amplitude for Hanle and inverted Hanle measurements. The net spin signal is proportional to [$\Delta V_{\phi=0^\circ}$+$\Delta V_{\phi=90^\circ}$]. It represents the signal amplitude between two extreme situations. In the first situation, the magnetization lies in the plane of the magnetic layer and the spin signal corresponding to the spins injected into the silicon is zero due to spin precession (minimum in the Hanle curve). For the second situation, the magnetization still lies in the plane of the magnetic layer but the spin signal is maximum, as the spins injected into the silicon have orientation parallel to the field and do not precess (maximum in the inverted Hanle curve). At 50 kOe in Fig. 6.2 (c), Hanle (red, ϕ=0°) and inverted Hanle (blue, ϕ=90°) curves are separated by ≈20 μV. This value is similar in magnitude to the signal obtained in the angle scan [Fig. 2(d)] between ϕ=0° and 90°. We note that for the same bias voltage and field, the tunnel contact with n-Si has smaller anisotropy compared to those on p-Si. In addition, the measured signal in the angle scan has minima at ϕ=90°, 270° and maxima at 0°, 180° and 360° for tunnel contacts with n-Si. The angle scans in Figs. 2(b) and (d) indicate that V_{meas} departs from the expected cos(ϕ) variation, implying that signals with different origin coexist.

In Fig. 6.3 we present the bias variation of anisotropic tunneling resistance for the tunnel contacts with Fe on p-Si [a-d] and n-Si [e-h]. The measured resistance at -172 mV in Fig. 6.3 (a) displays two fold symmetry with nearly square peaks at ϕ = 90° and 270°. At -30 mV [Fig. 6.3 (b)] the resistance at ϕ = 90° and 270° decreases whereas at 0° and 180° it starts to rise compared to minimum value. It becomes more clear in Fig. 6.3 (c) at 70 mV for which the resistances at 90° and 270° are no longer the maximum, while at 172 mV in Fig. 6.3 (d) it has become the minimum. The symmetry is no longer two-fold and highest resistance are found for 0° and 180°. New features with minima approximately at 38°, 145°, 219° and 325° can be seen in Figs. 6.3 (c) and (d) at 70 mV and 172 mV respectively. Also note that the amplitude of the signal decreases from negative to positive voltage.

The tunnel contact with n-Si [Fig. 6.3 (e-h)] has local minima at 90°, 270° and local maxima at 0°,180° and 360° within the investigated bias range. However, four minima positions are observed at the same angle for n-Si and p-Si, i.e., 39°, 147°, 219° and 330°. The overall shape of the curves for n-Si [Fig. 6.3 (e-h)] has little dependence on bias voltage [as opposed to p-type, see Fig. 6.3 (a-d)].

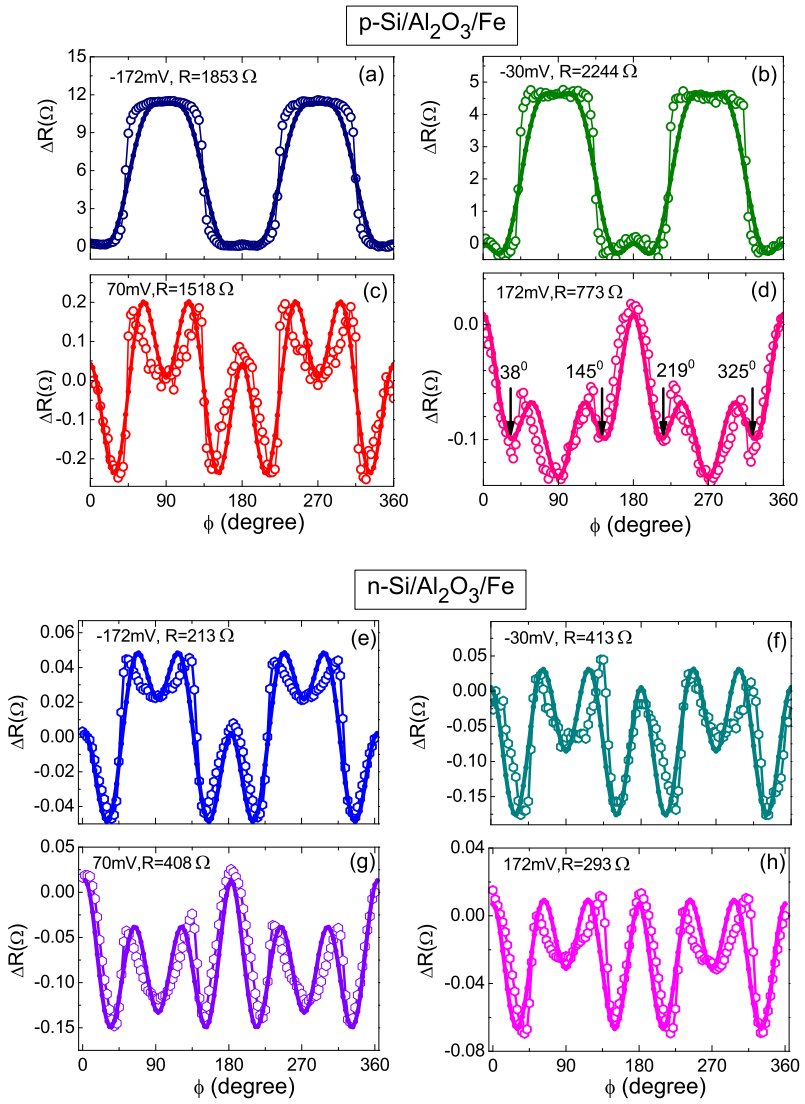

Figure 6.3: *ΔR (=R(ϕ)-R_{min}, R_{min} is the minimum resistance in the measurement) as a function of the field angle ϕ at -172 mV (a) -30 mV (b) 70 mv (c) and 172 mV (d) for p-Si/Al_2O_3/Fe. Similarly ΔR vs. ϕ at -172 mV (e) -30 mV (f) 70 mv (g) and 172 mV (h) for n-Si/Al_2O_3/Fe tunnel contacts. The junction resistance values at each bias are indicated in respective figure. Measurements have been taken on tunnel contacts at a field of 50 kOe and a temperature of 300 K. Note the different vertical scales for ΔR in each plot. Solid lines are fits using Eq. (6.4) in text.*

6.3.2 Tunnel contacts on n-type and p-type Si with Ni

Next, we will describe the field scan along with the angle scan measurements on tunnel contacts with Ni electrode. Considering the low saturation magnetization (M_s = 0.6T) for Ni and the fact that tunnel contacts with Ni have lower Hanle line width[56], Figs. 6.4 (a) and (c) display the data only up to 10 kOe for clarity. In Fig. 6.4 (a),

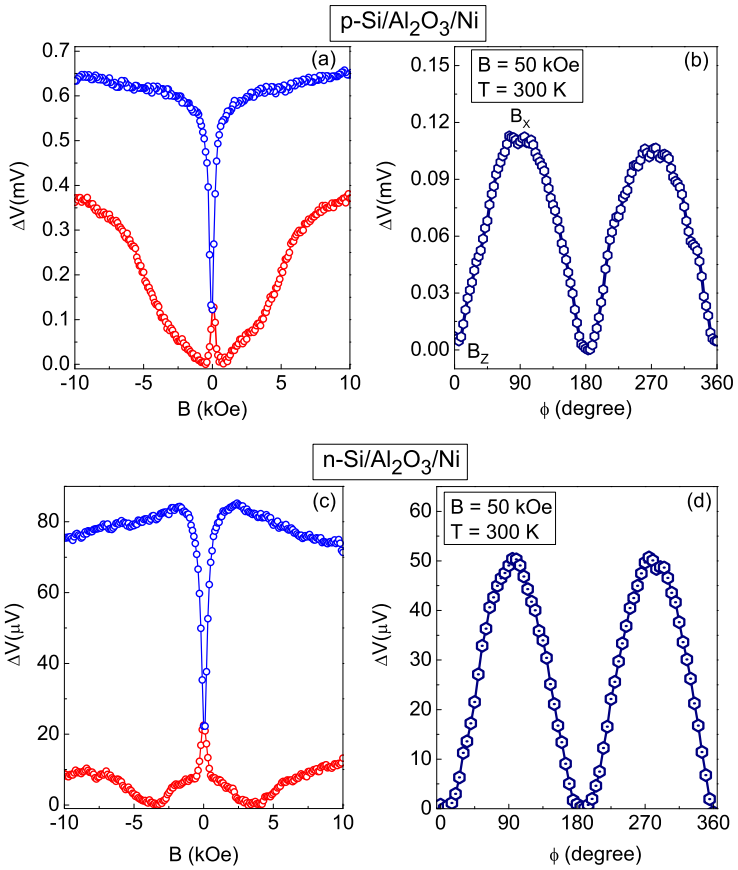

Figure 6.4: *Experimental data for p-Si/Al_2O_3/Ni tunnel contact (a) with field perpendicular (Hanle, red), parallel to the tunnel interface (inverted Hanle, blue) and (b) angular dependence of the measured signal at a bias of -172 mV (-171 μA). Similar data set for n-Si/Al_2O_3/Ni tunnel contact (c) Hanle (red), inverted Hanle (blue) and (d) angular dependence of the measured signal at a bias of -172 mV (-650 μA) . Data is shown after subtracting different offset voltages. In (b) and (d) a constant field of 50 kOe is applied.*

Hanle (red) and inverted Hanle (blue) measurements for p-Si/Al_2O_3/Ni tunnel contacts at -172 mV (hole injection in to p-Si) are shown. The voltage ΔV has been

obtained after subtracting a constant voltage V_0 = -172 mV. The Hanle curve has a very sharp peak at zero field. Around 0.5 kOe the signal rises very fast due to rotation of magnetization of the Ni layer. A change in the slope of the signal occurred around 6 kOe and it stays constant with further increase in field. The inverted Hanle curve (blue) has a dip around zero field and saturates at high magnetic field. In Fig. 6.4 (b) the angle scan at 50 kOe and a bias of -172 mV gives cos(ϕ) variation of ΔV=V_{meas}-V_0 vs. ϕ, with two maxima at ϕ=90° and ϕ=270°.

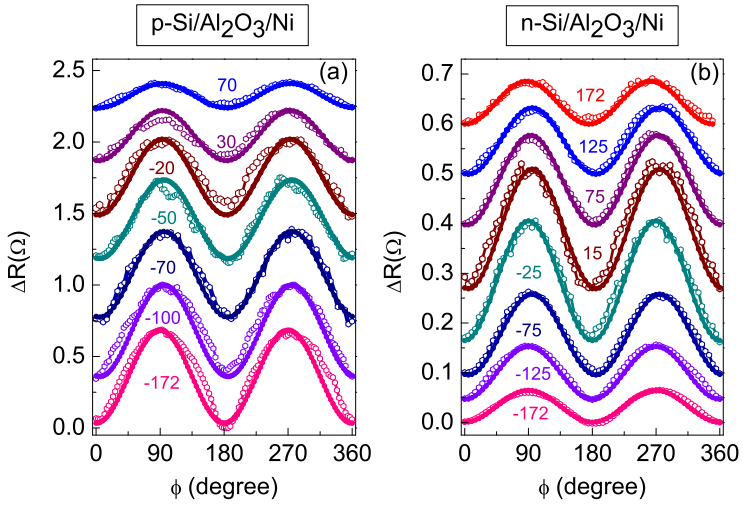

Figure 6.5: *ΔR as a function of field angle ϕ for (a) p-Si/Al_2O_3/Ni and (b) n-Si/Al_2O_3/Ni tunnel junctions at bias voltages indicated in each fig.(in mV). Vertical axis is ΔR=$R(\phi)$-R_{min}, where R_{min} is the minimum resistance value in measurement. Solid lines are fits obtained through Eq. (6.4) in text. Data are displaced vertically for clarity. All the measurements have been performed at 300 K and a field of 50 kOe.*

Fig. 6.4 (c) shows Hanle and inverted Hanle curves for n-Si/Al_2O_3/Ni tunnel contacts up to 10 kOe. We obtain a sharp Hanle peak around zero field, and with further increase in the field, the signal saturates at $\approx$ 7 kOe. For a field applied parallel to the tunnel interface, we observe the inverted Hanle effect with a dip in the signal around zero field and recovery of the signal at high field. In Fig. 6.4 (d) the angle scan at 50 kOe and at a bias of -172 mV gives a cos(ϕ) variation with two maxima at ϕ=90° and ϕ=270°, similar to tunnel contact with Ni on p-Si.

The detailed bias dependence of anisotropic tunnel resistance for tunnel contacts on p and n-Si with Ni is shown in Figs. 6.5 (a) and (b). The shape of the signal and two-fold symmetry along 90° and 270° do not change with bias voltage. However, the magnitude of the total signal decays with increasing bias voltage. Fig. 6.5 (b)

contains similar data set for n-Si/Al_2O_3/Ni tunnel contacts. Irrespective of the bias voltage, we have a cos(ϕ) variation with two-fold symmetry along ϕ=90° and 270°. Note that this behaviour is completely different from tunnel contacts with Fe [see Fig. 6.3]. We will have a more detailed discussion of this topic in the next section.

6.4 Bias variation of tunneling anisotropy and spin resistance

So far we have shown the angular variation of the tunneling resistance at different bias voltages for different tunnel contacts (on n and p Si) with Fe and Ni. To gain insight, we define the tunneling anisotropy as [($R_{\phi=90^\circ}$ - $R_{\phi=180^\circ}$)/$R_{\phi=180^\circ}$]$\times 100\%$, where R(ϕ) [see Fig. 6.2 (d)] corresponds to the resistance values at angle ϕ=90° and 180°. Angles ϕ=90° and 180° represent the in-plane and out-of-plane orientation of the field, respectively. We also define the spin-resistance as ΔR_{spin}=[$\Delta V_{B_{\phi=0^\circ}} + \Delta V_{B_{\phi=90^\circ}}$]$/I$, where I is the constant source current across tunnel contact, whereas $\Delta V_{B_{\phi=0^\circ}}$ and $\Delta V_{B_{\phi=90^\circ}}$ have been defined earlier in Fig. 6.2 (c). Hence, the ΔR_{spin} represents the sum of the Hanle and inverted Hanle signal amplitude, which is proportional to the spin accumulation $\Delta\mu$. In the next section we will discuss these parameters for tunnel contacts with Fe followed by Ni.

6.4.1 Tunnel contacts with Fe

Fig. 6.6 (a) shows the tunneling anisotropy of p-Si/Al_2O_3/Fe junction as a function of bias voltage. At negative bias (hole injection) we see that the anisotropy is maximum and that it decreases linearly by going towards positive bias. Along positive bias (hole extraction), the anisotropy becomes negative and does not decay much. Fig. 6.6 (b) shows the variation of the spin-resistance with bias voltage for the same tunnel junction. The spin resistance is asymmetric with respect to bias voltage, has a positive sign, and remain non-zero for all bias voltages. The measured voltage due to spin accumulation is proportional to the square of the TSP of the ferromagnet/insulator interface. As a result, the spin resistance ΔR_{spin} is always positive, independent of the sign of the spin accumulation or TSP. However, if there is a sign reversal of the TSP, the spin resistance must become zero at some bias voltage and become positive again. Since the observed ΔR_{spin} does not display a drop to zero, we conclude that the TSP does not change sign. In Fig. 6.6 (c), we show the variation of the junction resistance with the bias voltage. We see that the junction resistance decays with bias voltage and more strongly for positive bias. When a bias is applied across the tunnel contact, electrons tunnel through the Al_2O_3 and Schottky barrier before reaching the bulk bands of the SC. Along negative bias, i.e., when V$<$0, the depletion width in p-Si increases, while for V$>$0, the width of the Schottky barrier is reduced. As a

result the tunneling probability is enhanced (reduced) for V>0 (V<0), giving rise to the asymmetry in the junction resistance.

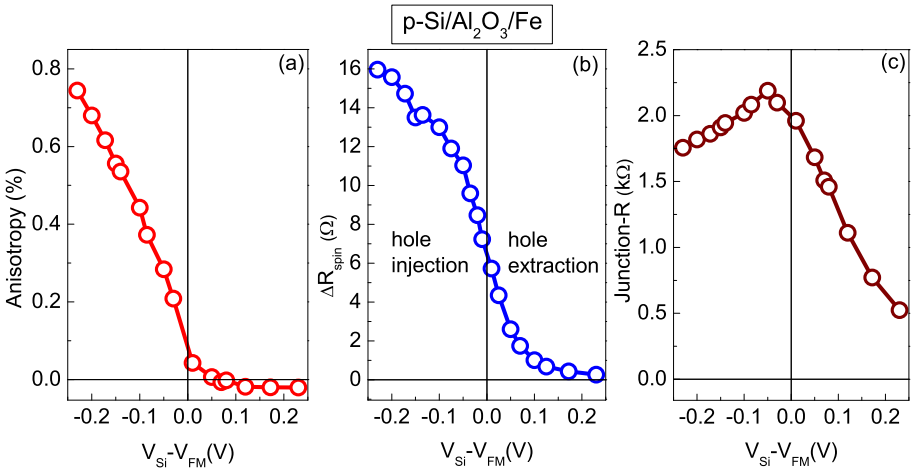

Figure 6.6: *Bias dependence of (a) tunneling anisotropy and (b) spin resistance* ΔR_{spin}=$[\Delta V_{B_{\phi=0^\circ}} + \Delta V_{B_{\phi=90^\circ}}]/I$, *shown together with (c) junction resistance for p-Si/Al*$_2$*O*$_3$*/Fe tunnel junction.* $\Delta V_{B_{\phi=0^\circ}}$ *and* $\Delta V_{B_{\phi=90^\circ}}$ *have been defined in Fig. 6.2 (c).*

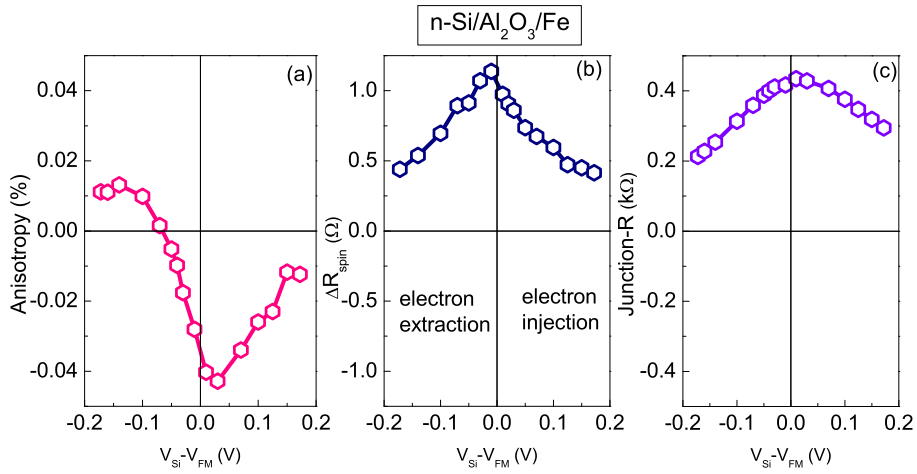

Figure 6.7: *Bias dependence of the (a) tunneling anisotropy (b) spin resistance,* ΔR_{spin} *and (c) junction resistance for n-Si/Al*$_2$*O*$_3$*/Fe tunnel junction.*

In Fig. 6.7 we show a similar set of data for n-Si/Al_2O_3/Fe tunnel contacts. Compared to p-type Si, a different qualitative variation is observed for the tunneling anisotropy and spin-resistance. Tunneling anisotropy [Fig. 6.7 (a)] has complex variation with bias voltage and it also changes sign with bias. However, the spin-resistance ΔR_{spin} in Fig. 6.7(b), displays quite different behavior. It decreases monotonically and equally fast at V$>$0 and V$<$0 and does not change sign. It also has much less variation with bias compared to p-type Si with Fe. At negative bias (electron extraction) the junction resistance [Fig. 6.7 (c)] decreases slightly faster compared to positive bias (electron injection). The weak variation of tunnel resistance with bias is due to smaller depletion layer width for heavily doped n-Si, in combination with low work function of the Fe(4.5eV)[135], which provides a lower Schottky barrier height for the tunnel contacts on n-Si.

6.4.2 Tunnel contacts with Ni

Fig. 6.8 displays the data for the tunnel contact on p-Si with Ni. Both the tunneling anisotropy (a) and ΔR_{spin} (b) decrease with bias voltage in approximately the same way and there is no sign reversal for the anisotropy. The tunneling anisotropy is always positive, meaning higher resistance for in plane field (ϕ=90°). The spin-resistance ΔR_{spin} and the tunneling anisotropy approach zero when the bias has reached a value of 172 mV. Thus, we see that for tunnel contacts with p-Si and Ni, the

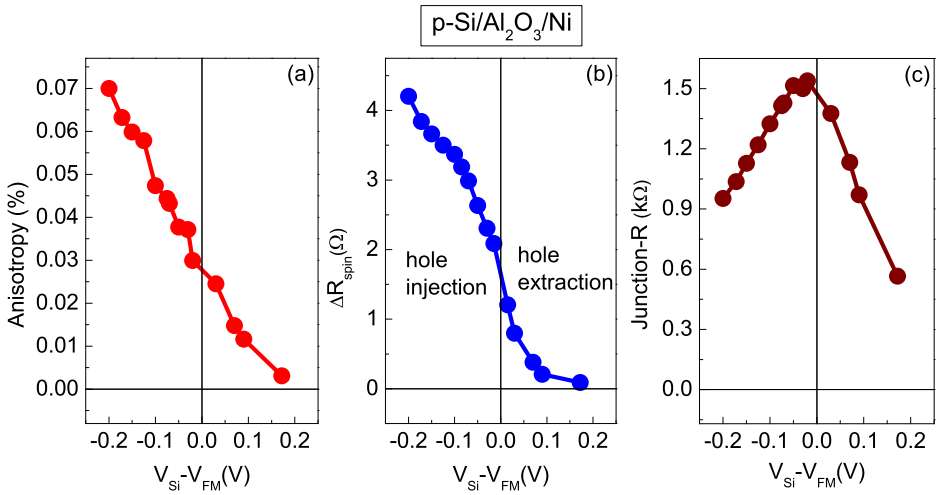

Figure 6.8: *Bias dependence of the (a) tunneling anisotropy (b) spin resistance and (c) junction resistance for p-Si/Al_2O_3/Ni tunnel junction.*

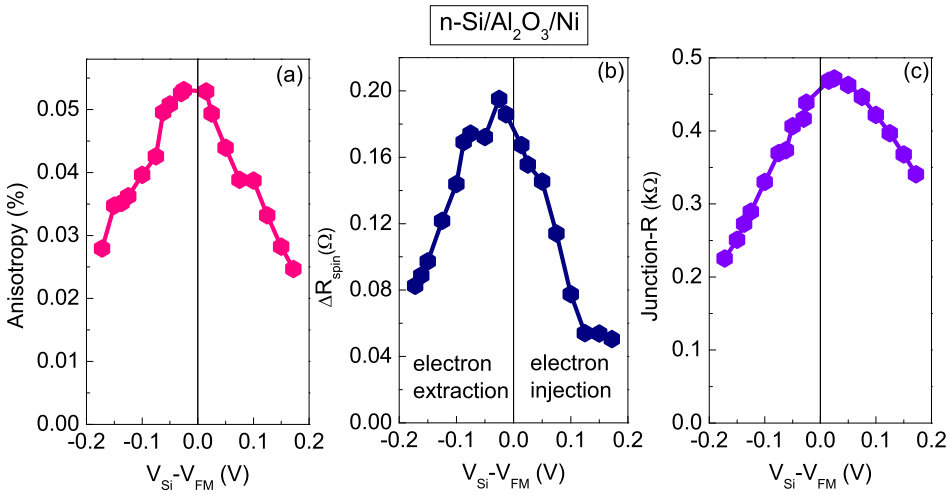

Figure 6.9: *Bias dependence of the (a) tunneling anisotropy and (b) spin resistance shown together with the (c) junction resistance for n-Si/Al_2O_3/Ni tunnel junction.*

tunneling anisotropy and spin-resistance behave similarly. In Fig. 6.8 (c) the junction resistance is shown. It decreases slowly at negative bias (hole injection) whereas at positive bias the decrease is more significant. However, the bias asymmetry of the junction resistance is weaker than for p-Si with Fe. The lower work function of the Fe(4.5 eV)[135] compared to Ni (5 eV) gives rise to a larger Schottky barrier for Fe on p-type Si. As a result, the bias asymmetry of the junction resistance is stronger for tunnel contacts on p-Si with Fe.

In Fig. 6.9, a similar data set for n-Si/Al_2O_3/Ni tunnel contacts is shown. The tunneling anisotropy [Fig. 6.9 (a)] decays almost equally fast at negative (electron extraction) and positive (electron injection) bias. It does not change sign in the bias range investigated. Qualitatively the spin-resistance decreases in both bias direction similar to the tunneling anisotropy. The junction resistance in Fig. 6.9 (c) has typical variation with bias voltage, reducing relatively fast (slow) for negative (positive) bias. Tunnel contacts on n-Si with large work function of Ni (5 eV) have a larger Schottky barrier as compared to the contact with Fe (4.5 eV). Larger Schottky barrier height results in a larger asymmetry in current across the tunnel contacts. As a result, the asymmetry of junction resistance in Fig. 6.9 (c) for contacts with Ni is larger than for contacts with Fe (Fig. 6.7 (c)).

6.5 Analysis and discussion

In this section, we will first discuss one of the sources of tunnel anisotropy that is well understood and originates from shape anisotropy, causing the magnetization direction to deviate from the direction of the applied magnetic field. Then we will describe the fitting equation that contains terms related to the TAMR and an anisotropic spin accumulation giving rise to the tunneling anisotropy. The sources of an ASA, namely the anisotropic TSP associated with ferromagnet/insulator interface and anisotropic spin relaxation time in Si, have been introduced earlier. We also discuss that by a suitable combination of tunnel contacts on n and p-Si with different FM (Fe or Ni), the different contributions to an ASA and to tunneling anisotropic magnetoresistance can be separated.

6.5.1 Anisotropic spin accumulation in Si due to Hanle spin precession

For a magnetic thin film, the shape anisotropy favours a magnetization direction parallel to the surface, i.e., within the film plane, whereas an external field of 50 kOe favours the magnetization to align with it. Consequently, the external field and magnetization are not perfectly aligned, but they are at angles ϕ and ϕ_M (see Fig. 6.1) with surface normal, respectively. The total energy of the magnetic layer consists of terms associated with the Zeeman energy and the demagnetizing energy due to shape anisotropy:

$$E_{total}(H,\phi,\phi_M) = -\mu_0 M_s H cos(\phi-\phi_M) - \frac{1}{2}\mu_0 M_s^2 sin^2(\phi_M), \tag{6.1}$$

Here μ_0, M_s and H are magnetic permeability of vacuum, saturation magnetization and external field respectively. The orientation of the magnetization (ϕ_M) w.r.t surface normal is determined by the energy minimization of the magnetic layer. Fig. 6.10 (a) shows $\phi_M - \phi$ as a function of field angle ϕ.

At ϕ =0° and 90° the field and magnetization are aligned perfectly. For intermediate values of ϕ, the difference $\theta = \phi_M - \phi$ has a maxima at ϕ=32.6° and 41.5° for Fe and Ni, respectively. We find that the difference $\phi_M - \phi$ is larger for Fe compared to Ni, which is attributed to larger shape anisotropy energy for Fe (M_s = 2.15 T) compared to Ni (M_s = 0.6 T). Due to misalignment of the magnetization with the field, the spins injected into silicon make an angle $\theta = \phi_M - \phi$ with the field, thereby leading to spin precession in Si even at a field of 50 kOe. The spin signal in terms of the angle θ between injected spins and magnetic field vector can be written as [16]:

$$\Delta\mu \propto \left[cos^2\theta + \frac{sin^2\theta}{1+(\omega_L\tau_s)^2}\right], \tag{6.2}$$

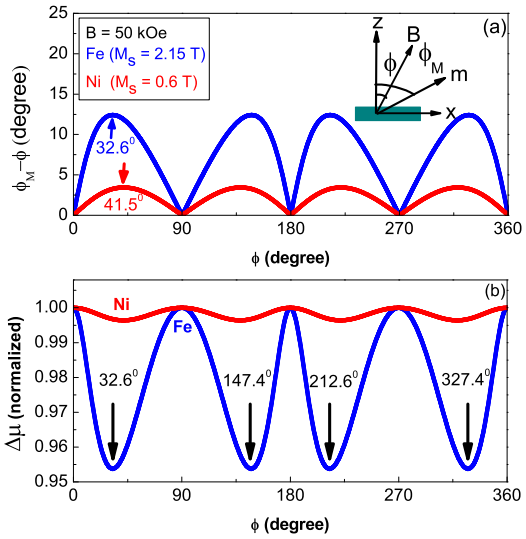

Figure 6.10: *(a) Magnetization angle ϕ_M and (b) normalized spin accumulation $\Delta\mu$ vs. field angle ϕ for Fe (blue) and Ni (red). In (a), at ϕ=0° and 90° field and magnetization are aligned. For intermediate values of ϕ the magnetization makes an angle of $\theta = (\phi_M - \phi)$ with the field. In (b) the spin accumulation has four pronounced minima (for Fe) at indicated ϕ values.*

where τ_s is the spin relaxation time and $\omega_L = g\mu_B B/\hbar$ is the Larmor frequency with g, μ_B and $\hbar$ being the Lande's g factor, Bohr magneton and reduced Planck constant respectively. In the limit $\omega_L\tau_s >> 1$ (due to large B = 50 kOe), the component of $\Delta\mu$ $\perp$ B is completely suppressed. Therefore in Eq. (6.2) the last term can be neglected. The net signal due to Hanle spin precession in the field will be:

$$\Delta\mu = \Delta\mu^0 \left[cos^2\theta\right] = \Delta\mu^0 cos^2(\phi_M - \phi). \tag{6.3}$$

where $\Delta\mu^0$ is the spin signal when ϕ_M = ϕ, i.e, when magnetization and field are perfectly aligned. Fig. 6.10 (b) shows the calculated $\Delta\mu$ vs. ϕ for Fe (blue) and Ni (red). There is a reduction of the spin signal with minima at ϕ=32.6°, 147.4°, 212.6° and 327.4° for the case of Fe. It is clear from Fig. 6.10 (a) that for Fe the angular separation, $\phi_M - \phi$ is larger than for Ni. This in turn causes the suppression (proportional to $\cos^2(\phi_M - \phi)$) of the signal in tunnel contacts with Fe to be more pronounced compared to those with Ni.

6.5.2 Fitting procedure

We found that the measured change in tunnel resistance , ΔR vs. ϕ can be fit using the following equation:

$$\Delta R = A_0 + A_1 cos(2\phi) + A_2 cos(6\phi) + \Delta R_{spin} cos^2(\phi_M - \phi), \tag{6.4}$$

where A_0 is a constant offset voltage, A_1 and A_2 are the fitting parameters. Reasonably good fits to the experimental data are obtained by considering the terms with two fold and six fold symmetry. The pre-factor [136] in the last term in the Eq. (6.4) represents the spin accumulation (i.e., ΔR_{spin}), which is modulated by a factor $cos^2(\phi_M - \phi)$, as noted in the previous section. The fits to the data using Eq. (6.4) are shown as solid lines in Figs. 6.3 and 6.5 for tunnel contacts with Fe and Ni, respectively. The parameters for the tunnel contacts with Fe are shown in Figs. 6.11 and 6.12, and for those with Ni in Fig. 6.13.

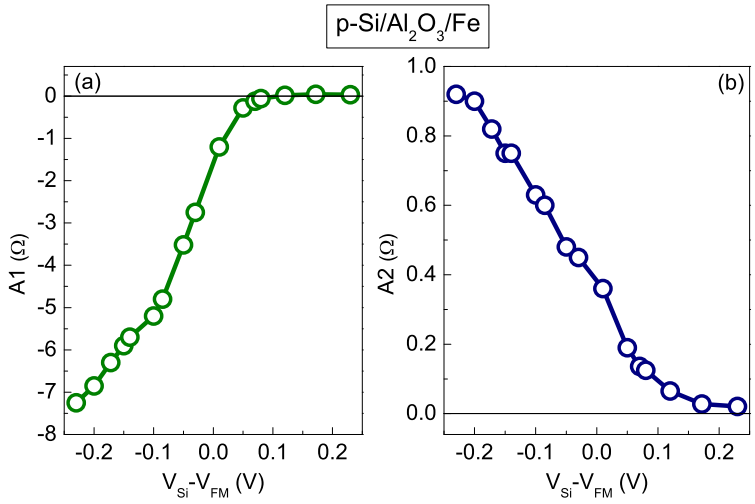

Figure 6.11: *Fitting parameters (a) A_1 and (b) A_2 in Ω as a function of bias for p-Si/Al_2O_3/Fe tunnel contact.*

We first discuss the results for tunnel contact on p-Si with Fe. At negative bias, A_1 is negative and reduces linearly as the bias voltage approaches zero. It changes sign at positive bias and thereafter does not vary much. Moving along positive bias (hole extraction), A_2 decays linearly up to 100 mV. Beyond that it becomes very small and close to zero. For the tunnel contact on n-Si with Fe, we find that A_1 changes sign and has a complex variation with bias voltage. A_2 reduces with increasing bias, and in the same way for positive and negative bias.

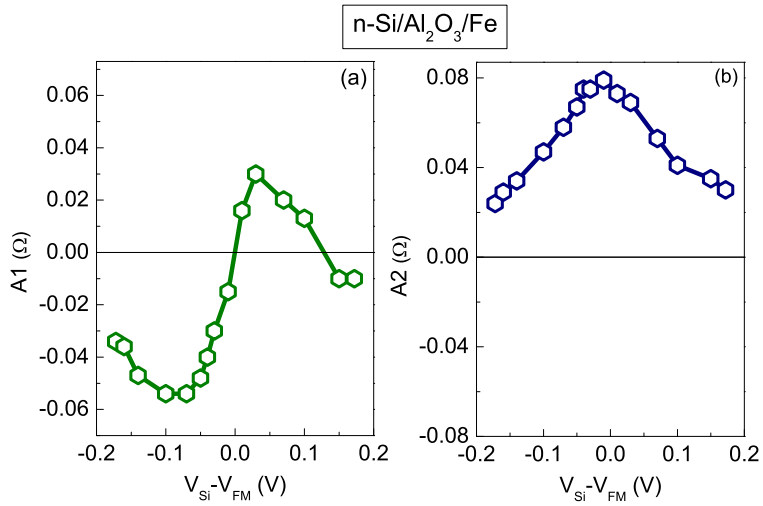

Figure 6.12: *Fitting parameters (a) A_1 and (b) A_2 as a function of bias for n-Si/Al_2O_3/Fe tunnel contact.*

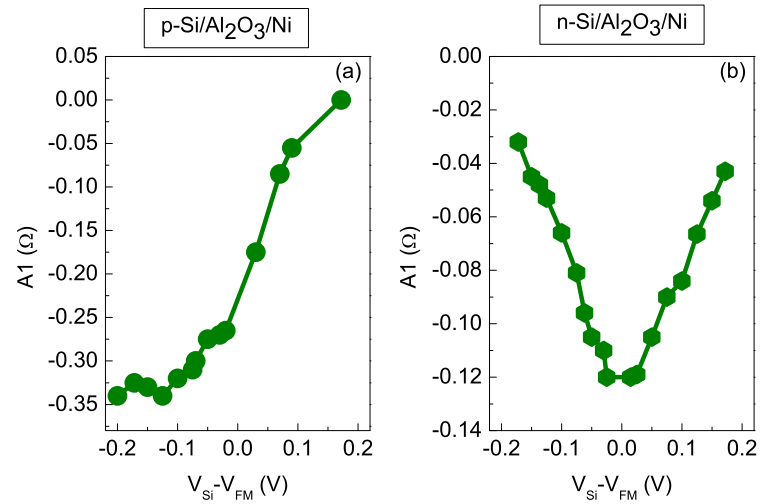

Figure 6.13: *Fitting parameter A_1 as a function of bias for (a) p-Si/Al_2O_3/Ni and (b) n-Si/Al_2O_3/Ni tunnel contacts.*

Figs. 6.13 (a) and (b) display the parameter A_1 for p-Si/Al_2O_3/Ni and n-Si/Al_2O_3/Ni tunnel contacts, respectively. Note that the data for tunnel contacts with Ni can be

fitted without considering the terms with A_2 and ΔR_{spin} as the pre-factor.

As pointed out in the previous section, due to the small shape anisotropy energy of Ni, the last term in Eqn. 6.4 can be neglected. For Ni contacts on p-type silicon (Fig. 6.13a), A_1 is negative and increases for negative bias, whereas it decreases to zero for positive bias. For tunnel contact on n-Si (in Fig. 6.13 (b)), A_1 is negative and decays almost symmetrically with bias voltage.

6.5.3 Strategy for data interpretation

Here we describe the criteria that will be adopted for interpreting the fitting results obtained above. We use the following two arguments for separating the different origins of the signal.

1. The spin resistance ΔR_{spin} is proportional to the spin accumulation $\Delta\mu$ in the Si. Therefore, if any one of the fitting parameters (i.e, A_1 or A_2) behaves as a function of V, in the same way as ΔR_{spin} does, then we assume that the corresponding anisotropy comes from the anisotropic spin accumulation (term $V_{ASA}(\Delta\mu(\phi))$). The anisotropy in $\Delta\mu$ can come from either the anisotropic TSP of the ferromagnet/insulator interface or from an anisotropic spin-relaxation time τ_s in Si. These two sources can be distinguished as follows:

   (a) A contribution to the anisotropic τ_s inside the Si should be independent of the type of ferromagnet (Fe or Ni) used in tunnel contacts.

   (b) A contribution to the anisotropy from anisotropic TSP should be different for tunnel contacts with Fe and Ni.

2. If any one of the fitting parameter does not vary with V as the ΔR_{spin} does, and the fitting parameter depends on the ferromagnet, then it is due to the TAMR.

6.5.4 Discussion

1. Let us first consider the tunnel contacts with Fe. The last term in Eq. 6.4 with a pre-factor ΔR_{spin} is dominant only in tunnel contacts with Fe. It comes from the misalignment of the magnetization and external field due to shape anisotropy of the thin magnetic film. This leads to four pronounced minima in the signal via the $\cos^2(\theta)$ term. Therefore this term partially accounts for the anisotropic spin accumulation inside Si.

2. The term A_2 with 6-fold symmetry is present in tunnel contacts with Fe and absent in those with Ni. Furthermore, A_2 has a bias variation similar to the

spin resistance ΔR_{spin}, implying that this anisotropy originates from the spin accumulation. Since the anisotropy with 6-fold symmetry is absent in Ni, a contribution due to anisotropic spin-relaxation time in Si is unlikely because it is not likely that contributions from TASP and anisotropic τ_s cancel at all bias voltages. We thus conclude that 6-fold anisotropy is due to anisotropy of $\Delta\mu$ arising from the anisotropic TSP of the magnetic tunnel contact.

3. In tunnel contacts with n-Si and Fe, A_1 does not vary with V as ΔR_{spin} does. Thus, A_1 has a contribution from TAMR and this is responsible for the change in a sign of the tunneling anisotropy.

4. The parameter A_1 (for p-Si) with two-fold symmetry has a polarity that is opposite to the tunneling anisotropy and spin resistance. A part of A_1, along positive V, does not vary with V as ΔR_{spin} does. This implies that A_1 has contributions due to anisotropic TSP of the FM and TAMR. The TAMR is responsible for the bias-induced inversion[130] of A_1, and gives rise to the experimentally observed change in tunneling anisotropy.

5. Let us now consider the tunnel contacts on n and p-Si with Ni electrode for which only two-fold anisotropy is observed. A_1 varies with bias voltage similar to the tunneling anisotropy and ΔR_{spin}, except that the polarity is opposite. This indicates that A_1 is due to the anisotropic spin accumulation $\Delta\mu$ in the Si. Furthermore, for tunnel contacts on n-Si with Fe and Ni, the bias variation of the tunneling anisotropy is different. Therefore, the term A_1 and the tunneling anisotropy in these tunnel contacts must have a contribution from anisotropic TSP of the ferromagnet/tunnel barrier interface. However, note that the presence of an additional contribution from an anisotropic τ_s cannot be excluded.

6. For tunnel contacts on p-Si with Fe and Ni, the tunneling anisotropy and ΔR_{spin} have similar variation with the bias voltage. The term A_1 with two fold symmetry decays similar to the tunneling anisotropy and ΔR_{spin}, but has opposite polarity. In tunnel contacts with Fe, the tunneling anisotropy and A_1 change sign along positive bias. This implies that for tunnel contact with Fe, the tunneling anisotropy and A_1 have contributions due to an ASA and TAMR. The TAMR is responsible for bias-induced inversion of the tunneling anisotropy and also A_1. The relative ratio $A_1/\Delta R_{spin}$ for tunnel contacts on p-Si with Fe and Ni is ≈ 0.43 and 0.087, respectively. This difference implies that the observed anisotropy must have a contribution from the anisotropy of the TSP of the ferromagnet/tunnel barrier interface. However, the presence of an additional contribution from an anisotropic τ_s cannot be excluded.

A brief summary of the conclusions is given in Table 6.1.

Table 6.1: *Summary of the different sources of tunneling anisotropy identified in this work for different tunnel contacts.*

Device	Fitting parameter	TAMR	ASA	
			TASP	τ_s
p-Si/Al_2O_3/Fe	A_1 (2ϕ)	yes	yes	possibly
	A_2 (6ϕ)	no	yes	no
n-Si/Al_2O_3/Fe	A_1 (2ϕ)	yes	yes	possibly
	A_2 (6ϕ)	no	yes	no
p-Si/Al_2O_3/Ni	A_1 (2ϕ)	no	yes	possibly
n-Si/Al_2O_3/Ni	A_1 (2ϕ)	no	yes	possibly

Let us finally compare the terms having two-fold and six-fold symmetry with the literature. Metal magnetic tunnel junctions with one FM electrode have shown two-fold symmetry of the anisotropy[127]. In addition, two-fold and four-fold symmetry has been observed for MTJ's with two FM electrodes[128]. These features are attributed to TAMR due to anisotropic density of states at the tunnel interface. The six-fold anisotropy term we observe here is, as shown, due to the spin accumulation in the Si, and is therefore not observed in metal MTJ's. The precise origin of the six-fold term is still unclear and requires further investigations.

6.6 Conclusions

We have observed out-of-plane tunneling anisotropy in Si/Al_2O_3/FM tunnel contacts. We find that different contributions to the tunneling anisotropy coexist. These can be distinguished using tunnel contacts on n as well as p-type silicon and different ferromagnets (Fe and Ni). We found that an important source of anisotropy comes from the anisotropy of the tunnel spin polarization (TASP) of the ferromagnet/tunnel barrier interface. It makes the spin accumulation in the silicon dependent on the absolute orientation of the magnetization of the magnetic layer. We did not find any conclusive evidence for anisotropy of the spin lifetime in silicon. Although the presence of a contribution from this mechanism cannot be excluded. The presence of tunneling anisotropic magnetoresistance (TAMR) in tunnel contacts with Fe gives rise to a bias-induced sign inversion of the tunneling anisotropy. In comparison, tunnel contacts with Ni do not display such a sign inversion of the tunneling anisotropy.

Chapter 7

Tunneling anisotropy in crystalline Si/MgO/Fe devices

In the previous chapter, we described the *out-of-plane* tunneling anisotropy in Si based magnetic tunnel devices with an amorphous Al_2O_3 as a tunnel barrier. In this chapter, we describe the influence of the crystalline order on the tunneling anisotropy when the magnetization of the magnetic layer is rotated within the plane of layer. We study the *in-plane* tunneling anisotropy in Si based tunnel devices with crystalline and polycrystalline MgO/Fe magnetic tunnel contacts. In addition magnetic tunnel devices on Si with an amorphous Al_2O_3 tunnel barrier and polycrystalline ferromagnetic electrode are also investigated. Out-of-plane tunneling anisotropy is studied only for crystalline Fe/MgO/Si tunnel devices. To rule out the spurious signals we present Hanle, inverted Hanle and tunneling anisotropy measurements on a control device that uses a non-magnetic layer (Au) between the ferromagnet and tunnel barrier.

The content of this chapter has previously been published in
S. Sharma, A. Spiesser, H. Saito, S. Yuasa, B.J. van Wees and R. Jansen, Phys. Rev. B **87**, 085307 (2013).

7.1 Introduction

In the field of semiconductor spintronics[14, 34, 35] remarkable progress has been made during the last few years, in particular with silicon[50, 51]. Magnetic tunnel contacts have emerged as a robust approach to inject and detect spin accumulation in a semiconductor (SC) at room temperature [29, 100], and significant understanding of the physics of spin transport across a magnetic tunnel contact to a semiconductor has been obtained[50, 51]. The progress in silicon spintronics has also stimulated research activities with other technologically important semiconductor materials, such as Ge[32, 93, 96, 97], while a variety of oxides (Al_2O_3 [29], SiO_2 [33] and crystalline MgO [30, 32, 93, 96, 110] have been successfully employed as tunnel barrier in spin tunnel contacts to a SC.

Calculations have predicted very high tunneling magnetoresistance[105, 106] (TMR) for crystalline Fe/MgO/Fe magnetic tunnel junctions (MTJs), and large room temperature TMR has indeed been realized[102, 137]. The high tunnel spin polarization (TSP) also makes the crystalline Fe/MgO system of interest for use in magnetic tunnel contacts to a semiconductor. Besides the large TSP, the crystalline nature of the contacts may also cause anisotropy in the TSP, as found previously for epitaxial (Ga,Mn)As/GaAs contacts[132]. For Si, anisotropy between in-plane and out-of plane magnetization has recently been reported for devices with an amorphous Al_2O_3 tunnel barrier (see Ch-6 and Ref.[138]). However, anisotropy of spin tunneling in MgO-based tunnel contacts to Si has not yet been investigated. Since the anisotropy ultimately arises from spin-orbit interaction, it is of interest to investigate the tunneling anisotropy (TA) in silicon devices with crystalline MgO/Fe tunnel contacts.

In this chapter, we describe the anisotropy of spin accumulation in silicon arising from the anisotropy of spin-polarized tunneling in crystalline Fe/MgO/Si tunnel devices, when the magnetization is rotated either *in-plane* or *out-of-plane*. For out-of-plane rotation of the magnetization, the tunnel resistance does not follow a simple cosine variation, implying that signals of different origin coexist. These tunnel devices also display an in-plane anisotropy with fourfold symmetry that reflects the cubic structure of the crystalline Si/MgO/Fe device. Surprisingly, we also observe in-plane anisotropy in silicon devices with an amorphous Al_2O_3 tunnel barrier and polycrystalline ferromagnet, suggesting a new mechanism of tunneling anisotropy. We attribute it to coherent spin-polarized tunneling across the contact, such that the anisotropy of the tunneling process reflects the cubic symmetry of the crystalline silicon electrode.

This chapter is organized as follows. Section. 7.3 describes the measurement principle. In Sec. 7.4, we first describe the experimental results for *out-of-plane* tunneling anisotropy in crystalline p-type Si/MgO/Fe tunnel devices. Then we describe the fitting procedure and discuss the results. This is followed by the data on *in-plane*

tunneling anisotropy obtained on magnetic tunnel contacts with a crystalline MgO/Fe contact, and with polycrystalline MgO or an amorphous Al_2O_3 barrier. At the end of this section similar measurements on a control device with zero TSP are shown. A summary is included at the end of the article in Sec. 7.7.

7.2 Device fabrication and structural characterization

Device fabrication and structural analysis for Fe/MgO/Si devices have been described in chapter 4. Details of fabrication of Si/Al_2O_3/ferromagnet tunnel devices can be found in chapter 3. In this chapter, we only describe the experimental results on tunneling anisotropy in the magnetic tunnel devices with crystalline, polycrystalline or amorphous tunnel barrier. It should be noted that all measurements have been performed on tunnel devices with contact area of 100×200 μm^2.

7.3 Measurement principle

Two types of anisotropy measurements, namely the field scan and the angle scan have been performed. In the field scan, the angle ϕ_{out} between applied field and the surface normal [see Fig. 7.1(a)] is kept fixed while varying the field strength. The Hanle [29] curve is obtained with the magnetic field perpendicular to the tunnel interface (i.e., ϕ_{out} = 0°, 180° and 360°) and the magnetization lying in the plane of the ferromagnetic layer. On the other hand, with a field parallel to the tunnel interface (i.e., ϕ_{out} = 90° and 270°) and the magnetization still in the plane of the layer, an inverted Hanle curve is obtained[56]. In the second type of measurement, the angle scan, the field strength is fixed at 50 kOe, and the direction of the field is changed by rotating the sample. This rotation can be done in the *out-of-plane* direction (i.e., by varying ϕ_{out}) or in the *in-plane* direction. For the latter, the in-plane field angle ϕ_{in} is defined as the angle between the field (or the magnetization direction) and the (100) crystal axis of the Si electrode, [Fig. 7.1(b)]. For fields of 50 kOe applied in-plane, the magnetization is always pointing along the field direction. However, with the applied field out-of-plane and $0° < \phi_{out} < 90°$, the magnetization of the magnetic thin film makes a finite angle θ=(ϕ_M-ϕ_{out}) with the applied field due to shape anisotropy[138] (see also Sec. 7.4.2). Here, ϕ_M represents the angle between the magnetization direction ($\vec{m}$) and the surface normal [Fig. 7.1(a)].

In Fig. 7.1, we depict the measurement geometry using the three-terminal method for spin injection and detection[29]. A constant current I_{bias} results in a voltage $V = V_{Si}$-V_{FM} across the tunnel contact. We adopt the bias convention such that $V < 0$ (or > 0) corresponds to hole injection (extraction) into (from) the valence band of p-type silicon. By changing the angle ϕ_{out} (or ϕ_{in}), and applying a fixed

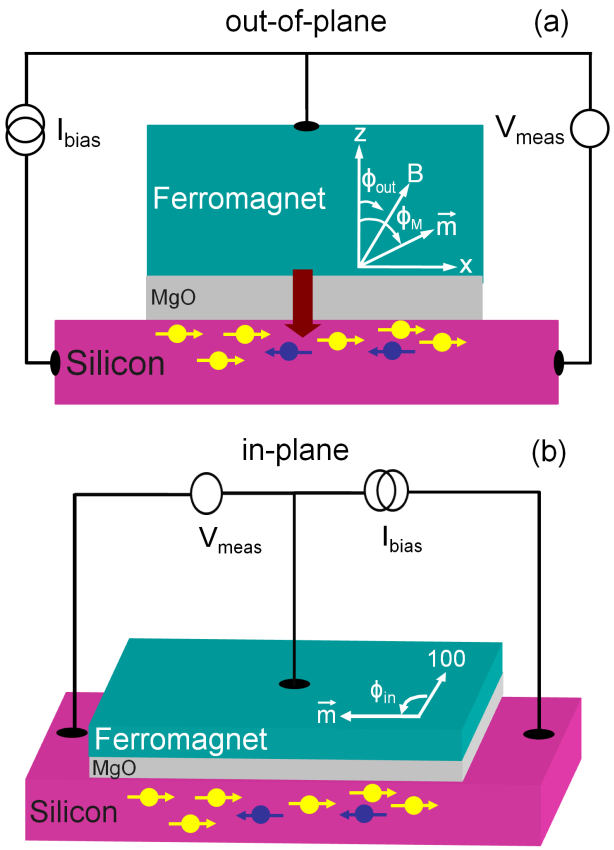

Figure 7.1: *Schematic of the three-terminal technique employed for measuring the* **(a)** *out-of-plane and* **(b)** *in-plane tunneling anisotropy. A constant current (I_{bias}), across the tunnel contact results in a voltage (V_{meas}), that changes when the magnetization is rotated, either from in-plane to out-of-plane or within the plane of the magnetic layer. In (a), ϕ_{out} represents the angle between the applied magnetic field and the surface normal, while ϕ_M is the angle between the magnetization ($\vec{m}$) and the surface normal directed along Z axis. The in-plane component of the magnetization lies along X. In (b), ϕ_{in} is the angle between the field (or magnetization) direction and the (100) crystal axis of the silicon.*

bias current I_{bias}, across the tunnel contact, the voltage is V_{meas} = V_0 + V_{TAMR} + $V_{ASA}(\Delta\mu(\phi_{out}, \phi_{in}))$. The first term on the right-hand side is a constant voltage. The second term (V_{TAMR}), is due to the regular tunneling anisotropic magnetoresistance [34, 122, 124, 125] (TAMR). This TAMR refers to the change in the tunnel resistance when the magnetization of the magnetic layer is rotated (either within the plane of the magnetic layer or rotated from in-plane to out-of-plane). The anisotropy origi-

nates from spin-orbit interaction at the interface between the ferromagnet and the tunnel barrier. The last term $V_{ASA}(\Delta\mu(\phi_{out}, \phi_{in}))$ refers to a voltage signal arising from an anisotropic spin accumulation (ASA), i.e., a spin accumulation $\Delta\mu(\phi_{out}, \phi_{in})$ that depends on ϕ_{out} and/or ϕ_{in}. This can be expected if the tunnel spin polarization of the magnetic contact is anisotropic which leads to a spin accumulation $\Delta\mu$ in the silicon that depends on ϕ_{out} and/or ϕ_{in}. In addition, an anisotropic spin-relaxation time τ_s in the silicon will also results in an anisotropy of $\Delta\mu$.

7.4 Out-of-plane tunneling anisotropy

We performed *out-of-plane* as well as *in-plane* tunneling anisotropy measurements on magnetic tunnel devices made on p-type silicon with crystalline MgO/Fe tunnel contact. On the other hand, only in-plane tunneling anisotropy measurements will be shown for tunnel contacts with amorphous Al_2O_3 and polycrystalline ferromagnetic layer. For the latter case, a detailed study of the *out-of-plane* tunneling anisotropy has been reported in chapter 6 and Ref.[138].

7.4.1 Crystalline MgO/Fe tunnel contacts to Si

The Hanle and inverted Hanle measurements are shown in Fig. 7.2(a) for a spin-tunnel contact with a 2.5 nm-thick MgO as a tunnel barrier. The field scan with the direction perpendicular to the tunnel interface results in a symmetric Hanle (red) peak around zero field. By increasing the field, the spin precession reduces the signal. A further increase of the field results in an upturn in the signal due to rotation of the magnetization of the ferromagnet towards the out-of-plane direction.

Approximately after 22 kOe, when the magnetization has aligned itself with the external field, meaning that there is no more spin precession, the signal settles (it increases only slightly with a linear slope, which is attributed to a background signal). On the other hand, when the applied field is parallel to the tunnel interface, the inverted Hanle curve (blue) is obtained. The inverted Hanle curve exhibits a suppression of the spin signal in the absence of external field due to spin precession in spatially inhomogeneous local magnetostatic fields arising from finite-roughness of the interface of the ferromagnetic layer[56]. At sufficiently large in-plane field, the signal recovers and becomes independent of the external field.

At 50 kOe, irrespective of the field direction, there is no spin precession because the magnetization, external field and spins injected into silicon all have the same orientation. Nevertheless, the Hanle and inverted Hanle curves settle at two different levels. As shown in Fig. 7.2(a), at 50 kOe these curves have a difference of about $\approx$ 440 μV. This result is reproduced in the angle scan measurement shown in Fig. 7.2(b)

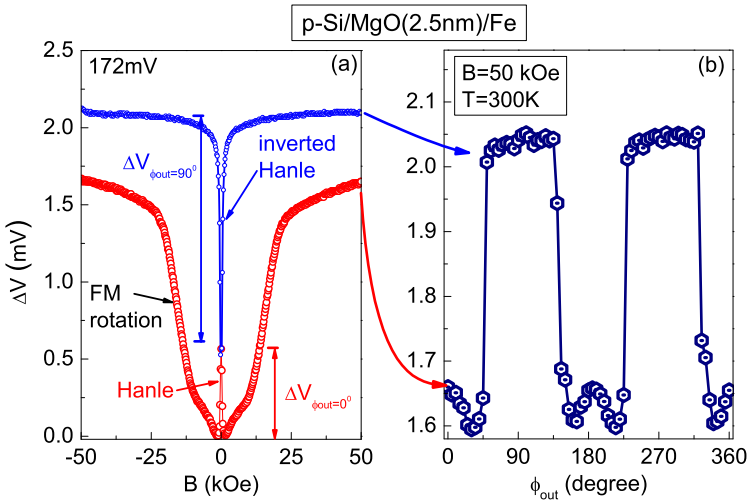

Figure 7.2: *Experimental data for crystalline p-Si/MgO/Fe tunnel contact. Data with field* **(a)** *perpendicular (Hanle, red) and parallel (inverted Hanle, blue) to the tunnel interface.* $\Delta V_{\phi_{out}=0^\circ}$ *and* $\Delta V_{\phi_{out}=90^\circ}$ *are the Hanle and inverted Hanle signal amplitudes, respectively.* **(b)** *Angular variation of the measured signal (for out-of-plane rotation of the magnetization) at same bias voltage. Data is shown after subtracting an offset of 172 mV (*I_{bias} *= 389* μA*).*

taken with a constant field of 50 kOe. Thus, the situations when the field is parallel or perpendicular to the tunnel interface are not equivalent. That is, there is an anisotropy in the measured voltage. It depends on the absolute orientation of the magnetization of the ferromagnetic electrode. Further, the angle scan in Fig. 7.2(b) shows that the measured voltage has a non-sinusoidal variation with the field angle. This suggests that different contributions to the tunneling anisotropy co-exist, as noted previously for tunnel contacts with amorphous Al_2O_3 barrier in chapter 6 and Ref.[138].

For the same tunnel device, Fig. 7.3 shows the bias variation of the change in resistance ΔR = R(ϕ_{out})- R($\phi_{out} = 0^\circ$), where R(ϕ_{out})= V_{meas}/I_{bias} is the resistance at a field angle ϕ_{out}. The tunnel resistance has four local minima at $\approx 40^\circ$, 160°, 215° and 340° for all bias voltages. Another two local minima can be seen at $\approx 90^\circ$ and $\approx 270^\circ$ but only for negative bias voltages. Nevertheless, the overall shape of the signal does not change much with bias voltage.

7.4.2 Analysis and discussion of out-of-plane anisotropy

For further analysis, we compare the anisotropy with the spin resistance, defined as ΔR_{spin}=[$\Delta V_{\phi_{out}=0^\circ}$+ $\Delta V_{\phi_{out}=90^\circ}$]/$I_{bias}$, where $\Delta V_{\phi_{out}=0^\circ}$ and $\Delta V_{\phi_{out}=90^\circ}$ are

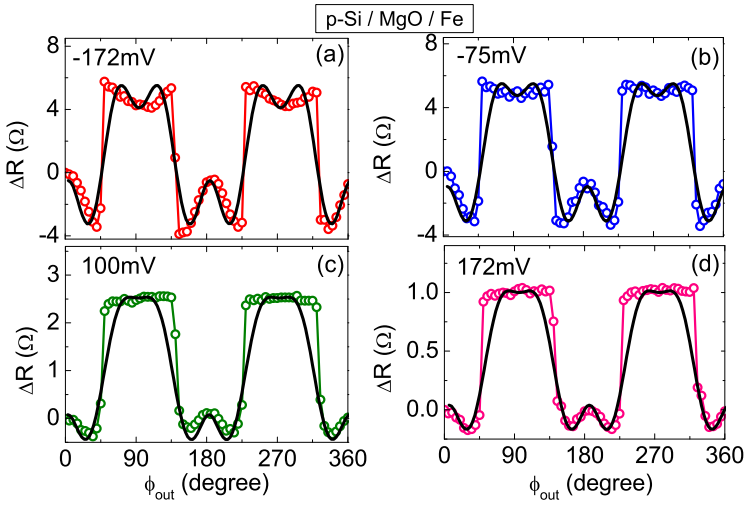

Figure 7.3: *Angular variation of the change in the tunnel resistance ΔR = R(ϕ_{out})-R($\phi_{out} = 0^{\circ}$), when the magnetization is rotated out-of-plane at* **(a)** *-172 mV* **(b)** *-75 mV* **(c)** *100 mV and* **(d)** *172 mV. All data were taken at 300 K and a field of 50 kOe. Solid black lines represent the fits obtained using Eqn. 7.1 described in the text.*

defined as the Hanle and inverted Hanle signal amplitudes as shown in Fig. 7.2(a). The quantity ΔR_{spin} is proportional to the spin accumulation. The bias variation of the spin resistance is shown in Fig. 7.4(a). As observed earlier[29, 120], the spin resistance is larger for V $<$ 0 (hole injection) and decays almost linearly for V $>$ 0 (hole extraction). We compare this to the *out-of-plane* anisotropy signal, i.e., $\Delta R_{out} = R_{\phi_{out}=90^{\circ}} - R_{\phi_{out}=180^{\circ}}$, shown in Fig. 7.4(c). It has a bias variation similar to spin resistance. We also define the *out-of-plane* tunneling anisotropy (TA) as [R($\phi_{out} = 90^{\circ}$)-R($\phi_{out} = 180^{\circ}$)]/R($\phi_{out} = 180^{\circ}$). As shown in Fig. 7.4(b) the tunneling anisotropy decays almost symmetrically with bias voltage. Finally, the regular resistance of the contact versus bias voltage is shown in Fig. 7.4(d). The junction resistance decreases for positive bias voltage whereas it is increasing for the negative bias voltages.

Next, we describe the fitting of the experimental data with an equation containing terms arising from an anisotropic spin accumulation, Hanle spin precession and/or TAMR. As found earlier for devices with Al_2O_3 tunnel barrier [124, 138], the measured tunnel resistance for out-of-plane rotation of the magnetization can be described by an equation that consists of terms with twofold and sixfold symmetry:

$$\Delta R = A_0 + A_1 cos(2\phi_{out}) + A_2 cos(6\phi_{out}) + \Delta R_{spin} cos^2(\phi_M - \phi_{out}), \quad (7.1)$$

where A_0 is a constant offset and A_1 and A_2 are the fitting parameters[136]. The

factor $\cos^2(\phi_M - \phi_{out})$ in the last term on the right hand side is due to the small misalignment between field and magnetization arising from magnetic shape anisotropy of the thin magnetic layer[138]. The magnetic shape anisotropy of a thin ($\approx$ 20nm) ferromagnetic film, favors a magnetization direction parallel to the surface, i.e., within the film plane, whereas an external field of 50 kOe favors the magnetization to align with it. As a result the external field and the magnetization are not perfectly aligned, but they make a different angle ϕ_{out} and ϕ_M [Fig. 7.1(a)] with the surface normal, respectively[138]. Due to this misalignment of the magnetization and the external field, the spins injected into silicon make an angle $\theta = \phi_M - \phi_{out}$ with the field, thereby leading to the spin precession in Si even at a field of 50 kOe. As a result, the

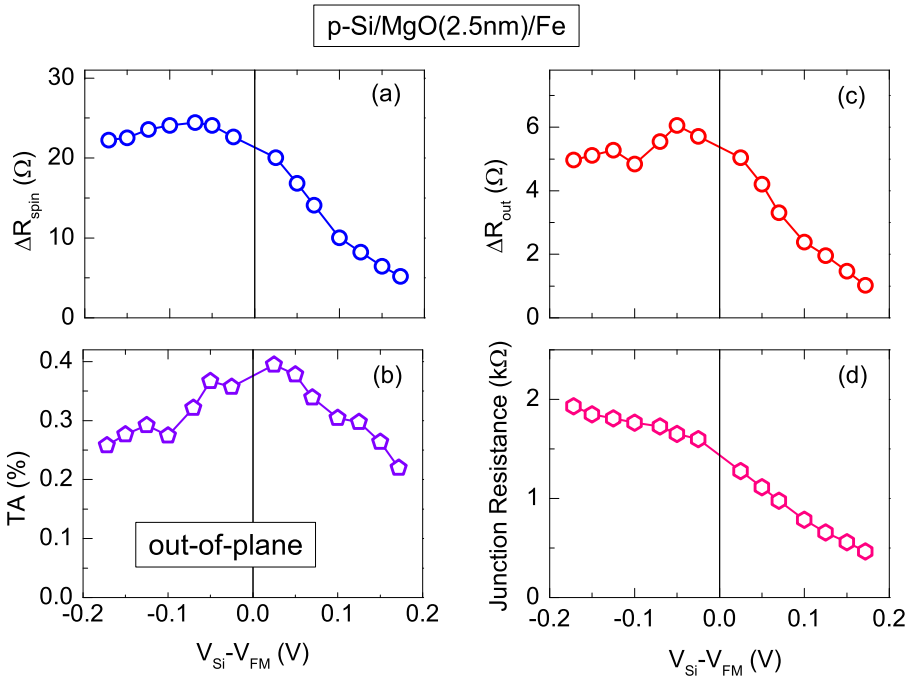

Figure 7.4: *Bias variation of* **(a)** *the spin resistance,* $\Delta R_{spin} = [\Delta V_{\phi_{out}=0^\circ} + \Delta V_{\phi_{out}=90^\circ}]/I_{bias}$, **(b)** *the tunneling anisotropy,* **(c)** *the change in resistance* ΔR_{out}=($R_{\phi_{out}=90^\circ}$-$R_{\phi_{out}=180^\circ}$) *and* **(d)** *the junction resistance* (V_{meas}/I_{bias}) *for a p-type Si/MgO/Fe tunnel device. Note that* $\Delta V_{\phi_{out}=0^\circ}$ *and* $\Delta V_{\phi_{out}=90^\circ}$ *have been defined in Fig. 7.2(a).*

net signal due to Hanle spin precession in the external field will be proportional to $\Delta R_{spin}\cos^2(\phi_M - \phi_{out})$.

The fits to the data using Eq. (7.1) are shown as solid black lines in Fig. 7.3. Rea-

sonably good fitting to the data can be achieved by considering terms with twofold and sixfold symmetry. It is found that inclusion of a tenfold term improves the fitting with the data (not shown), but it does not effect the other terms. We therefore limited ourselves to terms up to sixfold symmetry. The fitting parameters A_1 and A_2 for this tunnel contact are shown in Fig. 7.5. The A_1 is negative, over the full bias range. It is almost constant for $V < 0$ and reduces linearly for $V > 0$. On the other hand, A_2 is positive and decays towards positive bias.

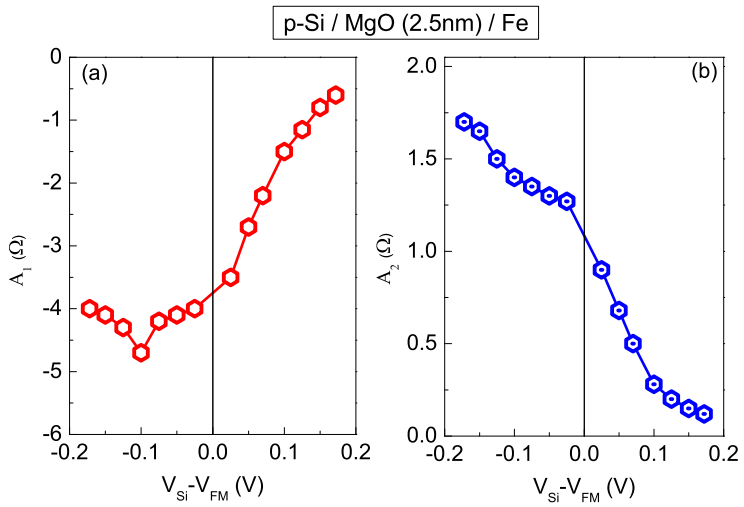

Figure 7.5: *(Color online) Bias variation of fitting parameters A_1 and A_2 corresponding to the out-of-plane tunneling anisotropy of a p-type Si/MgO/Fe tunnel device.*

For the interpretation of these results, we will use the following criteria [138]. The spin resistance ΔR_{spin} is proportional to the spin accumulation $\Delta\mu$ in the silicon. Thus, if any of the fitting parameters (i.e., A_1 or A_2) behaves as a function of bias in the same way as ΔR_{spin} does, then we assume that the corresponding anisotropy comes from the anisotropic spin accumulation term $V_{ASA}(\Delta\mu(\phi_{out}))$. Ignoring the polarity, the term A_1 with twofold symmetry has a bias variation similar to ΔR_{spin}, but also to the junction resistance. Also the term A_2 with sixfold symmetry has a bias variation similar to ΔR_{spin} as well as to junction resistance. The behavior of A_1 seems to follow that of ΔR_{spin} more closely except that polarity is opposite. It suggests that A_1 is due to an anisotropic spin accumulation in the silicon. On the other hand, the bias variation of the term A_2 resembles with the junction resistance as well as ΔR_{spin}. The former case implies a contribution due to TAMR whereas in the latter case anisotropic spin accumulation may result in same bias variation. Due to small difference in bias variation of these parameters different contributions (i.e.,

TAMR and spin-accumulation) cannot be distinguished.

7.5 In-plane tunneling anisotropy

In-plane tunneling anisotropy refers to the change in the tunneling resistance when the magnetization is rotated within the plane of the magnetic layer. We measure the signal in three-terminal configuration by rotating the sample (i.e., by changing the angle ϕ_{in}, see Fig. 7.1(b) in an in-plane field of 50 kOe which is large enough to ensure that the magnetization lies always along the field direction. Devices with crystalline and polycrystalline MgO/Fe tunnel contacts as well as those with an amorphous Al_2O_3 as a tunnel barrier and polycrystalline ferromagnet have been evaluated to investigate the exact source of in-plane tunneling anisotropy. We begin with magnetic tunnel contacts to p-Si with crystalline MgO barrier.

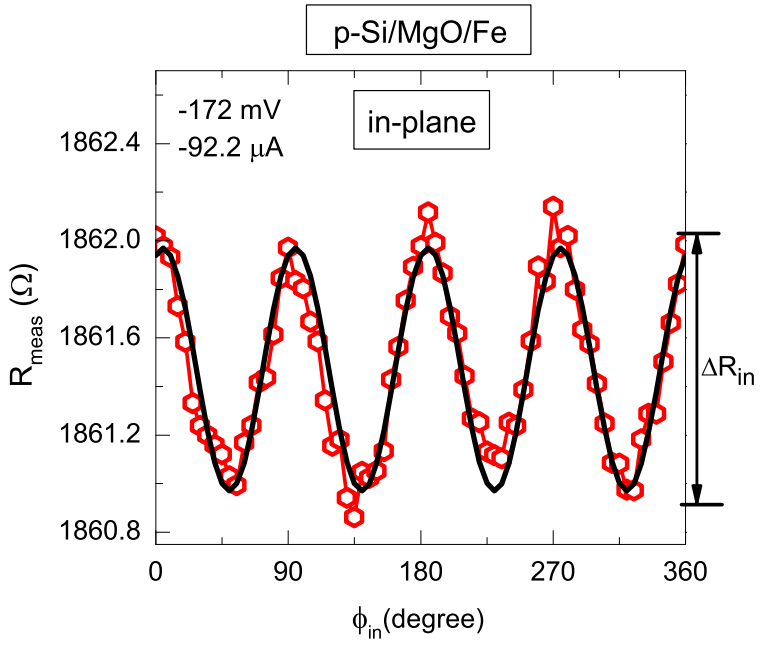

Figure 7.6: *Measured tunnel resistance R_{meas}=V_{meas}/I_{bias} vs. angle ϕ_{in} for a tunnel contact with 2.5 nm MgO at a bias voltages of -172 mV (-92.2 μA). Here ϕ_{in} refers to the in-plane angle between the magnetization and the (100) crystal axis of the Si electrode, (see, Fig. 7.1(b)). Data was taken at T = 300 K.*

7.5.1 Tunnel contacts with crystalline MgO barrier

A typical measurement on a crystalline MgO/Fe tunnel contact with 2.5 nm of MgO is shown in Fig. 7.6, taken at a bias voltage (current) of -172 mV (-92.2 μA). The tunnel resistance displays an in-plane anisotropy with fourfold symmetry. It has four minima at $\approx 45°$, 135°, 225° and 315°.

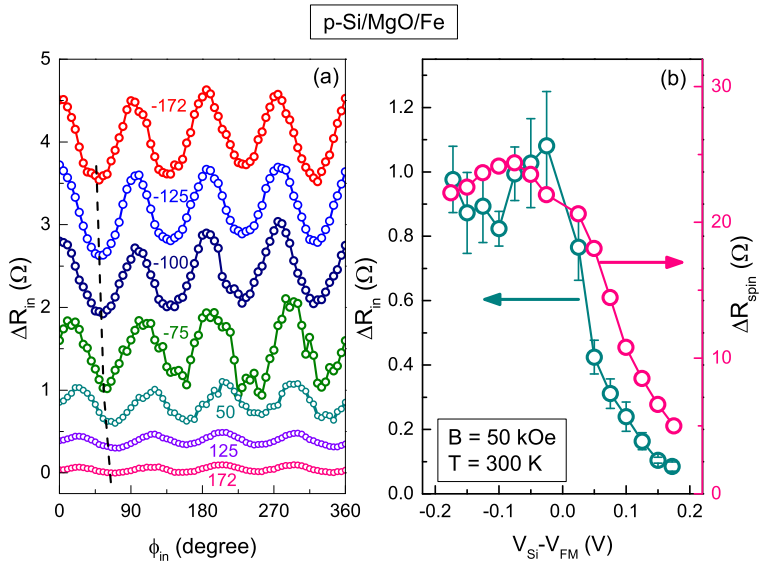

Figure 7.7: **(a)** *Change in resistance (ΔR_{in}) at different bias voltages (in mV) when the magnetization is rotated in the plane of the magnetic layer. Data are displaced vertically for clarity. The black dotted line indicates the shift of the first minima position when the bias voltage is changed from -172 mV to 172 mV. Note that vertical scale is the measured negative voltage.* **(b)** *Bias variation of ΔR_{in} shown together with ΔR_{spin}. Note that ΔR_{in} is the peak-to-peak change in tunnel resistance when the magnetization is rotated within the plane of the magnetic layer. All data were taken at 300 K.*

We define the anisotropy in the tunneling resistance ΔR_{in} as the maximum peak-to-peak change in tunnel resistance when the magnetization is rotated within the plane of the magnetic layer [see Fig. 7.6]. In Fig. 7.7(a), bias variation of the change in tunnel resistance is shown. A fourfold symmetry is obtained at all bias voltages. At -172 mV, the first minimum in resistance occurs at $\approx 45°$. By increasing the bias voltage from -172 mV to 172 mV, the first minimum position gradually shifts from 45° to 70°. The shift in the position of the minima is indicated by a black dotted line in Fig. 7.7(a). The bias variation of ΔR_{in} is shown together with the spin resistance ΔR_{spin} in Fig. 7.7(b). It is found that ΔR_{in} and ΔR_{spin} have the same qualitative

variation with bias voltage. For V < 0 (hole injection), ΔR_{in} does not vary much whereas it decays linearly for V > 0 (hole extraction).

7.5.2 Tunnel contacts with polycrystalline MgO barrier

The crystalline quality of the tunnel contacts has been found to influence the spin accumulation created in a semiconductor[110]. Here we examine the effect of crystalline structure of the tunnel contact on the in-plane tunneling anisotropy using a p-Si/MgO/Fe tunnel device with a polycrystalline MgO/Fe tunnel contact. A measurement at a fixed bias current of -582 μA (-172 mV) is shown in Fig. 7.8. We obtain a signal with fourfold symmetry and amplitude $\approx$ 40 μV, which is less than the signal ($\approx$100 μV) obtained for a tunnel device with a crystalline MgO/Fe contact.

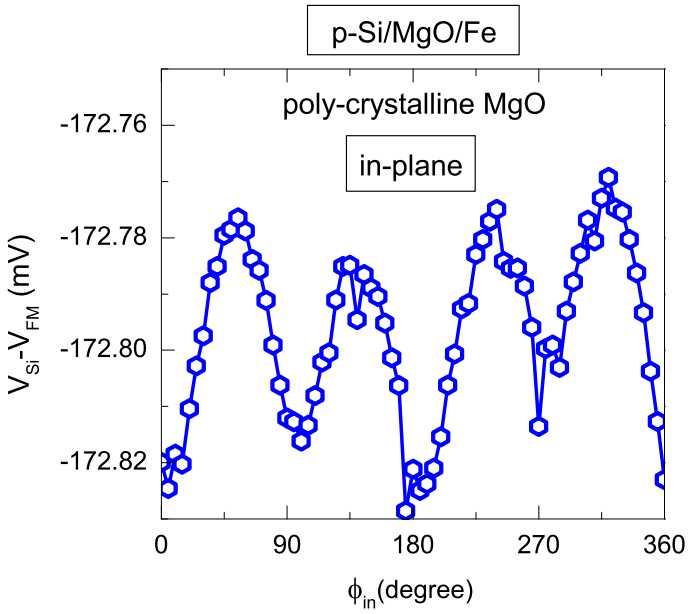

Figure 7.8: *(Color online) The angular variation in the measured voltage for in-plane rotation of the magnetization for a tunnel device on p-Si with polycrystalline MgO/Fe contact. The measurement was taken with a bias current I_{bias} = -582 μA (-172 mV) at 300 K. Note that the vertical scale is the measured (negative) voltage, and that the current is also negative, such that the maximum of resistance occurs at 0°, 90°, 180°, 270° and 360°, just as in Fig. 7.6.*

7.5.3 Tunnel contacts with amorphous Al_2O_3 barrier

The observed in-plane tunneling anisotropy may have different origins, e.g., anisotropic tunnel spin polarization of the magnetic contact and/or the anisotropic spin relaxation time τ_s in silicon[138]. In order to investigate the origin of the anisotropy, we study the devices with an amorphous tunnel barrier and polycrystalline ferromagnet. We performed angle scans on tunnel contacts to p-Si as well as n-Si which contain a polycrystalline ferromagnet (Fe or Ni or $Ni_{80}Fe_{20}$) and an Al_2O_3 tunnel barrier that is known to be amorphous[75, 139]. Fig. 7.9 displays angle scans for these tunnel devices at -172 mV. For the p-Si/Al_2O_3/Fe device, we observe a fourfold symmetry

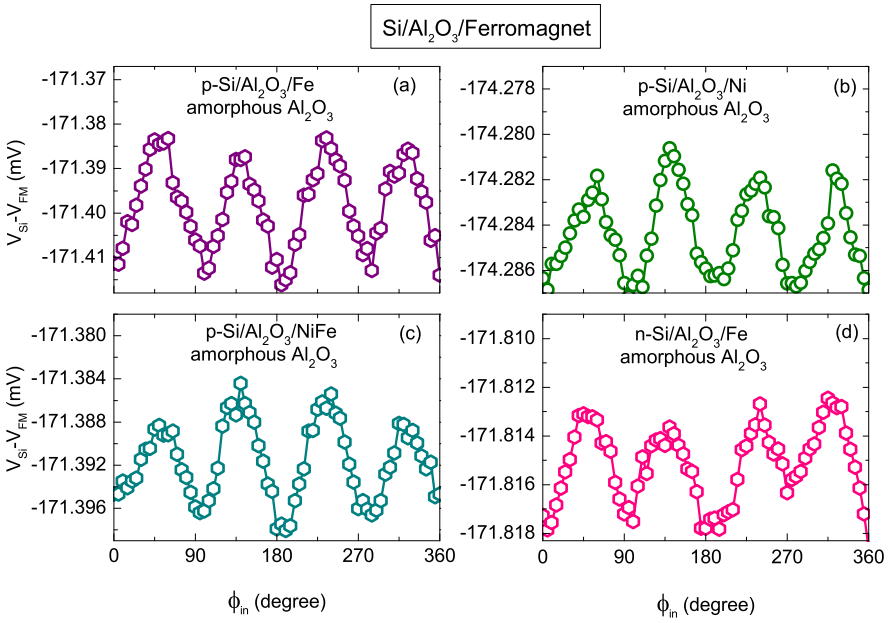

Figure 7.9: *The angular variation in the measured voltage for in-plane rotation of the magnetization for* **(a)** *p-Si/Al_2O_3/Fe at I_{bias} = -97.13 μA,* **(b)** *p-Si/Al_2O_3/Ni at I_{bias} = -192 μA,* **(c)** *p-Si/Al_2O_3/NiFe at I_{bias} = -480 μA,* **(d)** *n-Si/Al_2O_3/Fe at I_{bias} = -777 μA. Note that these devices have amorphous Al_2O_3 and polycrystalline ferromagnet. All measurements were taken at 300 K. Note that the vertical scale is the measured (negative) voltage, and that the current is also negative, such that the maximum of resistance occurs at 0°, 90°, 180°, 270° and 360°, just as in Fig. 7.6.*

with $\approx$ 20-25 μV change in the signal [Fig. 7.9(a)]. Similar fourfold features are observed for tunnel devices on p-type Si with Al_2O_3 barrier and Ni [Fig. 7.9(b)] and $Ni_{80}Fe_{20}$ [Fig. 7.9(c)] as ferromagnetic electrode. However, the change in signal is small, 4-6 μV and 8-10 μV for tunnel devices with Ni and $Ni_{80}Fe_{20}$ electrodes, re-

spectively. Finally, in Fig. 7.9(d), it is shown that a device with an Al_2O_3/Fe magnetic tunnel contact to n-type Si has the same fourfold symmetry, with a signal amplitude $\approx$ 4-6 μV.

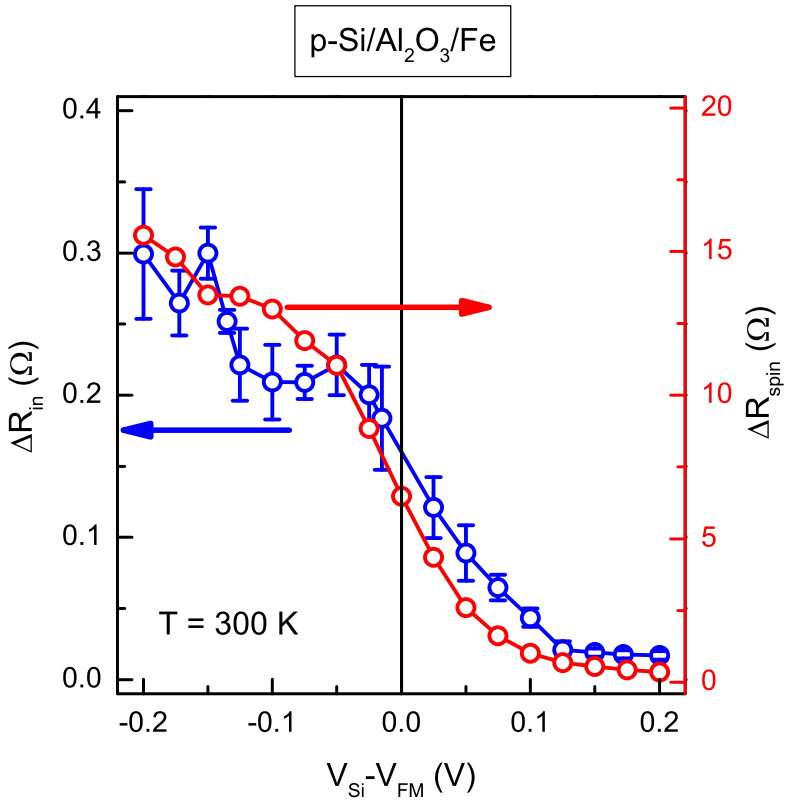

Figure 7.10: **(a)** *Bias variation of the in-plane anisotropy in tunnel resistance ΔR_{in} shown together with the spin resistance, i.e., ΔR_{spin} for a p-type Si/Al_2O_3/Fe tunnel device. Note that vertical axis is the measured negative voltage.*

For the p-Si/Al_2O_3/Fe tunnel contact the bias variation of ΔR_{in} is shown together with ΔR_{spin} in Fig. 7.10. We see that ΔR_{in} and ΔR_{spin} have qualitatively the same variation with bias voltage.

7.5.4 Discussion of in-plane tunneling anisotropy

In Table 7.1 we have collected the relevant parameters, i.e., the in-plane anisotropy signal ΔR_{in}, the tunnel resistance (R_{tun}=V_{meas}/I_{bias}) and the spin resistance ΔR_{spin},

obtained on the various tunnel devices at -172 mV. The magnitude of ΔR_{in} depends on the crystalline quality of the tunnel contact as can be seen from the ratios $\Delta R_{in}/R_{tun}$ and $\Delta R_{in}/R_{spin}$ for these devices.

Table 7.1: *Summary of the in-plane anisotropy data obtained at -172 mV on tunnel contacts to p-Si and n-Si. Here R_{tun} is the tunnel resistance, ΔR_{spin} is the spin resistance and ΔR_{in} is the maximum peak-to-peak signal for in-plane rotation of the magnetization.*

Parameters Units	ΔR_{in} (Ω)	R_{tun} (Ω)	$\Delta R_{in}/R_{tun}$ ($\%$)	ΔR_{spin} (Ω)	$\Delta R_{in}/\Delta R_{spin}$ ($\%$)
Crystalline MgO					
p-Si/MgO/Fe	0.976	1865	0.052	22.22	4.39
Polycrystalline MgO					
p-Si/MgO/Fe	0.077	295	0.026	2.44	3.15
Amorphous Al_2O_3					
p-Si/Al_2O_3/Fe	0.265	1811	0.015	14.72	1.8
p-Si/Al_2O_3/Ni	0.026	895	0.002	3.84	0.68
p-Si/Al_2O_3/NiFe	0.021	358	0.005	4.29	0.49
n-Si/Al_2O_3/Fe	0.006	221	0.003	0.44	1.46

The ratios of these parameters are larger for tunnel devices on p-type Si with crystalline MgO/Fe contact and smaller for the devices with an amorphous Al_2O_3 barrier and polycrystalline Fe as a magnetic electrode. An intermediate value is obtained for the device with a polycrystalline MgO/Fe contact. For the other devices on Si with Al_2O_3, the ratio of these parameters changes by a small amount but does not differ significantly. In crystalline tunnel contacts as well as those with polycrystalline ferromagnet and an amorphous tunnel barrier, the signal ΔR_{in} due to in-plane anisotropy is a few percent (2 to 5 $\%$) of the spin resistance (ΔR_{spin}) and ΔR_{in} qualitatively has the same bias variation as ΔR_{spin}. This suggests that the observed tunneling anisotropy is due to anisotropic spin accumulation in the silicon. Although the amplitude of the signal depends on the degree of crystallinity of the tunnel contact, in-plane rotation of the magnetization produces a change in tunnel resistance that has a fourfold symmetry for all the tunnel devices, irrespective of the type of ferromagnet, silicon (n or p-type) or crystalline structure of the tunnel contact. For the crystalline p-type Si/MgO/Fe tunnel devices, a fourfold in-plane symmetry is a natural consequence of the cubic crystal structure of the MgO/Fe contact. The crystalline MgO/Fe tunnel contacts on p-type Si display a fourfold symmetry with first minima at 45° at a bias of -172 mV. The minima positions gradually shifts to 70° with change in bias voltage. It is known that in the Fe/MgO system the states with different symmetries have different tunneling probability[105, 106]. Their relative contribution may

change with bias voltage and this may lead to a change in the position of the minima.

An in-plane TAMR or tunneling anisotropy was not expected in tunnel contacts with amorphous Al_2O_3 tunnel barrier and polycrystalline ferromagnet. However, these contacts also displayed fourfold in-plane symmetry. Below, we discuss the possible sources which may produce the observed in-plane tunneling anisotropy.

(a) An in-plane TA could arise if the Al_2O_3 tunnel barrier has a crystalline structure so that propagating states from the ferromagnet decay into the tunnel barrier with the symmetry of the ferromagnet/Al_2O_3 contact. Recently, evidence for crystalline growth of α-Al_2O_3 on silicon has been reported[112]. However, the Al_2O_3 has hexagonal structure. Thus, any in-plane anisotropy, if it exists, would not have the fourfold symmetry that we observe. More importantly, it is known that the Al_2O_3 and ferromagnet in our devices are, respectively, amorphous and polycrystalline[75, 139]. Therefore, we do not expect any kind of anisotropy arising from the crystallinity of the Al_2O_3/ferromagnet contact.

(b) An anisotropy of the spin-relaxation time (τ_s) in silicon will lead to an anisotropic spin accumulation. We discuss the possible mechanisms that may produce an anisotropy in the spin-relaxation time and hence in spin accumulation. In bulk and unstrained silicon the spin-relaxation time is expected to be isotropic[140]. The Dresselhaus type of spin-orbit coupling fields (SOCF) are absent for silicon due to its bulk inversion symmetry. However, due to symmetry breaking at the silicon interface, a contribution from Dresselhaus spin-orbit coupling can be present. This would produce an anisotropy in the spin-relaxation time with fourfold as well as twofold symmetry [see Fig. 4 of Ref.[124]]. Then, a twofold and fourfold anisotropy would be produced in the spin accumulation in the silicon. However, we observe only a fourfold anisotropy in the measured voltage, implying that this mechanism is absent.

Heterostructures such as Si/oxide/ferromagnet have a built-in potential gradient in the growth direction and hence an electric field perpendicular to the tunnel interfaces. This leads to an effective Rashba spin-orbit coupling field[124]. However, the magnitude of the Rashba field is isotropic within the plane of the interface, and will thus not generate an in-plane tunneling anisotropy.

(c) Given that the previous two mechanisms are not the source of the in-plane anisotropy, we attribute the anisotropy to a different mechanism that can arise if the tunneling process is coherent. In that case, the propagating states from the ferromagnet couple directly to empty states in the Si. The tunneling states thereby “inherit" part of the character and crystal symmetry of the Si electrode, which is a crystalline wafer with (001) orientation. Together with spin-orbit

interaction at the ferromagnet/oxide interface, this may produce an in-plane cubic anisotropy of the tunneling spin polarization, and thereby of the spin accumulation. We suggest that this mechanism, that has previously not been considered, can produce a crystal-induced anisotropy in devices in which only the non-magnetic electrode (silicon) is crystalline, but the tunnel oxide and ferromagnet are not.

Thus, we conclude that the observed *in-plane* anisotropy in devices with an amorphous Al_2O_3 barrier is due to a contribution from coherent spin-polarized transport across the tunnel device and reflects the cubic structure of the crystalline silicon electrode.

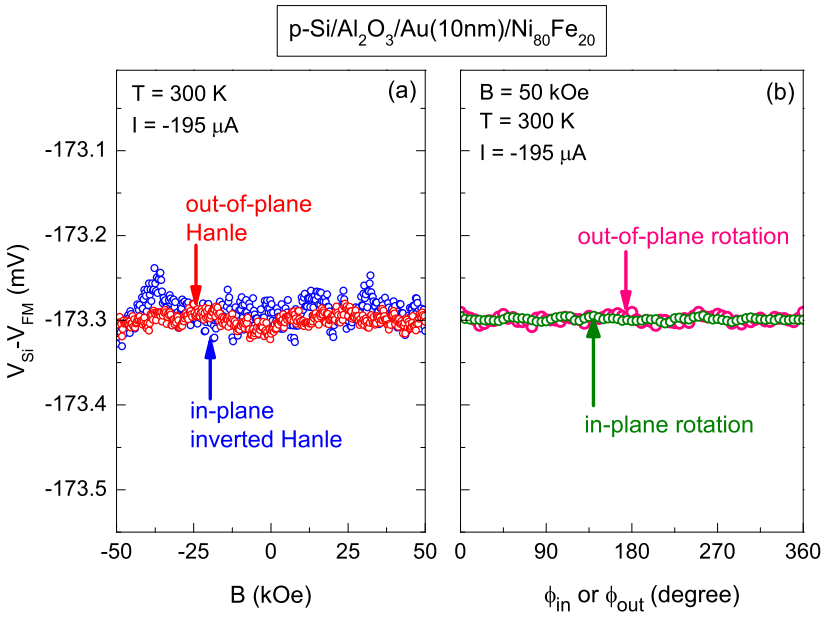

Figure 7.11: *Control experiment with a p-type Si device having a non-magnetic nanolayer (10 nm Au) inserted between the ferromagnetic electrode ($Ni_{80}Fe_{20}$) and the tunnel barrier (Al_2O_3), which suppresses the tunnel spin polarization to zero.* **(a)** *Hanle (red) and inverted Hanle (blue) measurements yield a null result.* **(b)** *Similarly, a null result is obtained when the magnetization is rotated from in-plane to out-of-plane or within the plane of the magnetic layer (right panel).*

7.6 Control device

In spin-transport measurements on semiconductor based magnetic tunnel devices, it is important to rule out any source of spurious signals that may interfere with the spin signal. A suitable control experiment was introduced[29, 63] that can be used to prove or disprove spin transport across semiconductor/oxide/ferromagnet tunnel devices. It exploits the extreme interface sensitivity of the spin-polarized tunneling. A nonmagnetic nanolayer inserted between a ferromagnet and a tunnel barrier suppresses the tunnel spin polarization of the magnetic tunnel contact to a negligible value. In such a device, the spin related effects disappear without removing the FM materials and the associated spurious effects[63]. We studied a control sample with structure p-type Si/Al_2O_3/Au(10 nm)/$Ni_{80}Fe_{20}$. It contains a nonmagnetic nanolayer (10 nm of Au) in between the ferromagnet and the tunnel barrier. Fig. 7.11(a), displays the Hanle and inverted Hanle measurements on this device at a bias current of -195 μA. The absence of Hanle, inverted Hanle signals [Fig. 7.11(a)] and of any tunneling anisotropy (*in-plane* or *out-of-plane*, [Fig. 7.11(b)]) suggest that signals obtained on the tunnel devices without a non-magnetic layer are due to spin polarized transport across the tunnel contact. Therefore, the observed anisotropy is genuine and due to anisotropy of the spin accumulation in the Si.

7.7 Summary

We have investigated the crystal-structure dependent anisotropy of spin accumulation in Si/MgO/Fe and Si/Al_2O_3/ferromagnet tunnel devices. The *in-plane* tunneling anisotropy in Si/oxide/ferromagnet tunnel devices displays a fourfold symmetry that reflects the crystal structure of the Si and/or MgO/Fe tunnel contact. The presence of fourfold in-plane anisotropy in devices with an amorphous Al_2O_3 barrier indicates a new mechanism of tunneling anisotropy. It arises from the direct coupling of states from the ferromagnet to states in the crystalline Si, as in coherent tunneling, which results in an anisotropy that reflects the cubic structure of the silicon.

Bibliography

[1] D. Kahng. Electric field controlled semiconductor device. (US 3.102.230), 08 1963.

[2] Y. Taur and T. H. Ning. *Fundamentals of modern VLSI devices*. Cambridge University Press, New York, NY, USA, 1998.

[3] International technology roadmap for semiconductors, http://www.itrs.net (2010).

[4] G. E. Uhlenbeck and S. Goudsmit. Spinning electrons and the structure of spectra. *Nature*, 117:264, 1926.

[5] M. N. Baibich, J. M. Broto, A. Fert, F. Nguyen Van Dau, F. Petroff, P. Etienne, G. Creuzet, A. Friederich, and J. Chazelas. Giant magnetoresistance of (001) fe/(001) cr magnetic superlattices. *Phys. Rev. Lett.*, 61:2472, 1988.

[6] B. Dieny, V. S. Speriosu, S. S. P. Parkin, B. A. Gurney, D. R. Wilhoit, and D. Mauri. Giant magnetoresistive in soft ferromagnetic multilayers. *Phys. Rev. B*, 43:1297, 1991.

[7] W. J. Gallagher and S. S. P. Parkin. Development of the magnetic tunnel junction mram at ibm: from first junctions to a 16-mb mram demonstrator chip. *IBM J. Res. Dev.*, 50(1):5, 2006.

[8] W. H. Butler. Tunneling magnetoresistance from a symmetry filtering effect. *Science and Technology of Advanced Materials*, 9(1):014106, 2008.

[9] T. Kawahara, K. Ito, R. Takemura, and H. Ohno. Spin-transfer torque ram technology: Review and prospect. *Microelectronics Reliability*, 52(4):613, 2012.

[10] L. Berger. Emission of spin waves by a magnetic multilayer traversed by a current. *Phys. Rev. B*, 54:9353, 1996.

[11] J. C. Slonczewski. Current-driven excitation of magnetic multilayers. *Journal of Magnetism and Magnetic Materials*, 159(1-2):L1, 1996.

[12] J. König, M. C. Bønsager, and A. H. MacDonald. Dissipationless spin transport in thin film ferromagnets. *Phys. Rev. Lett.*, 87:187202, Oct 2001.

[13] S. Murakami, N. Nagaosa, and S. C. Zhang. Dissipationless quantum spin current at room temperature. *Science*, 301(5638):1348, 2003.

[14] D. D. Awschalom and M. E. Flatte. Challenges for semiconductor spintronics. *Nat Phys*, 3(3):153–159, 2007.

[15] J. F. Gregg, I. Petej, E. Jouguelet, and C. Dennis. Spin electronics a review, 2002.

[16] F. Meier and B. P. Zakharchenya (Editors). *Optical Orientation*. Elsevier, Amsterdam, 1984.

[17] G. Lampel. Nuclear dynamic polarization by optical electronic saturation and optical pumping in semiconductors. *Phys. Rev. Lett.*, 20:491, 1968.

[18] G. Schmidt, D. Ferrand, L. W. Molenkamp, A. T. Filip, and B. J. van Wees. Fundamental obstacle for electrical spin injection from a ferromagnetic metal into a diffusive semiconductor. *Phys. Rev. B*, 62:R4790, 2000.

[19] J. Y. Veuillen, J. Derrien, P. A. Badoz, E. Rosencher, and C. d'Anterroches. Co/si(111) interface: Formation of an initial cosi[sub 2] phase at room temperature. *Applied Physics Letters*, 51(18):1448, 1987.

[20] J. S. Tsay, C. S. Yang, Y. Liou, and Y. D. Yao. Magnetic properties of ultrathin co films on si(111) and cosi[sub 2] surfaces. *Journal of Applied Physics*, 85(8):4967, 1999.

[21] E. I. Rashba. Theory of electrical spin injection: Tunnel contacts as a solution of the conductivity mismatch problem. *Phys. Rev. B*, 62:R16267, 2000.

[22] A. Fert and H. Jaffrès. Conditions for efficient spin injection from a ferromagnetic metal into a semiconductor. *Phys. Rev. B*, 64(18):184420, 2001.

[23] D. L. Smith and R. N. Silver. Electrical spin injection into semiconductors. *Phys. Rev. B*, 64:045323, 2001.

[24] I. Appelbaum, B. Huang, and D. J. Monsma. Electronic measurement and control of spin transport in silicon. *Nature*, 447(7142):295, 2007.

[25] B. Huang, D. J. Monsma, and I. Appelbaum. Coherent spin transport through a 350 micron thick silicon wafer. *Phys. Rev. Lett.*, 99:177209, 2007.

[26] B. T. Jonker, G. Kioseoglou, A. T. Hanbicki, C. H. Li, and P. E. Thompson. Electrical spin-injection into silicon from a ferromagnetic metal/tunnel barrier contact. *Nat Phys*, 3(8):542, 2007.

[27] R. Fiederling, M. Keim, G. Reuscher, W. Ossau, G. Schmidt, A. Waag, and L. W. Molenkamp. Injection and detection of a spin-polarized current in a light-emitting diode. *Nature*, 402(6763):787, 1999.

[28] O. M. J. van 't Erve, A. T. Hanbicki, M. Holub, C. H. Li, C. Awo-Affouda, P. E. Thompson, and B. T. Jonker. Electrical injection and detection of spin-polarized carriers in silicon in a lateral transport geometry. *Applied Physics Letters*, 91(21):212109, 2007.

[29] S. P. Dash, S. Sharma, R. S. Patel, M. P. de Jong, and R. Jansen. Electrical creation of spin polarization in silicon at room temperature. *Nature*, 462(7272):491, 2009.

[30] T. Sasaki, T. Oikawa, T. Suzuki, M. Shiraishi, Yoshishige Suzuki, and Katsumichi Tagami. Electrical spin injection into silicon using mgo tunnel barrier. *Applied Physics Express*, 2(5):053003, 2009.

[31] K. R. Jeon, B. C. Min, I. J. Shin, C. Y. Park, H. S. Lee, Y. H. Jo, and S. C. Shin. Electrical spin accumulation with improved bias voltage dependence in a crystalline cofe/mgo/si system. *Applied Physics Letters*, 98(26):262102, 2011.

[32] H. Saito, S. Watanabe, Y. Mineno, S. Sharma, R. Jansen, S. Yuasa, and K. Ando. Electrical creation of spin accumulation in p-type germanium. *Solid State Communications*, 151(17):1159, 2011.

[33] C. H. Li, O. M. J. van t̂ Erve, and B. T. Jonker. Electrical injection and detection of spin accumulation in silicon at 500 k with magnetic metal/silicon dioxide contacts. *Nat Commun*, 2:245, 2011.

[34] J. Fabian, A. Matos-Abiague, C. Ertler, P. Stano, and I. Žutić. Semiconductor spintronics. *Acta Phys. Slov.*, 57:565, 2007.

[35] I. Žutić, J. Fabian, and S. D. Sarma. Spintronics: Fundamentals and applications. *Rev. Mod. Phys.*, 76(2):323, 2004.

[36] R. R. Parsons. Band-to-band optical pumping in solids and polarized photoluminescence. *Phys. Rev. Lett.*, 23:1152, 1969.

[37] B. I. Zakharchenya, V. G. Fleisher, R. I. Dzhioev, Y. P. Veshchunov, and I. B. Rusanov. Effect of Optical Orientation of Electron Spins in a GaAs Crystal. *ZhETF Pis ma Redaktsiiu*, 13:195, 1971.

[38] G. Fishman and G. Lampel. Spin relaxation of photoelectrons in p-type gallium arsenide. *Phys. Rev. B*, 16:820, 1977.

[39] J. M. Kikkawa and D. D. Awschalom. Resonant spin amplification in n-type gaas. *Phys. Rev. Lett.*, 80:4313, 1998.

[40] J. M. Kikkawa and D. D. Awschalom. All-optical magnetic resonance in semiconductors. *Science*, 287(5452):473, 2000.

[41] M. W. Wu, J. H. Jiang, and M. Q. Weng. Spin dynamics in semiconductors. *Physics Reports*, 493(2-4):61, 2010.

[42] Y. Ohno, D. K. Young, B. Beschoten, F. Matsukura, H. Ohno, and D. D. Awschalom. Electrical spin injection in a ferromagnetic semiconductor heterostructure. *Nature*, 402(6763):790, 1999.

[43] H. J. Zhu, M. Ramsteiner, H. Kostial, M. Wassermeier, H.-P. Schönherr, and K. H. Ploog. Room-temperature spin injection from fe into gaas. *Phys. Rev. Lett.*, 87:016601, 2001.

[44] A. T. Hanbicki, B. T. Jonker, G. Itskos, G. Kioseoglou, and A. Petrou. Efficient electrical spin injection from a magnetic metal/tunnel barrier contact into a semiconductor. *Applied Physics Letters*, 80(7):1240, 2002.

[45] R. Jansen, B. C. Min, S. P. Dash, S. Sharma, G. Kioseoglou, A. T. Hanbicki, O. M. J. van 't Erve, P. E. Thompson, and B. T. Jonker. Electrical spin injection into moderately doped silicon enabled by tailored interfaces. *Phys. Rev. B*, 82(24):241305, 2010.

[46] Y. Ando, K. Hamaya, K. Kasahara, Y. Kishi, K. Ueda, K. Sawano, T. Sadoh, and M. Miyao. Electrical injection and detection of spin-polarized electrons in silicon through an fe[sub 3]si/si schottky tunnel barrier. *Applied Physics Letters*, 94(18):182105, 2009.

[47] M. Tran, H. Jaffrès, C. Deranlot, J.-M. George, A. Fert, A. Miard, and A. Lemaître. Enhancement of the spin accumulation at the interface between a spin-polarized tunnel junction and a semiconductor. *Phys. Rev. Lett.*, 102(3):036601, 2009.

[48] R. Jansen, A. M. Deac, H. Saito, and S. Yuasa. Thermal spin current and magnetothermopower by seebeck spin tunneling. *Phys. Rev. B*, 85:094401, 2012.

[49] R. Jansen, A. M. Deac, H. Saito, and S. Yuasa. Injection and detection of spin in a semiconductor by tunneling via interface states. *Phys. Rev. B*, 85:134420, 2012.

[50] R. Jansen. Silicon spintronics. *Nat Mater*, 11(5):400, 2012.

[51] R. Jansen, S. P. Dash, S. Sharma, and B. C. Min. Silicon spintronics with ferromagnetic tunnel devices. *Semiconductor Science and Technology*, 27(8):083001, 2012.

[52] H. Jaffrès and A. Fert. Spin injection from a ferromagnetic metal into a semiconductor. *Journal of Applied Physics*, 91(10):8111, 2002.

[53] A. Fert, J. M. George, H. Jaffrès, and R. Mattana. Semiconductors between spin-polarized sources and drains. *Electron Devices, IEEE Transactions on*, 54(5):921, 2007.

[54] R. W. Wood and A. Ellett. Polarized resonance radiation in weak magnetic fields. *Phys. Rev.*, 24:243, 1924.

[55] W. Hanle. The magnetic influence on the polarization of resonance fluorescence. *Z. Physik.*, 30, 1924.

[56] S. P. Dash, S. Sharma, J. C. Le Breton, J. Peiro, H. Jaffrès, J. M. George, A. Lemaître, and R. Jansen. Spin precession and inverted hanle effect in a semiconductor near a finite-roughness ferromagnetic interface. *Phys. Rev. B*, 84:054410, 2011.

[57] M. Johnson and R. H. Silsbee. Interfacial charge-spin coupling: Injection and detection of spin magnetization in metals. *Phys. Rev. Lett.*, 55:1790, 1985.

[58] F. J. Jedema, H. B. Heersche, A. T. Filip, J. J. A. Baselmans, and B. J. van Wees. Electrical detection of spin precession in a metallic mesoscopic spin valve. *Nature*, 416(6882):713, 2002.

[59] X. Lou, C. Adelmann, M. Furis, S. A. Crooker, C. J. Palmstrøm, and P. A. Crowell. Electrical detection of spin accumulation at a ferromagnet-semiconductor interface. *Phys. Rev. Lett.*, 96:176603, 2006.

[60] X. Lou, C. Adelmann, S. A. Crooker, E. S. Garlid, J. Zhang, K. S. M. Reddy, S. D. Flexner, C. J. Palmstrom, and P. A. Crowell. Electrical detection of spin transport in lateral ferromagnet-semiconductor devices. *Nat Phys*, 3(3):197, 2007.

[61] V. V. Osipov and A. M. Bratkovsky. Spin accumulation in degenerate semiconductors near modified schottky contact with ferromagnets: Spin injection and extraction. *Phys. Rev. B*, 72:115322, 2005.

[62] F. G. Monzon, M. Johnson, and M. L. Roukes. Strong hall voltage modulation in hybrid ferromagnet/semiconductor microstructures. *Applied Physics Letters*, 71(21):3087, 1997.

[63] R. S. Patel, S. P. Dash, M. P. de Jong, and R. Jansen. Magnetic tunnel contacts to silicon with low-work-function ytterbium nanolayers. *Journal of Applied Physics*, 106(1):016107, 2009.

[64] L. Grenet, M. Jamet, P. Noe, V. Calvo, J. M. Hartmann, L. E. Nistor, B. Rodmacq, S. Auffret, P. Warin, and Y. Samson. Spin injection in silicon at zero magnetic field. *Appl. Phys. Lett.*, 94(3):032502, 2009.

[65] G. Kioseoglou, A. T. Hanbicki, R. Goswami, O. M. J. van 't Erve, C. H. Li, G. Spanos, P. E. Thompson, and B. T. Jonker. Electrical spin injection into si: A comparison between fe/si schottky and fe/al[sub 2]o[sub 3] tunnel contacts. *Applied Physics Letters*, 94(12):122106, 2009.

[66] C. H. Li, G. Kioseoglou, O. M. J. van 't Erve, P. E. Thompson, and B. T. Jonker. Electrical spin injection into si(001) through a sio_2 tunnel barrier. *Applied Physics Letters*, 95(17):172102, 2009.

[67] P. Li and H. Dery. Theory of spin-dependent phonon-assisted optical transitions in silicon. *Phys. Rev. Lett.*, 105:037204, 2010.

[68] B. G. Park, T. Banerjee, B. C. Min, J. C. Lodder, and R. Jansen. Tunnel spin polarization of $ni_{80}fe_{20}/sio_2$ probed with a magnetic tunnel transistor. *Phys. Rev. B*, 73:172402, 2006.

[69] O. van't Erve, C. Awo-Affouda, A. T. Hanbicki, C. H. Li, P. E. Thompson, and B. T. Jonker. Information processing with pure spin currents in silicon: Spin

injection, extraction, manipulation, and detection. *Electron Devices, IEEE Transactions on*, 56(10):2343, 2009.

[70] T. Sasaki, T. Oikawa, T. Suzuki, M. Shiraishi, Y. Suzuki, and K. Noguchi. Temperature dependence of spin diffusion length in silicon by hanle-type spin precession. *Applied Physics Letters*, 96(12):122101, 2010.

[71] T. Sasaki, T. Oikawa, T. Suzuki, M. Shiraishi, Y. Suzuki, and K. Noguchi. Evidence of electrical spin injection into silicon using mgo tunnel barrier. *Magnetics, IEEE Transactions on*, 46(6):1436, 2010.

[72] T. Sasaki, T. Oikawa, T. Suzuki, M. Shiraishi, Y. Suzuki, and K. Noguchi. Local and non-local magnetoresistance with spin precession in highly doped si. *Applied Physics Letters*, 98(26):262503, 2011.

[73] T. Sasaki, T. Oikawa, M. Shiraishi, Y. Suzuki, and K. Noguchi. Comparison of spin signals in silicon between nonlocal four-terminal and three-terminal methods. *Applied Physics Letters*, 98(1):012508, 2011.

[74] M. Shiraishi, Y. Honda, E. Shikoh, Y. Suzuki, T. Shinjo, T. Sasaki, T. Oikawa, K. Noguchi, and T. Suzuki. Spin transport properties in silicon in a nonlocal geometry. *Phys. Rev. B*, 83:241204, 2011.

[75] B. C. Min, K. Motohashi, C. Lodder, and R. Jansen. Tunable spin-tunnel contacts to silicon using low-work-function ferromagnets. *Nat Mater*, 5(10):817, 2006.

[76] B. G. Park, T. Banerjee, J. C. Lodder, and R. Jansen. Tunnel spin polarization versus energy for clean and doped al_2o_3 barriers. *Phys. Rev. Lett.*, 99:217206, 2007.

[77] K. R. Jeon, B. C. Min, I. J. Shin, C. Y. Park, H. S. Lee, Y. H. Jo, and S. C. Shin. Unconventional hanle effect in a highly ordered cofe/mgo/ n-si contact: non-monotonic bias and temperature dependence and sign inversion of the spin signal. *New Journal of Physics*, 14(2):023014, 2012.

[78] S. O. Valenzuela, D. J. Monsma, C. M. Marcus, V. Narayanamurti, and M. Tinkham. Spin polarized tunneling at finite bias. *Physical Review Letters*, 94(19):196601, 2005.

[79] Y. Ando, K. Kasahara, K. Yamane, Y. Baba, Y. Maeda, Y. Hoshi, K. Sawano, M. Miyao, and K. Hamaya. Bias current dependence of spin accumulation signals in a silicon channel detected by a schottky tunnel contact. *Applied Physics Letters*, 99(1):012113, 2011.

[80] Y. Ando, K. Kasahara, S. Yamada, Y. Maeda, K. Masaki, Y. Hoshi, K. Sawano, M. Miyao, and K. Hamaya. Temperature evolution of spin accumulation detected electrically in a nondegenerated silicon channel. *Phys. Rev. B*, 85:035320, Jan 2012.

[81] C. H. Shang, J. Nowak, R. Jansen, and J. S. Moodera. Temperature dependence of magnetoresistance and surface magnetization in ferromagnetic tunnel junctions. *Phys. Rev. B*, 58:R2917, 1998.

[82] J. L. Cheng, M. W. Wu, and J. Fabian. Theory of the spin relaxation of conduction electrons in silicon. *Phys. Rev. Lett.*, 104:016601, 2010.

[83] G. Feher, J. C. Hensel, and E. A. Gere. Paramagnetic resonance absorption from acceptors in silicon. *Phys. Rev. Lett.*, 5:309, 1960.

[84] J. L. Cheng, M. W. Wu, and J. Fabian. Theory of the spin relaxation of conduction electrons in silicon. *Phys. Rev. Lett.*, 104:016601, 2010.

[85] P. Li and H. Dery. Spin-orbit symmetries of conduction electrons in silicon. *Phys. Rev. Lett.*, 107:107203, 2011.

[86] V. L. Korenev. Optical orientation in ferromagnet/semiconductor hybrids. *Semiconductor Science and Technology*, 23(11):114012, 2008.

[87] I. A. Merkulov, Al. L. Efros, and M. Rosen. Electron spin relaxation by nuclei in semiconductor quantum dots. *Phys. Rev. B*, 65:205309, 2002.

[88] J. Strand, B. D. Schultz, A. F. Isakovic, C. J. Palmstrøm, and P. A. Crowell. Dynamic nuclear polarization by electrical spin injection in ferromagnet-semiconductor heterostructures. *Phys. Rev. Lett.*, 91:036602, 2003.

[89] S. Demokritov, E. Tsymbal, P. Grünberg, W. Zinn, and I. K. Schuller. Magnetic-dipole mechanism for biquadratic interlayer coupling. *Phys. Rev. B*, 49:720, 1994.

[90] A. Nogaret. Electron dynamics in inhomogeneous magnetic fields. *Journal of Physics: Condensed Matter*, 22(25):253201, 2010.

[91] K. Ando and E. Saitoh. Observation of the inverse spin hall effect in silicon. *Nat Commun*, 3:629, 2012.

[92] E. Shikoh, K. Ando, E. Saito, T. Shinjo, and M. Shiraishi. Spin-pumping-induced spin transport in p-type Si at room temperature. *ArXiv e-prints*, 2011.

[93] S. Iba, H. Saito, A. Spiesser, S. Watanabe, R. Jansen, S. Yuasa, and K. Ando. Spin accumulation in nondegenerate and heavily doped p-type germanium. *Applied Physics Express*, 5(2):023003, 2012.

[94] S. Iba, H. Saito, A. Spiesser, S. Watanabe, R. Jansen, S. Yuasa, and K. Ando. Spin accumulation and spin lifetime in p-type germanium at room temperature. *Applied Physics Express*, 5(5):053004, 2012.

[95] Esther M. Conwell. Impurity band conduction in germanium and silicon. *Phys. Rev.*, 103:51, 1956.

[96] K. R. Jeon, B. C. Min, Y. H. Jo, H. S. Lee, I. J. Shin, C. Y. Park, S. Y. Park, and S. C. Shin. Electrical spin injection and accumulation in cofe/mgo/ge contacts at room temperature. *Phys. Rev. B*, 84:165315, 2011.

[97] A. Jain, L. Louahadj, J. Peiro, J. C. Le Breton, C. Vergnaud, A. Barski, C. Beigné, L. Notin, A. Marty, V. Baltz, S. Auffret, E. Augendre, H. Jaffrès, J. M. George, and M. Jamet. Electrical spin injection and detection at al[sub 2]o[sub 3]/n-type germanium interface using three terminal geometry. *Applied Physics Letters*, 99(16):162102, 2011.

[98] K. Kasahara, Y. Baba, K. Yamane, Y. Ando, S. Yamada, Y. Hoshi, K. Sawano, M. Miyao, and K. Hamaya. Spin accumulation created electrically in an n-type germanium channel using schottky tunnel contacts. *Journal of Applied Physics*, 111(7):07C503, 2012.

[99] Y. Zhou, W. Han, L. T. Chang, F. Xiu, M. Wang, M. Oehme, I. A. Fischer, J. Schulze, R. K. Kawakami, and K. L. Wang. Electrical spin injection and transport in germanium. *Phys. Rev. B*, 84:125323, 2011.

[100] T. Suzuki, T. Sasaki, T. Oikawa, M. Shiraishi, Y. Suzuki, and K. Noguchi. Room-temperature electron spin transport in a highly doped si channel. *Applied Physics Express*, 4(2):023003, 2011.

[101] S. Yuasa, A. Fukushima, T. Nagahama, K. Ando, and Y. Suzuki. High tunnel magnetoresistance at room temperature in fully epitaxial fe/mgo/fe tunnel junctions due to coherent spin-polarized tunneling. *Japanese Journal of Applied Physics*, 43(4B):L588, 2004.

[102] S. S. P. Parkin, C. Kaiser, A. Panchula, P. M. Rice, B. Hughes, M. Samant, and S. H. Yang. Giant tunnelling magnetoresistance at room temperature with mgo (100) tunnel barriers. *Nat Mater*, 3(12):862, 2004.

[103] R. Jansen and B. C. Min. Detection of a spin accumulation in nondegenerate semiconductors. *Phys. Rev. Lett.*, 99(24):246604, 2007.

[104] R. Biagi, P. Fantini, V. De Renzi, M. Grazia B., C. Mariani, and U. del Pennino. Photoemission investigation of the alkali-metal-induced two-dimensional electron gas at the $\mathrm{Si}(111)(1 \times 1)$: H surface. *Phys. Rev. B*, 67:155325, Apr 2003.

[105] W. H. Butler, X. G. Zhang, T. C. Schulthess, and J. M. MacLaren. Spin-dependent tunneling conductance of $\mathrm{Fe|MgO|Fe}$ sandwiches. *Phys. Rev. B*, 63:054416, 2001.

[106] J. Mathon and A. Umerski. Theory of tunneling magnetoresistance of an epitaxial fe/mgo/fe(001) junction. *Phys. Rev. B*, 63:220403, 2001.

[107] C. Tiusan, F. Greullet, M. Hehn, F. Montaigne, S. Andrieu, and A. Schuhl. Spin tunnelling phenomena in single-crystal magnetic tunnel junction systems. *Journal of Physics: Condensed Matter*, 19(16):165201, 2007.

[108] A. T. Hanbicki, S. F. Cheng, R. Goswami, O. M. J. van t̂ Erve, and B.T. Jonker. Electrical injection and detection of spin accumulation in ge at room temperature. *Solid State Communications*, 152(4):244, 2012.

[109] X. Jiang, R. Wang, R. M. Shelby, R. M. Macfarlane, S. R. Bank, J. S. Harris, and S. S. P. Parkin. Highly spin-polarized room-temperature tunnel injector for semiconductor spintronics using mgo(100). *Phys. Rev. Lett.*, 94:056601, 2005.

[110] A. Spiesser, S. Sharma, H. Saito, R. Jansen, S. Yuasa, and K. Ando. Electrical spin injection in p-type si using fe/mgo contacts. *Proc. SPIE*, 8461:84610K, 2012.

[111] C. Chappert, A. Fert, and F. N. Van Dau. The emergence of spin electronics in data storage. *Nat Mater*, 6(11):813, 2007.

[112] T. Inokuchi, M. Ishikawa, H. Sugiyama, Y. Saito, and N. Tezuka. Spin injection and detection between cofe/alo$_x$ junctions and soi investigated by hanle effect measurements. *Journal of Applied Physics*, 111(7):07C316, 2012.

[113] M. Ishikawa, H. Sugiyama, T. Inokuchi, K. Hamaya, and Y. Saito. Effect of the interface resistance of cofe/mgo contacts on spin accumulation in silicon. *Applied Physics Letters*, 100(25):252404, 2012.

[114] S. Takahashi and S. Maekawa. Spin injection and detection in magnetic nanostructures. *Phys. Rev. B*, 67:052409, 2003.

[115] Y. Song and H. Dery. Spin transport theory in ferromagnet/semiconductor systems with noncollinear magnetization configurations. *Phys. Rev. B*, 81:045321, 2010.

[116] J. Robertson. High dielectric constant gate oxides for metal oxide si transistors. *Reports on Progress in Physics*, 69(2):327, 2006.

[117] Y. Xu, D. Ephron, and M. R. Beasley. Directed inelastic hopping of electrons through metal-insulator-metal tunnel junctions. *Phys. Rev. B*, 52:2843, 1995.

[118] T. Uemura, K. Kondo, J. Fujisawa, K. Matsuda, and M. Yamamoto. Critical effect of spin-dependent transport in a tunnel barrier on enhanced hanle-type signals observed in three-terminal geometry. *Applied Physics Letters*, 101(13):132411, 2012.

[119] S. Yuasa and D D Djayaprawira. Giant tunnel magnetoresistance in magnetic tunnel junctions with a crystalline mgo(001) barrier. *Journal of Physics D: Applied Physics*, 40(21):R337, 2007.

[120] S. P. Dash, S. Sharma, J. C. Le Breton, and R. Jansen. Silicon spintronics at room temperature. *Proc. SPIE*, 7760(1):77600J, 2010.

[121] M. Julliere. Tunneling between ferromagnetic films. *Physics Letters A*, 54(3):225, 1975.

[122] C. Gould, C. Rüster, T. Jungwirth, E. Girgis, G. M. Schott, R. Giraud, K. Brunner, G. Schmidt, and L. W. Molenkamp. Tunneling anisotropic magnetoresistance: A spin-valve-like tunnel magnetoresistance using a single magnetic layer. *Phys. Rev. Lett.*, 93:117203, 2004.

[123] C. Rüster, C. Gould, T. Jungwirth, J. Sinova, G. M. Schott, R. Giraud, K. Brunner, G. Schmidt, and L. W. Molenkamp. Very large tunneling anisotropic magnetoresistance of a $(\mathrm{Ga},\mathrm{Mn})\mathrm{As}/\mathrm{GaAs}/(\mathrm{Ga},\mathrm{Mn})\mathrm{As}$ stack. *Phys. Rev. Lett.*, 94:027203, 2005.

[124] A. M. Abiague and J. Fabian. Anisotropic tunneling magnetoresistance and tunneling anisotropic magnetoresistance: Spin-orbit coupling in magnetic tunnel junctions. *Phys. Rev. B*, 79(15):155303, 2009.

[125] H. Saito, S. Yuasa, and K. Ando. Origin of the tunnel anisotropic magnetoresistance in $\mathrm{ga}_{1-x}\mathrm{mn}_x\mathrm{As}/\mathrm{ZnSe}/\mathrm{ga}_{1-x}\mathrm{mn}_x\mathrm{As}$ magnetic tunnel junctions of ii-vi/iii-v heterostructures. *Phys. Rev. Lett.*, 95:086604, 2005.

[126] T. Akiho, T. Uemura, M. Harada, K. Matsuda, and M. Yamamoto. Effect of mgo barrier insertion on spin-dependent transport properties of cofe/n-gaas heterojunctions. *Japanese Journal of Applied Physics*, 51(2):02BM01, 2012.

[127] B. G. Park, J. Wunderlich, D. A. Williams, S. J. Joo, K. Y. Jung, K. H. Shin, K. Olejník, A. B. Shick, and T. Jungwirth. Tunneling anisotropic magnetoresistance in multilayer co/pt/alo$_x$/pt structures. *Phys. Rev. Lett.*, 100:087204, 2008.

[128] L. Gao, X. Jiang, S. H. Yang, J. D. Burton, E. Y. Tsymbal, and S. S. P. Parkin. Bias voltage dependence of tunneling anisotropic magnetoresistance in magnetic tunnel junctions with mgo and $\mathrm{al}_2\mathrm{o}_3$ tunnel barriers. *Phys. Rev. Lett.*, 99:226602, 2007.

[129] A. B. Shick, F. Máca, J. Mašek, and T. Jungwirth. Prospect for room temperature tunneling anisotropic magnetoresistance effect: Density of states anisotropies in copt systems. *Phys. Rev. B*, 73(2):024418, 2006.

[130] J. Moser, A. M. Abiague, D. Schuh, W. Wegscheider, J. Fabian, and D. Weiss. Tunneling anisotropic magnetoresistance and spin-orbit coupling in $\mathrm{Fe}/\mathrm{GaAs}/\mathrm{Au}$ tunnel junctions. *Phys. Rev. Lett.*, 99:056601, 2007.

[131] A. Einwanger, M. Ciorga, U. Wurstbauer, D. Schuh, W. Wegscheider, and D. Weiss. Tunneling anisotropic spin polarization in lateral (ga,mn)as/gaas spin esaki diode devices. *Applied Physics Letters*, 95(15):152101, 2009.

[132] M. Ciorga, A. Einwanger, U. Wurstbauer, D. Schuh, W. Wegscheider, and D. Weiss. In-plane anisotropy of tunneling magnetoresistance and spin polarization in lateral spin injection devices with (ga,mn)as/gaas spin-esaki diode contacts. *Physica E:*, 42(10):2673, 2010.

[133] N. Tombros, S. Tanabe, A. Veligura, C. Jozsa, M. Popinciuc, H. T. Jonkman, and B. J. van Wees. Anisotropic spin relaxation in graphene. *Phys. Rev. Lett.*, 101:046601, 2008.

[134] Y. A. Bychkov and E. I. Rashba. Oscillatory effects and the magnetic susceptibility of carriers in inversion layers. *J. Phys. C: Solid State Phys.*, 17(33):6039, 1984.

[135] H. B. Michaelson. The work function of the elements and its periodicity. *Journal of Applied Physics*, 48(11):4729, 1977.

[136] *In principle, the pre-factor in the last term should include A_1 and A_2. However, during fitting we observed that inclusion of these terms does not affect previously extracted value of A_1 and A_2. Retaining ΔR_{spin} as a pre-factor, makes the fitting procedure simple*.

[137] S. Yuasa, T. Nagahama, A. Fukushima, Y. Suzuki, and K. Ando. Giant room-temperature magnetoresistance in single-crystal fe/mgo/fe magnetic tunnel junctions. *Nat Mater*, 3(12):868–871, 2004.

[138] S. Sharma, S. P. Dash, H. Saito, S. Yuasa, B. J. van Wees, and R. Jansen. Anisotropy of spin polarization and spin accumulation in si/al$_2$o$_3$/ferromagnet tunnel devices. *Phys. Rev. B*, 86:165308, 2012.

[139] B. C. Min. *Ph.D Thesis*. Koninklijke Wöhrmann, Zutphen, The Netherlands, 2007.

[140] Y. Song and H. Dery. Analysis of phonon-induced spin relaxation processes in silicon. *Phys. Rev. B*, 86:085201, 2012.

Summary

The research work described in this thesis was aimed at the understanding of the spin-polarized transport across a magnetic tunnel contact to Si. The successful demonstration of an all-electrical injection and detection of the spins and their manipulation via Hanle effect has been achieved in magnetic tunnel contacts to n-type as well as p-type Si with different tunnel barriers (Al_2O_3 and MgO) and types of ferromagnet (Fe, Co, Ni, $Ni_{80}Fe_{20}$). Importantly, this was achieved at room temperature. Significant understanding of the physics of spin polarized transport across these tunnel devices has been generated. However, certain new issues such as large spin signals, their variation with barrier thickness and lower effective spin lifetime have surfaced and need to be examined in more detail. We present below the summary of the research work described in the thesis.

This thesis

This thesis is divided into three main parts. In the first part, we describe the principle of electrical spin injection into a semiconductor. The second part describes the fundamental results of spin injection and detection in Si at room temperature. This part also includes the detailed study of how spin signal varies with parameters like the voltage, the current density, temperature, interface roughness, barrier thickness and tunnel barrier materials (Al_2O_3 and MgO). The third part of the thesis is devoted to the investigation of the tunneling anisotropy in Si/oxide/ferromagnet devices. For all measurements, we have used the three-terminal geometry for spin injection and detection.

Chapter 2: Principle of spin injection and detection

First, we introduced the principle of electrical injection and detection of spin polarization induced in a semiconductor via tunneling. In a magnetic tunnel contact between a ferromagnet and a semiconductor, the tunnel current is spin-polarized because majority ($\uparrow$) and minority ($\downarrow$) spins have different tunneling conductance. Hence, one type (majority) of spins are injected into the semiconductor at a higher rate than the other type (minority), resulting in a net spin density in the semiconductor. The spins injected into a semiconductor undergo relaxation and if a steady state is maintained, a non-equilibrium spin accumulation $\Delta\mu$ in semiconductor is obtained. This non-equilibrium spin accumulation can be detected via the Hanle effect. We described the Hanle effect, which is considered as a standard test to prove or disprove the existence of the spin accumulation in a non-magnetic material. We pointed out the difference in analyzing the data with a pure Lorentzian approach and another one that considers vertical spin diffusion. We concluded that the time constant extracted from the pure Lorentzian should be treated as a lower bound to the spin lifetime. We also discussed the three-terminal and two-terminal device geometry for spin injection and detection. Finally, we emphasized the importance of performing a control experiment to rule out spurious signals.

Chapters 3-5: Spin Injection into Si

This part of the thesis describes the successful implementation of the magnetic tunnel contacts to Si to electrically create and detect the spin accumulation. In chapter 3, we demonstrated the spin injection, detection and their manipulation via the Hanle effect, in both n-type as well as p-type Si at room temperature. We studied the variation of the spin signals with the voltage, the current density, temperature and different tunnel barrier materials. The control experiments with a non-magnetic layer (Yb or Au) between the ferromagnet and the tunnel barrier confirm that the large room-temperature spin signal is genuine and originates from spin-polarized tunneling and spin accumulation in the Si. The spin signals are found to differ by several order of magnitude from the standard theory. We discussed the possible causes of the disagreement between experiment and theory. Further, the enhancement of the spin signal due to spin accumulation in the localized states was ruled out in an experiment that uses Cs treatment of the silicon surface.

The effective spin lifetime extracted from the Hanle curve is found to be smaller than that obtained from electron spin resonance measurements. This indicates that the spin lifetime is reduced by extrinsic factors that are related to the tunnel contacts. We discussed that the process of spin tunneling into Si is sensitive to the interface

roughness. The interface roughness gives rise to magnetostatic fields B^{ms}, whose magnitude depends upon the amplitude and period of the roughness. Due to these magnetostatic fields, the injected spins precess even in the absence of an external field. This produces an artificial broadening of the Hanle curve, that depends on the direction and the magnitude of B^{ms}, which in turn is proportional to the magnetization of the ferromagnet. As a result the width of the Hanle curve depends on the ferromagnet used, i.e., the width increases from Ni, to $Ni_{80}Fe_{20}$, to Co, to Fe. An inverted Hanle effect is introduced as an experimental signature. It denotes the increase of the spin accumulation in an applied (in-plane) magnetic field.

Chapter 4 describes the use of crystalline Si/MgO/Fe tunnel devices for creating spin polarization in Si at room temperature. The main motivation behind this work was to investigate the expected possibility of large tunnel spin polarization across crystalline Si/MgO/Fe tunnel devices as previously demonstrated for metal-based (Fe/MgO/Fe) magnetic tunnel junctions. From the structural characterization we found that highly ordered crystalline tunnel contacts can be obtained on an annealed Si surface. After the oxide removal, the annealing of Si substrate at 700°C gives rise to a 2×1 reconstructed surface. Subsequent deposition of MgO and Fe at 300°C and 100°C, respectively, results in crystalline tunnel contacts and successful spin injection was observed into n-type as well as p-type Si at 300 K. From transmission electron microscopy images we concluded that with optimum etching time of the SiO_2, a smoother interface between Si and MgO can be obtained.

We also evaluated the influence of the interface roughness on the relative ratio of the Hanle and inverted Hanle signals. We observed that the devices with a more rough interface have a larger inverted Hanle signal compared to the ones with a relatively smoother interface. Thus, we conclude that the magnetostatic fields arising from the rough interface produce stronger inverted Hanle signal and a broadening of the Hanle curve.

In chapters 3 & 4, we concluded that ferromagnetic tunnel contacts to Si provide a robust and technologically viable approach to create and detect the spin-polarized carriers in Si. However, we observed that the magnitude of the spin signals differs by orders of magnitude from the existing theory for spin injection and diffusion. In theory, the spin accumulation ($\Delta\mu$) is predicted to be proportional to the injected spin current. In chapter 5, we present a method to check this prediction by varying the tunnel barrier thickness, which changes the current density J exponentially. The spin accumulation is expected to exhibit a similar exponential variation, such that $\Delta\mu$/J remains constant. Instead, we found that the measured spin signals in Si/oxide/ferromagnet devices scale anomalously with the tunnel resistance and violate the expected proportionality of spin voltage and injected spin current. The obtained results are incompatible with any of the known theories, including those based

on direct tunneling and/or two-step tunneling via localized states. In addition, the results on a control sample rule out signal enhancement by spin accumulation in localized states in the tunnel barrier. The origin of exceptionally large spin signal is still unclear and further theoretical as well as experimental investigations are required.

Chapters 6-7: Tunneling Anisotropy

The third main part of the thesis is devoted to the study of the contribution of the spin accumulation to tunneling anisotropy in Si/oxide/ferromagnet devices. Tunneling anisotropy in these devices is investigated for two cases. For the first case, the magnetization of the magnetic layer is rotated from *in-plane* to perpendicular to the tunnel interface and the resulting change in the tunnel resistance is measured. For the second case, the magnetization is rotated within the plane of the magnetic layer and the change in the tunnel resistance is measured. These investigations have been performed for devices with either amorphous tunnel barrier (Al_2O_3) and poly-crystalline ferromagnetic electrode or devices with crystalline MgO/Fe tunnel contacts to Si.

In chapter 6, we have first investigated *out-of-plane* tunneling anisotropy in Si/Al_2O_3/ferromagnet tunnel devices. A complex dependence of the tunnel resistance on the bias voltage and the field angle was found, which are distinctly different for tunnel devices with different ferromagnetic electrodes (i.e., Fe or Ni). We find that different contributions to the tunneling anisotropy coexist. These can be distinguished using tunnel contacts on n-type as well as p-type silicon and different ferromagnets (Fe and Ni). We found that an important source of anisotropy comes from the anisotropy of the tunnel spin polarization (TASP) of the ferromagnet/tunnel barrier interface. It makes the spin accumulation in the silicon dependent on the absolute orientation of the magnetization of the magnetic layer. We did not find any conclusive evidence for anisotropy of the spin lifetime in silicon, although the presence of a contribution from this mechanism cannot be excluded. The presence of tunneling anisotropic magnetoresistance (TAMR) in tunnel contacts with Fe gives rise to a bias-dependent sign inversion of the tunneling anisotropy. In comparison, tunnel contacts with Ni do not display such a sign inversion of the tunneling anisotropy. Further, we noticed that due to the magnetic shape anisotropy of the thin magnetic layers the magnetization of the magnetic layer and the external field are not perfectly aligned. As a result, the spins injected into the Si undergo some degree of Hanle spin precession that changes when the field direction is changed. This mechanism is shown to contribute to the anisotropy in the spin accumulation. From the analysis of the data we found a term with six-fold symmetry which is associated with the ferromagnet (Fe) and its precise origin is not yet clear.

In chapter 7, the effect of crystalline order on the anisotropy of spin accumu-

lation in Si/oxide/ferromagnet tunnel devices has been investigated. The tunneling anisotropy has been studied in Si based tunnel devices with crystalline and polycrystalline MgO and amorphous Al_2O_3 tunnel barriers. The induced spin accumulation in silicon changes when the magnetization is rotated out-of-plane or within the plane of the magnetic layer. The observed fourfold *in-plane* anisotropy reflects the cubic structure of the Si and/or the MgO/Fe tunnel contact. The anisotropy is proportional to the spin accumulation and is a few percent of it. This together with the null result for Hanle, inverted Hanle and tunneling anisotropy on a control sample suggest that the observed anisotropy is due to anisotropic spin accumulation in silicon. Most likely, it is due to the anisotropic tunnel spin polarization of the magnetic tunnel contact. The presence of fourfold in-plane anisotropy in devices with an amorphous Al_2O_3 barrier indicates a new mechanism of tunneling anisotropy. It arises from the direct coupling of states from the ferromagnet to states in the crystalline Si, as in coherent tunneling, which results in an anisotropy that reflects the cubic structure of the silicon electrode.

The present research work has made a key advancement in the development of silicon-based spintronics devices by using ferromagnetic tunnel contacts. Following a similar approach, the spin injection and detection has now also been established in Ge, another technologically important material. The successful injection, manipulation and detection of spin polarization in a semiconductor at room temperature have proved these tunnel devices to be a robust and reliable buildings block of silicon spintronics. These advancements have enabled us to investigate the influence of the various parameters which may affect the spin transport and the spin dynamics in such devices. Significant understanding of the physics, materials engineering and technology of silicon-based spin-transport devices has been generated, although certain aspects such as the magnitude of the spin accumulation and the spin lifetime require further investigations. The demonstration of the electrical field control of the spins in the channel is, however, still a big challenge. Another challenge is to demonstrate efficient spin injection in Si (n and p-type) with lower doping density so that complementary devices can be realized on the same chip. The present work has significantly brought us closer to the point where we can address the prospects for realizing spin functionality in semiconductor based spintronics devices.

Samenvatting

Het onderzoek beschreven in dit proefschrift is gericht op het begrijpen van spin-gepolariseerd transport in silicium structuren met een ferromagnetisch tunnelcontact. De volledig elektrische injectie en detectie van spin polarisatie in het Si en de manipulatie van de spins via het Hanle effect is bereikt in magnetische tunnelcontacten op n-type en p-type Si met verschillende tunnelbarrières (Al_2O_3 en MgO) en ferromagnetische materialen (Fe, Co, Ni, $Ni_{80}Fe_{20}$). Cruciaal is dat dit is gedaan bij kamertemperatuur. Het onderzoek heeft een belangrijk begrip opgeleverd van de fysica van spin-gepolariseerd transport in silicium structuren met dergelijke tunnelcontacten. Er zijn ook bepaalde onverwachte aspecten opgedoken, zoals de grootte van de spin signalen, de rol van de dikte van de tunnelbbarrière en de kortere effectieve spin levensduur. Deze aspecten dienen nader onderzocht te worden. Hieronder is een samenvatting gegeven van het onderzoek beschreven in dit proefschrift.

Dit proefschrift

Dit proefschrift is verdeeld in drie delen. In het eerste deel wordt het beginsel van elektrische spin injectie in een halfgeleider beschreven. Het tweede deel beschrijft de fundamentele experimentele resultaten van spin injectie en detectie in Si bij kamertemperatuur. Dit deel bevat ook een gedetailleerde studie van de afhankelijkheid van het spin signaal van parameters zoals de spanning, stroomdichtheid, temperatuur, ruwheid van het grensvlak en de dikte van de tunnelbarrière, waarbij tevens verschillende materialen (Al_2O_3 en MgO) zijn gebruikt. Het derde deel van het proefschrift betreft het onderzoek aan de tunnel anisotropie in Si/oxyde/ferromagneet structuren.

Hoofdstuk 2: Principe van spin injectie en detectie

In dit hoofdstuk is allereerst het principe beschreven van de elektrische injectie en detectie van spin polarisatie in een halfgeleider door middel van een tunnelstroom. Deze tunnelstroom is spin-gepolariseerd in een magnetisch tunnelcontact van een ferromagneet op een halfgeleider, omdat elektronen met meerderheidspin een andere tunnelkans hebben dan elektronen met minderheidspin. Daardoor wordt een groter aantal spins van een bepaald type (bijvoorbeeld de meerderheidspin) geïnjecteerd in de halfgeleider. Hierdoor ontstaat een netto spindichtheid in de halfgeleider. De geïnjecteerde spins ondergaan spin verstrooiing in de halfgeleider, en in een "steady-state" situatie wordt een netto spin accumulatie in de halfgeleider verkregen. Deze spin accumulatie kan worden gedetecteerd met behulp van het Hanle effect. Dit effect wordt algemeen beschouwd als een goede test om het bestaan van een spin accumulatie in een niet-magnetisch materiaal te bewijzen. De Hanle metingen kunnen worden beschreven met behulp van een Lorentz curve, of met een aangepaste curve indien diffusie van de spins loodrecht op het tunnel grensvlak wordt meegenomen. Een belangrijke conclusie is dat een beschrijving van de metingen met een zuivere Lorentz curve niet de spin levensduur geeft, maar slechts een ondergrens daaraan. Verder zijn in dit hoofdstuk de verschillende meetgeometrieën (driepunts en vierpunts) besproken, en is het belang benadrukt van controle experimenten om valse signalen te indentificeren en uit te sluiten. Alle spin-transport experimenten beschreven in dit proefschrift zijn gedaan met driepuntsmetingen.

Hoofdstuk 3-5: Spin injectie in silicium

Dit deel van het proefschrift beschrijft het succesvolle gebruik van magnetische tunnelcontacten op Si voor de elektrische creatie en detectie van een spin polarisatie in het Si. Hoofdstuk 3 beschrijft experimenten die laten zien dat het inderdaad mogelijk is om een spin accumulatie in het silicium te induceren, detecteren en tevens te manipuleren (met behulp van het Hanle effect), en dat alles bij kamertemperatuur. De variatie van de spin signalen als functie van de aangelegde spanning, de stroomdichtheid, en de temperatuur is bestudeerd voor verschillende materialen. Controle experimenten, waarbij een zeer dunne niet-magnetische laag (Yb of Au) tussen de ferromagneet en de tunnelbarrière wordt opgenomen, laten eenduidig zien dat de spin signalen daadwerkelijk het resultaat zijn van spin-gepolariseerd transport en het ontstaan van een spin polarisatie in het silicium. Er werd gevonden dat de spin signalen vele ordes van grootte verschillen van wat verwacht werd op basis van de bestaande theorie. De mogelijke oorzaken van dit verschil zijn besproken, waarbij een voorgestelde versterking van het spin signaal door tunnelen via gelokaliseerde

toestanden aan het halfgeleidergrensvlak werd uitgesloten met behulp van speciaal daarvoor ontworpen experimenten.

De effectieve spin levensduur in het silicium, zoals bepaald uit de Hanle metingen, blijkt kleiner te zijn dan werd verwacht op basis van eerdere metingen van de bulk spin levensduur met behulp van elektron spin resonantie. Dit geeft aan dat de spin levensduur in het Si onder het tunnelcontact wordt gelimiteerd door externe factoren. Er werd gevonden dat de spin levensduur afhangt van de ruwheid van de contacten. Ruwheid van de grensvlakken produceerd locale magnetostatische strooivelden, met een grootte die afhangt van de amplitude en typische lengteschaal van de ruwheid. Als gevolg van deze locale velden wordt de accumulatie en dynamica (precessie) van de spins in de buurt van het grensvlak veranderd. In de afwezigheid van een extern magnetisch veld wordt de spin accumulatie al onderdrukt, terwijl tevens een inhomogene verbreding van de Hanle curve optreedt waardoor de bepaalde spin levensduur korter lijkt te zijn. De kunstmatige verbreding hangt af van de grootte en de richting van de locale strooivelden, en daarmee tevens van de magnetisatie van de ferromagneet. Er werd inderdaad gevonden dat de breedte van de Hanle curve toeneemt als een ferromagneet met een grotere magnetisatie wordt gebruikt (bijvoorbeeld Fe of Co in plaats van Ni of $Ni_{80}Fe_{20}$). Als experimenteel kenmerk is het geïnverteerde Hanle effect geïntroduceerd. Dit effect beschrijft de toename van de spin accumulatie in een aangelegd magnetisch veld parallel aan de magnetisatie van de ferromagneet, waardoor de invloed van de locale strooivelden wordt onderdrukt.

Hoofdstuk 4 beschrijft het gebruik van kristallijne Si/MgO/Fe tunnelcontacten voor het creëren van spin polarisatie in Si bij kamertemperatuur. De belangrijkste motivatie voor dit werk is dat een grote tunnel spin polarisatie kan worden verwacht, zoals reeds was aangetoond voor magnetische tunneljuncties met twee metalen magnetische elektroden (Fe/MgO/Fe). Er werd gevonden dat de preparatie van het silicium een belangrijke factor is. Na het verwijderen van de oxydelaag werd het Si substraat verhit tot 700°C, waarbij een oppervlak met een 2×1 reconstructie ontstaat. Depositie van MgO en Fe bij, respectievelijk, 300°C en 100°C resulteert vervolgens in kristallijne tunnelcontacten waarmee spin injectie en detectie bij kamertemperatuur inderdaad werd waargenomen, zowel voor n-type als voor p-type Si. Tevens werd gevonden dat de ruwheid van het oppervlak kan worden verbeterd door een juiste keuze van de etstijd voor de verwijdering van de oxydelaag op het Si. Dit heeft niet alleen invloed op de grootte van het spin signaal, maar ook op de relatieve grootte van de Hanle en geïnverteerde Hanle signalen. Voor contacten met grotere ruwheid van de grensvlakken werd gevonden dat het geïnverteerde Hanle effect meer prominent aanwezig is. Dit strookt met magnetostatische strooivelden als de oorzaak van het geïnverteerde Hanle effect.

Op basis van de resultaten uit de hoofdstukken 3 en 4 concluderen we dat ferromagnetische tunnelcontacten op Si een robuuste en technologisch haalbare benadering vormen voor het creëren en detecteren van spin-gepolariseerde ladingsdragers in Si bij kamertemperatuur. De gevonden spin accumulatie was echter veel groter dan was verwacht op basis van de bestaande theorie voor injectie en diffusie van spins in niet-magnetische materialen. Ook voorspelt de theorie een compleet ander gedrag van het spin signaal als functie van de dikte van de tunnelbarrière. Volgens de theorie is de spin accumulatie ($\Delta\mu$) evenredig met de geïnjecteerde spinstroom. Hoofdstuk 5 beschrijft experimentele resultaten voor tunnel contacten met verschillende dikte van de tunnelbarrière, waarmee de stroomdichtheid J exponentieel wordt gevarieerd. De spin accumulatie zou dan naar verwachting een vergelijkbare exponentiële variatie moeten laten zien. Er werd echter gevonden dat $\Delta\mu$ slechts zeer zwak afhangt van de barrière dikte, zodat $\Delta\mu$/J geen constante is, maar, geheel onverwacht, evenredig is met de tunnelweerstand. De verkregen resultaten zijn onverenigbaar met de bestaande theorieën, zowel die voor direct tunneltransport alsmede die voor tunneltransport in twee stappen via gelokaliseerde toestanden. De verklaring voor de onverwacht grote spin signalen en het gedrag als functie van de dikte van de tunnelbarrière is vooralsnog onbekend.

Hoofdstuk 6-7: Anisotropie van het tunnel spin transport

Het derde deel van dit proefschrift is gewijd aan de studie van de anisotropie in Si/oxyde/ferromagneet tunnelcontacten en de bijdrage daaraan van de spin accumulatie. De tunnel anisotropie is onderzocht voor twee configuraties. In de eerste configuratie wordt de magnetisatie van de ferromagnetische laag gedraaid van parallel aan het tunnelgrensvlak naar loodrecht op het grensvlak. In de tweede configuratie wordt de magnetisatie gedraaid in het vlak van het tunnelcontact. In beide gevallen wordt de verandering van de tunnelweerstand gemeten. Dit is gedaan voor contacten op Si met een tunnelbarrière van amorf Al_2O_3 en een polykristallijne ferromagnetische elektrode, en voor structuren met een kristallijn MgO/Fe contact.

In hoofdstuk 6 worden de resultaten beschreven van onderzoek aan de anisotropie in Si/Al_2O_3/ferromagneet tunnelcontacten in de loodrechte configuratie. Er werd een complexe afhankelijkheid van de tunnelweerstand van de richting van het aangelegde magnetische veld gevonden, met duidelijke verschillen voor tunnelcontacten met verschillende ferromagnetische elektroden (bijvoorbeeld Fe of Ni). Er wordt geconcludeerd dat er meerdere bijdragen aan de anisotropie naast elkaar bestaan. Deze bijdragen kunnen worden gescheiden door experimenten met tunnelcontacten op n-type en p-type silicium en met verschillende ferromagneten (Fe en Ni). Er blijkt dat de anisotropie van de tunnel spin polarisatie van het ferromagneet/tunnelbarrière

grensvlak een belangrijke bron van anisotropie is. Het maakt dat de spin accumulatie in het silicium afhankelijk is van de absolute oriëntatie van de magnetisatie van de ferromagnetische laag. Er werden geen aanwijzingen gevonden voor anisotropie van de spin levensduur in het silicium, alhoewel een bijdrage hiervan niet geheel kan worden uitgesloten. Verder werd gevonden dat in deze metingen tevens een extra anisotropie ontstaat door de magnetische vormanisotropie van de dunne magnetische lagen. Hierdoor staan de magnetisatie en het externe magnetische veld niet exact parallel, waardoor de spins die in de halfgeleider zijn geïnjecteerd Hanle precessie ondergaan die verandert wanneer het veld van richting verandert.

In hoofdstuk 7 worden experimenten beschreven die laten zien dat er een bijdrage aan de anisotropie is door de kristallijne aard van de Si/oxyde/ferromagneet tunnelcontacten. Hiertoe werden metingen in de tweede configuratie gedaan (magnetisatie in het vlak van het tunnelcontact) aan structuren met kristallijne en polykristallijne MgO tunnelbarrières en aan structuren met amorf Al_2O_3. De geïnduceerde spin accumulatie in het Si verandert wanneer de magnetisatie in het vlak van het tunnel contact wordt gedraaid. De waargenomen anisotropie heeft een viervoudige symmetrie die de kubische structuur van het Si en/of het MgO/Fe tunnel contact weerspiegelt. De sterkte van de anisotropie is evenredig met de spin accumulatie en bedraagt een paar procent daarvan. Een dergelijke anisotropie is afwezig in controle experimenten met structuren waarin de tunnel spin polarisatie nul is zodat er geen spin accumulatie is. We concluderen daarom dat de waargenomen viervoudige anisotropie in het vlak van het tunnelcontact gerelateerd is aan de spin accumulatie, en hoogstwaarschijnlijk onstaat door de anisotropie van de tunnel spin polarisatie van het magnetische tunnelcontact. Geheel onverwacht werd deze viervoudige anisotropie ook gevonden in structuren met amorf Al_2O_3 als tunnelbarrière. Dit suggereert een nieuw mechanisme van anisotropie. Het ontstaat door de directe koppeling van elektronische toestanden van de ferromagneet met die van het kristallijne Si, zoals in coherent tunneltransport. Dit resulteert in een anisotropie die de kubische structuur van de silicium elektrode weerspiegelt.

Het onderzoek beschreven in dit proefschrift is een belangrijke stap voorwaarts in de ontwikkeling van silicium spintronica, mogelijk gemaakt door het gebruik van ferromagnetische tunnelcontacten. Deze tunnelcontacten zijn uitermate geschikt gebleken voor de injectie, manipulatie en detectie van spin polarisatie in halfgeleiders bij kamertemperatuur, en vormen een betrouwbare bouwsteen van silicium spintronica. Volgens een soortgelijke aanpak is spin injectie en detectie nu ook waargenomen in germanium, een ander technologisch belangrijk materiaal. Deze ontwikkelingen hebben ons tevens in staat gesteld de invloed te onderzoeken van de verschillende parameters die het transport en de dynamica van spins in dergelijke structuren beïnvloeden. Belangrijk begrip is verkregen van de fysica, materiaalkunde en technolo-

gie van spin-transport structuren die zijn gebaseerd op silicium, hoewel bepaalde aspecten, zoals de grootte van de spin accumulatie en de spin levensduur, verder onderzoek vereisen. Een grote uitdaging is het manipuleren van de spin polarisatie in het silicium met een elektrisch, in plaats van een magnetisch, veld. Er is ook nog verder onderzoek nodig aan spin injectie in silicium met een lagere concentratie van ladingsdragers. Desalniettemin, door het beschreven onderzoek zal het in de nabije toekomst mogelijk zijn een goed onderbouwde inschatting te maken van de mogelijkheden en potentie van silicium spintronica.

Acknowledgements

I have been waiting for this part since last four years. The endless support from my colleagues, family members and friends has helped me to reach at this stage. Now, I am in a position to acknowledge those who have motivated and enabled me to achieve my goal.

First of all, I wish to express my gratitude to Prof. Bart J. van Wees for being my *promotor* and extending his support all the time. The timely support that you offered during the shift of workplace from Twente to Tsukuba, helped me to concentrate on my research work.

I wish to thank my thesis supervisor and *assistant promoter*, Dr. Ron Jansen for giving me the opportunity to work as his PhD student. I must admit his patience in explaining me the same topic again and again. Your continuous encouragement, inspiring guidance, crystal clear explanations of the concepts and support throughout these four years has helped me a lot in understanding and pushing my research work. Discussion with you was always illuminating. After working with you, I have learned how to plan the experiments, analyze the results and present them. Thanks for inculcating these things in me.

I would like to express my gratitude to the members of the reading committee who have taken time out of their busy schedules and given me invaluable comments.

I wish to acknowledge Dr. Saroj Prasad Dash (now faculty at Chalmers University, Sweden), who informed me about the new PhD position. Fortunately, I was called for an interview and got the opportunity to work at the University of Twente. He was instrumental in getting me started. I had never thought that a person with whom I shared a bench in the classroom at IIT-Delhi will supervise my PhD work!!. Thanks Saroj, for motivating me, strengthening me during my tough time, putting me on the track, introducing me to the MESA$^+$ lab and the new world of semiconductor spintronics. Thanks for providing me the cakes almost every evening so that I can stay with you in the lab for longer duration !!!!.

During my PhD tenure, I got the opportunity to work with many people. I wish to thank Dr. Michel P. de Jong, Dr. Tian Gang, T. L. A. Tran, Johnny Sanderink, Thijs Bolhuis and Martin Siekman, the team members of Nano Electronic group, for their involvement in the technical work during my short stay at University of Twente. I miss the time spent with you people at Hogekamp.

In October-2010, I got another opportunity to work with a new team at AIST-Tsukuba in Japan. I am thankful to Dr. Shinji Yuasa and Dr. Hidekazu Saito for giving me the access to their research facilities. I wish to thank Dr. Takehiko Yorozu, Dr. Koji Moriyama and Ms. Mie Yamamoto for their help in getting me acquainted with new lab. A special thanks to Dr. Takehiko Yorozu for the care he has shown when I fell sick. Thanks to other members: Dr. Satoshi Iba, Dr. Aurelie Spiesser, Sugu Watanabe, Sato-kun of the spintronics group at AIST for their help in scientific work.

It is my pleasure to express my gratitude to Dr. Tamalika Banerjee, Dr. Yunjae Lee, Dr. Ivan Vera-Marun, Subir Parui, K. G. Rana, Alok Chubal and Saurabh Roy for assisting me in many ways. Thanks to Himansu Shekhar Nanda, Neeraj, Tilak Bhattacharjee, Mrinalini Mishra, Shipra Chauhan, Ganesh and Sathish for sharing their valuable time and making my stay pleasant at Tsukuba.

I wish to thank my colleagues at Semiconductor Lab (SCL) Mohali, India, with whom I worked, learned the semiconductor fundamentals and developed interests in research. Thanks to Dr. Jatin Roy, Dr. Chumki Saha, Dr. Uma Pati, Dr. D. N. Singh for supporting my decision. Also, I am thankful to Vikram Singh Chauhan, Vinita Mishra, Monika Gupta, Uday Khambete Purushotam, Sudipto Das Gupta, Satadru Sarkar and Amit Singh for sharing their knowledge and time with me.

I appreciate the administrative support from Lydia van der Vlist, Anna McEwan-Bos, J.C. Wierbos-Post, Tomoko Fukuda and Kazuko Sato.

Now moving towards more personal acknowledgments, I am indebted to my parents, sisters and brother-in-laws for their selfless support and continuous encouragement during these four years. I wish to express my gratitude to my sisters and Pankaj and Pardeep for sharing their valuable time with my son “Shivaansh". Your involvement has helped me to strengthen myself and made it possible for me to be at this stage. Ammi and Abbu, I have always seen you working hard to support our education. Now, I hope that this will make your year’s work more valuable. Again, I wish to thank you for taking care of “Shivaansh" in my absence. It would have never been possible without your encouragement and support.

Specially, I would like to dedicate this thesis to my son *“Shivaansh"*. I always feel sorry that I couldn’t see you growing in front of me, be with you during your childhood. But, there was not a single moment when I did not think about you. I was always with you and after this assignment, again we will learn together.

Sandeep Sharma
February 2013, Tsukuba

Publications

[1] S. Sharma, A. Spiesser, S. P. Dash, S. Iba, S. Watanabe, B.J. van Wees, H. Saito, S. Yuasa and R. Jansen. Anomalous scaling of spin accumulation in ferromagnetic tunnel devices with silicon and germanium. http://arxiv.org/abs/1211.4460

[2] S. Sharma, A. Spiesser, H. Saito, S. Yuasa, B. J. van Wees and R. Jansen. Crystal-induced anisotropy of spin accumulation in Si/MgO/Fe and Si/Al_2O_3/Ferromagnet tunnel devices. Phys. Rev. B **87**, 085307 (2013).

[3] S. Sharma, S. P. Dash, H. Saito, S. Yuasa, B. J. van Wees and R. Jansen. Anisotropy of spin polarization and spin accumulation in Si/Al_2O_3/ferromagnet tunnel devices. Phys. Rev. B **86**, 165308 (2012).

[4] R. Jansen, S. P. Dash, S. Sharma, and B. C. Min. Silicon spintronics with ferromagnetic tunnel devices. Semicond. Sci. Technol. **27**, 083001 (2012), Review 27p.

[5] A. Spiesser, S. Sharma, H. Saito, R. Jansen, S. Yuasa and K. Ando. Electrical spin injection in p-type Si using Fe/MgO contacts. Proc. SPIE, **8461**, 84610K (2012).

[6] J. C. Le Breton, S. Sharma, H. Saito, S. Yuasa and R. Jansen. Thermal spin current from a ferromagnet to silicon by Seebeck spin tunnelling. Nature **475**, 82-85 (2011).

[7] H. Saito, S. Watanabe, Y. Mineno, S. Sharma, R. Jansen, S. Yuasa, and K. Ando. Electrical creation of spin accumulation in p-type Germanium. Sol. State. Comm. **151**, 1159-1161 (2011).

[8] S. P. Dash, S. Sharma, J. C. Le Breton, J. Peiro, H. Jaffrès, J. M. George, A. Lemaître, and R. Jansen. Spin precession and inverted Hanle effect in a semiconductor near a finite-roughness ferromagnetic interface. Phys. Rev. B **84**, 054410 (2011).

[9] S. P. Dash, S. Sharma, J. C. Le Breton and R. Jansen. Silicon spintronics at room temperature. Proc. SPIE, **7760**, 7760J (2010).

[10] R. Jansen, B. C. Min, S. P. Dash, S. Sharma, G. Kioseoglou, A. T. Hanbicki, O. M. J. van't Erve, P. E. Thompson, and B. T. Jonker. Electrical spin injection into moderately doped silicon enabled by tailored interfaces. Phys. Rev. B **82**, 241305 (2010).

[11] S. P. Dash, S. Sharma, R. S. Patel, M. P. de Jong and R. Jansen. Electrical creation of spin polarization in silicon at room temperature. Nature **462**, 491-494 (2009).

[12] S. Sharma, A. Barman, M. Sharma, L. R. Shelford, W. Kruglyak and R. J. Hicken. Structural and magnetic properties of electro-deposited Cobalt nanowires arrays. Sol. State. Comm. **149**, 1650 (2009).

[13] A. B. Bhattacharyya, G. Desai, C. Saha, S. Sharma, A. K. Singh and D. N. Singh. Temperature dependence of compact alpha power MOSFET model parameters. Proc. IWPSD **1082**, (2005).